

NOTE TO USERS

This reproduction is the best copy available.

UMI[®]

Design and Development of a Cam-Driven Laboratory Ball Mill

Lei Geng

Department of Mechanical Engineering
McGill University, Montreal

August, 2004

A Thesis submitted to the Faculty of Graduate studies and Research
In partial fulfilment of the requirements for the degree of
Master of Engineering

© Lei Geng, 2004



Library and
Archives Canada

Bibliothèque et
Archives Canada

Published Heritage
Branch

Direction du
Patrimoine de l'édition

395 Wellington Street
Ottawa ON K1A 0N4
Canada

395, rue Wellington
Ottawa ON K1A 0N4
Canada

Your file Votre référence

ISBN: 0-494-12603-5

Our file Notre référence

ISBN: 0-494-12603-5

NOTICE:

The author has granted a non-exclusive license allowing Library and Archives Canada to reproduce, publish, archive, preserve, conserve, communicate to the public by telecommunication or on the Internet, loan, distribute and sell theses worldwide, for commercial or non-commercial purposes, in microform, paper, electronic and/or any other formats.

The author retains copyright ownership and moral rights in this thesis. Neither the thesis nor substantial extracts from it may be printed or otherwise reproduced without the author's permission.

AVIS:

L'auteur a accordé une licence non exclusive permettant à la Bibliothèque et Archives Canada de reproduire, publier, archiver, sauvegarder, conserver, transmettre au public par télécommunication ou par l'Internet, prêter, distribuer et vendre des thèses partout dans le monde, à des fins commerciales ou autres, sur support microforme, papier, électronique et/ou autres formats.

L'auteur conserve la propriété du droit d'auteur et des droits moraux qui protègent cette thèse. Ni la thèse ni des extraits substantiels de celle-ci ne doivent être imprimés ou autrement reproduits sans son autorisation.

In compliance with the Canadian Privacy Act some supporting forms may have been removed from this thesis.

Conformément à la loi canadienne sur la protection de la vie privée, quelques formulaires secondaires ont été enlevés de cette thèse.

While these forms may be included in the document page count, their removal does not represent any loss of content from the thesis.

Bien que ces formulaires aient inclus dans la pagination, il n'y aura aucun contenu manquant.


Canada

ABSTRACT

In mineral processing industries, grinding processes can be defined as the particles reduced in size by a combination of impact and abrasion. It is performed in tumbling mills that describe a class of mills delimited by a cylindrical chamber filled with balls and/or rock that rotate around its longitudinal axis. Tumbling mills, whether they are autogenous, semi-autogenous, ball or rod, are classed according the nature of the discharge as centre peripheral discharge mills, end peripheral discharge mills, overflow mills, and grate discharge mills. These mills are used in at least three industries: mining, cement and metal powders industries to grind different materials (ore, clinker and metal powder) to desired quality specifications as principally described by a size distribution. These tumbling mills range in size from small 0.3 m diameter lab mills to a 16 m diameter semi-autogenous industrial mill and are driven by chain and sprocket (lab mills), gear and pinion (pilot and industrial scale mills) and gearless drives in very large diameter mill (8 to 12 m dia.). All of these mill drives present advantages and limitations.

In this thesis, we focus on the design and development of a cam-driven laboratory ball mill. An alternative drive system is presented that uses a newly patented speed-o-cam technology and applies it to a 5 ft diameter lab mill. We introduce polynomials to modify the cam profile around both the cusp and the blunt point of the profile to improve pressure angle and shock impact. We build models of mechanical systems, simulate the full-motion behavior of the models, and analyze multiple design variations. We integrate the theoretical, virtual and experimental analyses in order to design an optimal mechanical system. Moreover, the analysis of static and dynamic forces of cam mechanism is reported in the thesis.

RESUME

Dans l'industrie du traitement du minerai, le broyage peut être défini comme la réduction de la taille des particules par une combinaison d'impacts et de frottements. Ce procédé est accompli à l'aide de broyeurs. Ces broyeurs sont constitués d'une large chambre cylindrique, remplie de boulets et de roche, tournant sur son axe longitudinal à la manière d'un boulier. Les broyeurs, peu importe leur procédé de broyage sont classés selon leur système de décharge. Celui-ci peut être à décharge autogène, semi-autogène, balle ou tringle. Ces broyeurs sont utilisés dans au moins trois industries: l'industrie minière, celle du ciment et celle des poudres métalliques. Leur tâche se résume au concassage de différents matériaux jusqu'à ce que la matière concassée réponde à des normes de qualité pré-établies. La majorité du temps, ces normes dictent la grosseur des particules désirée à la fin du procédé. Les dimensions d'un broyeur varient. Aussi petites qu'un (1) pied de diamètre pour un broyeur expérimental en laboratoire elles peuvent atteindre quarante (40) pieds de diamètre pour un broyeur industriel. Les plus petits broyeurs sont entraînés par un système à chaîne alors que ceux de moyenne et de grosse dimension sont habituellement entraînés par un système d'engrenage. Les broyeurs de très grande dimension (30 à 40 pieds de diamètre) sont propulsés par voie électromagnétique. Chacun de ces systèmes d'entraînement comporte ses avantages et ses inconvénients.

Cette thèse, porte sur le développement d'un broyeur à boulets expérimental doté d'un nouveau système d'entraînement à cames. Le système d'entraînement « *speed-o-cam* » de ce broyeur de cinq (5) pieds de diamètre utilise une technologie nouvellement brevetée issue du monde de la robotique. L'introduction de polynômes a permis de modifier le profil des cames afin d'améliorer les performances dynamiques et cinématiques du système pour son application dans le domaine du broyage. Différents modèles mécaniques ont été construits et, à l'aide de simulateurs, leur comportement a pu être analysé. En intégrant la théorie, les résultats d'expériences et les données obtenues par simulations numériques, il a été possible d'optimiser le système. L'analyse des forces statiques et dynamiques exercées sur les cames fait aussi partie de cette thèse.

ACKNOWLEDGEMENTS

I am indebted to thank my thesis supervisor Professor Peter Radziszewski, for his continued supervision, guidance, and invaluable support throughout the course of my thesis research. His patience and encouragement made it possible for me to finish this thesis.

I would like to express my gratitude to Professor Jorge Angeles for his clarification of many concepts about speed-o-cam in my research area.

Special thanks are due to Professional Engineer Rafael Perlin for his help time to time in producing the cam-driven ball mill.

I would like to acknowledge the support of COREM and NSERC as well as the companies Brunswick Mines and Troilus.

I am also thankful to Chao Chen, Shaoping Bai, Weimin Zhang, Xiang Zhang, and Chinpun Teng, for their contributions to the cam design as well as Gary Savard, Dan Ringuette, Ray Lemay and especially John Boisvert for the contributions to the manufacture of this mill.

Last but not least, I would like to thank the staff, secretaries, and all my colleagues of Comminution Dynamics Lab, and of the Department of Mechanical Engineering, McGill University, for their help, support and making my stay at McGill a pleasant experience.

TABLE OF CONTENTS

ABSTRACT.....	i
RESTRACT.....	ii
ACKNOWLEDGEMENTS.....	iii
LIST OF FIGURES.....	vi
LIST OF TABLES.....	x
SYMBOLS AND ABBREBIATIONS.....	xi
CHAPTER 1. Introduction.....	1
1.1. Types of Mill.....	1
1.2. Review of the current drive systems	6
1.2.1. Chain & Sprocket Drives.....	6
1.2.2. Geared Drives.....	6
1.2.3. Gearless Drives.....	7
1.3. Objective of this work	8
CHAPTER 2. Design Parameters of Ball Mill.....	10
2.1. Derivation for Speed	10
2.2. Power prediction.....	12
2.3. Drive Selection.....	15
CHAPTER 3. The Synthesis of Planar Speed-o-Cam	17
3.1. Cam Profile Determination	17
3.2. Pressure Angle Determination	20
3.3. Cam Curvature	21
3.4. Undercutting of the Cam Profile.....	23
3.5. Polynomial.....	23
3.5.1. The Fifth Order Polynomial	29
3.5.2. The Sixth Order Polynomial.....	33
CHAPTER 4. Design and Development	36
4.1. Optimization by Virtual Prototype Technology.....	36

4.2. Design and Optimization of Speed-o-Cam	38
4.2.1. Version I of Speed-o-Cam.....	39
4.2.2. Version II of Speed-o-Cam	42
4.2.3. Version III of Speed-o-Cam.....	46
4.2.4. Version IV of Speed-o-Cam.....	50
4.3. Design and Optimization of other components	55
CHAPTER 5. Finite Element Analyses of Cam Profile	58
5.1. The static forces analysis.....	59
5.2. The dynamic forces analysis.....	61
CHAPTER 6. The Cam Drive Fabrication & Assessment.....	64
6.1. The Cam Drive Fabrication.....	64
6.2. The Cam Drive Assessment.....	67
CHAPTER 7. Conclusions and Recommendations for Future Work	68
7.1. Conclusions	68
7.2. Recommendations for Future Work	69
REFERENCES	71
APPENDIX A. Engineering Drawings of the Cam-Driven Laboratory	
Ball Mill and its Components	75
A.1. Drawings of the Cam-Driven Laboratory Ball Mill and Components	75

LIST OF FIGURES

1.1	Tumbling mill.....	1
1.2	Rod mill.....	2
1.3	Overflow Ball Mill.....	2
1.4	Diaphragm (Grate) Discharge Ball Mill.....	2
1.5	Central peripheral discharge mill.....	3
1.6	End peripheral discharge mill	3
1.7	Overflow mill.....	3
1.8	Grate discharge mill.....	3
1.9	Overflow Rod Mill.....	4
1.10	End peripheral Discharge Rod Mill.....	4
1.11	Rod/Ball Compartmented Mill.....	4
1.12	Ball Compartmented Mill.....	5
1.13	Motion of charge in a tumbling mill.....	5
1.14	Gear/pinion on ball mill.....	7
1.15	Ball mill with gearless ring motor.....	8
1.16	Prototype of planar Speed-o-Cam.....	8
2.1	Discrete ball charge at rest	12
2.2	Charge profile simulation (4.75 m dia., 45% filling, 12.5 cm top size ball, 80% crit. Speed, 1 m length).....	14
2.3	Slurry pool overlapping with ball charge (4.75 m dia., 45% filling, 12.5 cm top size ball, 80% crit. Speed, 1 m length).....	14
2.4	Combined data set: Observed vs predicted power	15
3.1	Two distinct views of external Speed-o-Cam.....	17
3.2	External planar speed-o-cam	18
3.3	The pressure angle distribution	21
3.4	Curvature for external speed-o-cam.....	23

3.5	Cam profile.....	23
3.6	Toggle position	23
4.1	Design process steps (ADAMS/View 12.0, 2001).....	38
4.2	Cam.....	39
4.3	Speed-O-Cam.....	39
4.4	Plotting of cam kinematics: (a) cam profile; (b) pressure angle; (c) curvature: $a_1 = 906mm$, $a_3 = 870mm$, $a_4 = 11mm$, and $N = 40$	40
4.5	Version I of Speed-o-Cam simulation: (a) model and result; (b) detail about component of contact force on x axis at contact 1; (c) detail about component of contact force on y axis at contact 1; (d) detail about component of contact force on x axis at contact 41; (e) detail about component of contact force on y axis at contact 41: $a_1 = 906mm$, $a_3 = 870mm$, $a_4 = 11mm$, and $N = 40$	41
4.6	Plotting of cam kinematics: (a) cam profile; (b) pressure angle; (c) curvature: $a_1 = 906mm$, $a_3 = 870mm$, $a_4 = 11mm$, $N = 40$, $\varepsilon = 0.1$, and $\lambda = \frac{2}{3}$	43
4.7	Version II of Speed-o-Cam simulation: (a) model and result; (b) detail about component of contact force on x axis at contact 1; (c) detail about component of contact force on y axis at contact 1; (d) detail about component of contact force on x axis at contact 41; (e) detail about component of contact force on y axis at contact 41: $a_1 = 906mm$, $a_3 = 870mm$, $a_4 = 11mm$, $N = 40$, $\varepsilon = 0.1$, and $\lambda = \frac{2}{3}$	44
4.8	Comparison between version I and II of the Speed-o-Cam simulation: (a) model and result; (b) detail about component of contact force on x axis at contact 1; (c) detail about component of contact force on y axis at contact 1;	

	(d) detail about component of contact force on x axis at contact 41;	
	(e) detail about component of contact force on y axis at contact 41.....	45
4.9	A toggle position.....	46
4.10	Simulation failure.....	46
4.11	Plotting of cam kinematics: (a) cam profile; (b) pressure angle;	
	(c) curvature: $a_1 = 906mm$, $a_3 = 870mm$, $a_4 = 11mm$,	
	$a_4' = a_4 + 0.25mm$, $N = 40$, $\sigma_A = 0.1$, and $\sigma_F = 0.2$	47
4.12	Version III of Speed-o-Cam simulation: (a) model and result;	
	(b) detail about component of contact force on x axis at contact 1;	
	(c) detail about component of contact force on y axis at contact 1;	
	(d) detail about component of contact force on x axis at contact 41;	
	(e) detail about component of contact force on y axis at contact 41:	
	$a_1 = 906mm$, $a_3 = 870mm$, $a_4 = 11mm$, $a_4' = a_4 + 0.25mm$,	
	$N = 40$, $\sigma_A = 0.1$, and $\sigma_F = 0.2$	48
4.13	Comparison between version II and III of the Speed-o-Cam simulation:	
	(a) model and result;	
	(b) detail about component of contact force on x axis at contact 1;	
	(c) detail about component of contact force on y axis at contact 1;	
	(d) detail about component of contact force on x axis at contact 41;	
	(e) detail about component of contact force on y axis at contact 41.....	49
4.14	Plotting of cam kinematics: (a) cam profile; (b) pressure angle;	
	(c) curvature: $a_1 = 906mm$, $a_3 = 870mm$, $a_4 = 11mm$,	
	$a_4' = a_4 + 0.25mm$, $N = 40$, $\sigma_A = 0.1$, $\sigma_F = 0.5$, $u_{EC} = 0.5$	
	and $u_{BG} = 0.8$	51
4.15	Version IV of Speed-o-Cam simulation: (a) model and result;	
	(b) detail about component of contact force on x axis at contact 1;	
	(c) detail about component of contact force on y axis at contact 1;	
	(d) detail about component of contact force on x axis at contact 41;	
	(f) detail about component of contact force on y axis at contact 41:	

	$a_1 = 906mm$, $a_3 = 870mm$, $a_4 = 11mm$, $a_4' = a_4 + 0.25mm$, $N = 40$, $\sigma_A = 0.1$, $\sigma_F = 0.5$, $u_{EC} = 0.5$ and $u_{BG} = 0.8$52
4.16	Comparison between version III and IV of the Speed-o-Cam simulation: (a) model and result; (b) detail about component of contact force on x axis at contact 1; (c) detail about component of contact force on y axis at contact 1; (d) detail about component of contact force on x axis at contact 41; (e) detail about component of contact force on y axis at contact 41.....53
4.17	Comparison between version I , II, III and IV of the Speed-o-Cam simulation: (a) model and result; (b) detail about component of contact force on x axis at contact 1; (c) detail about component of contact force on y axis at contact 1; (d) detail about component of contact force on x axis at contact 41; (e) detail about component of contact force on y axis at contact 41.....54
4.18	The cam follower disc.....55
4.19	The support for disc shaft.....56
4.20	The support for cam shaft.....56
4.21	The base of cam driven ball mill.....57
4.22	The cam driven ball mill.....57
5.1	The function command.....59
5.2	Simulation results obtained from the final computational FAE.....60
5.3	The Array Parameters and the time interval62
5.4	Simulation results obtained from the final computational FAE.....63
6.1	Cam Assembly.....65
6.2	Cam rollers disk.....65
6.3	Cam shaft and motor modification66
6.4	Prony brake66

LIST OF TABLES

2.1	Average % of Critical Speed.....	11
2.2	Net power estimates for the lab mill design	15
2.3	Estimated comparison of different drive systems	16
4.1	Cam Profile Points with $a_1 = 906mm$, $a_3 = 870mm$, $a_4 = 11mm$, and $N = 40$	40
4.2	Cam Profile Points with $a_1 = 906mm$, $a_3 = 870mm$, $a_4 = 11mm$, $N = 40$, $\varepsilon = 0.1$, and $\lambda = \frac{2}{3}$	43
4.3	Cam Profile Points with $a_1 = 906mm$, $a_3 = 870mm$, $a_4 = 11mm$, $a'_4 = a_4 + 0.25mm$, $N = 40$, $\sigma_A = 0.1$, and $\sigma_F = 0.2$	47
4.4	Cam Profile Points with $a_1 = 906mm$, $a_3 = 870mm$, $a_4 = 11mm$, $a'_4 = a_4 + 0.25mm$, $N = 40$, $\sigma_A = 0.1$, $\sigma_F = 0.5$, $u_{EC} = 0.5$ and $u_{BG} = 0.8$	50
4.5	Accepted tolerance limits for cam & disc manufacture.....	55
5.1	Force on the cam.....	62

SYMBOLS AND ABBREVIATIONS

N_c : critical speed in rpm;

D : mill diameter inside liners specified in meters.

N_p : peripheral speed in rpm;

D : mill diameter inside liners ;

N_m : mill speed in rpm.

m_e : the mass of the charge [kg],

$m_{slurry\ e}$: the mass of the slurry elements [kg],

r_i : the element radial position [m],

ϕ_i : the element angular position [rad],

ω_o : the mill rotation speed [rad/s].

a_1 : distance between input and output axes;

a_3 : distance between input and roller axes;

a_4 : radius of the roller;

ψ : angle of rotation of cam;

$\tilde{\phi}$: angular displacement of the follower;

$\tilde{\phi}'$: derivative of the angular displacement of the follower with respect to ψ ,
also known as the *velocity ratio*;

N : number of indexing steps, its reciprocal being the *velocity ratio*.

γ : the transmission angle, which is that between vector $\overrightarrow{O_1O_2}$ and the normal
vector \overrightarrow{CP} .

S_c : the maximum compressive stress;

K : constant, which depend on the materials and the treatments of the cam and the
roller

F_n : the normal load;

b : the cam width;

κ_c : the curvature of the cam at the contact point;

κ_r : the curvature of the roller at the contact point.

CHAPTER 1

INTRODUCTION

In mineral processing industries, grinding processes can be defined as the particles reduced in size by a combination of impact and abrasion. It is performed in tumbling mills that describe a class of mills delimited by a cylindrical chamber filled with balls and/or rock that rotate around its longitudinal axis.

1.1. Types of Mill

Tumbling mills, whether they are autogenous, semi-autogenous, ball or rod, are classed according the nature of the discharge as centre peripheral discharge mills, end peripheral discharge mills, overflow mills, and grate discharge mills (as shown in Figure 1.1 to 1.12). These mills are used in at least three industries: mining, cement and metal powders industries to grind different materials (ore, clinker and metal powder) to desired quality specifications as principally described by a size distribution. These tumbling mills range in size from small 1 ft diameter lab mills to a 40 ft diameter semi-autogenous industrial mill.

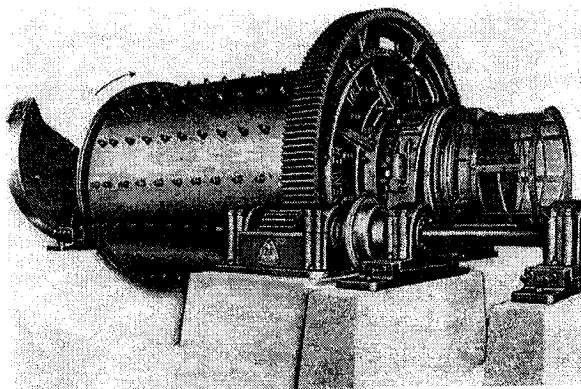


Figure 1.1: Tumbling mill (Mular and Jergensen, 1982)

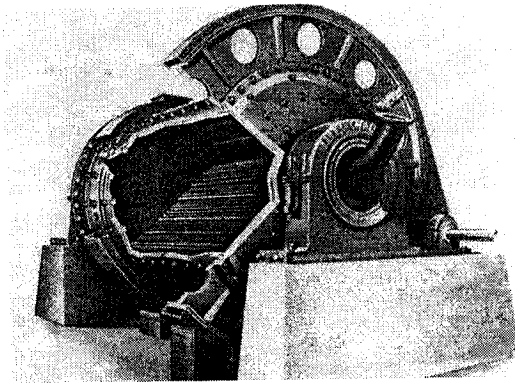


Figure 1.2: Rod mill (Mular and Jergensen, 1982)

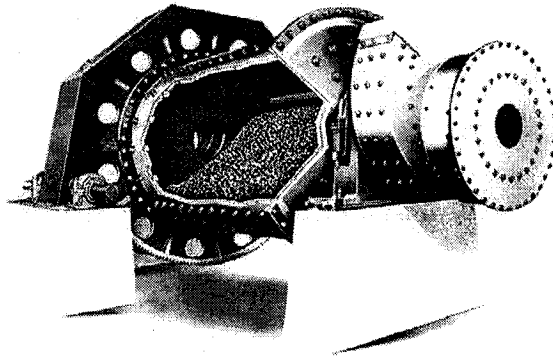


Figure 1.3: Overflow Ball Mill (Mular and Jergensen, 1982)

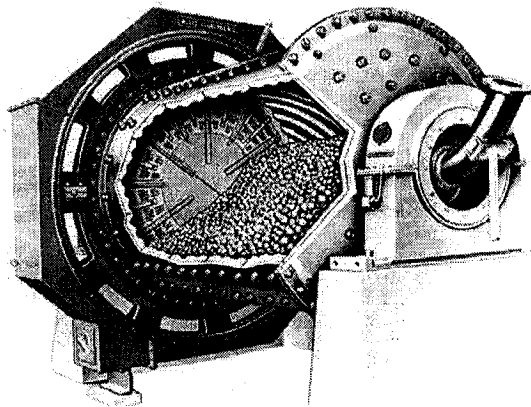


Figure 1.4: Diaphragm (Grate) Discharge Ball Mill
(Mular and Jergensen, 1982)

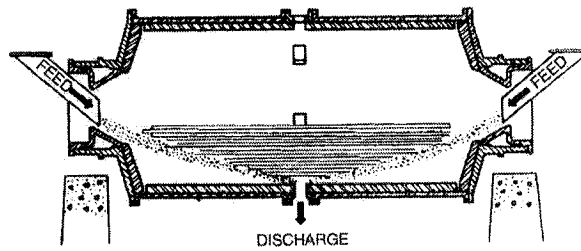


Figure 1.5: Central peripheral discharge mill (Wills, 1997)

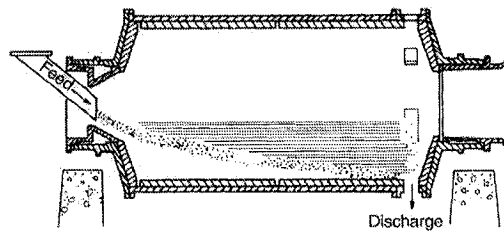


Figure 1.6: End peripheral discharge mill (Wills, 1997)

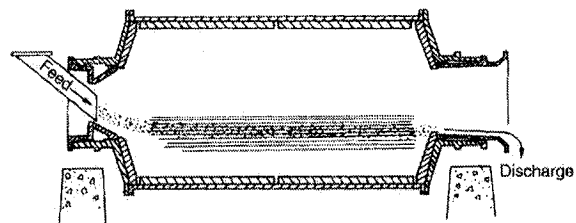


Figure 1.7: Overflow mill (Wills, 1997)

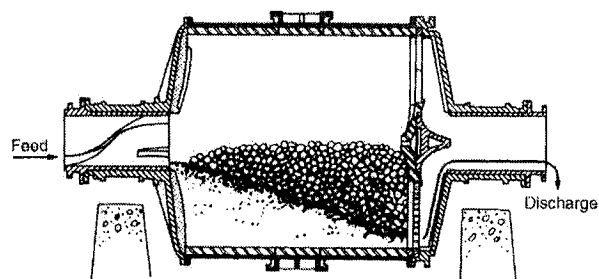


Figure 1.8: Grate discharge mill (Wills, 1997)

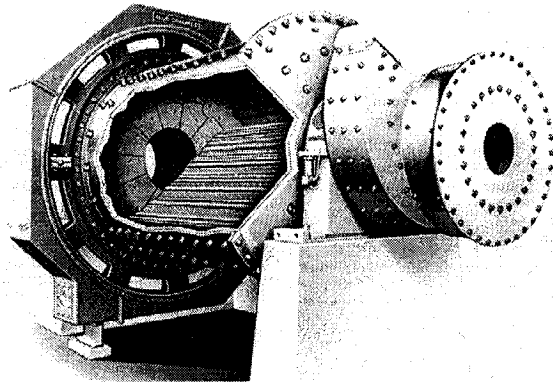


Figure 1.9: Overflow Rod Mill (Mular and Jergensen, 1982)

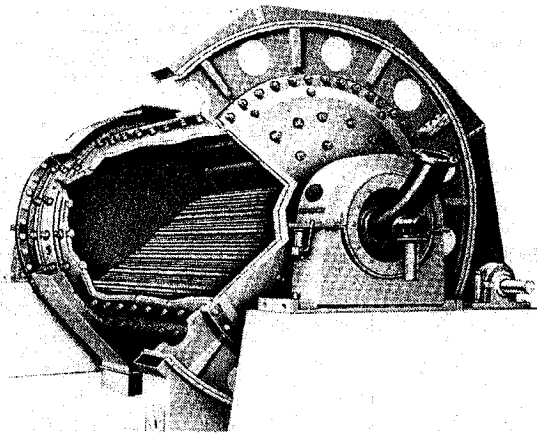


Figure 1.10: End peripheral Discharge Rod Mill
(Mular and Jergensen, 1982)

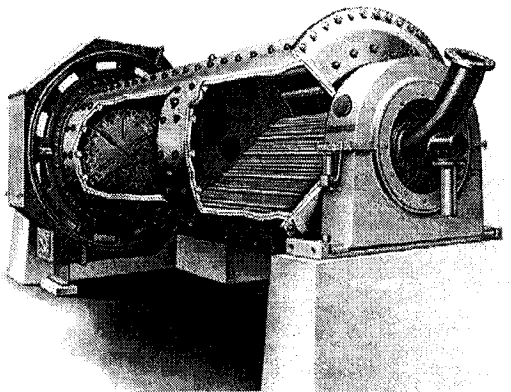


Figure 1.11: Rod/Ball Compartmented Mill
(Mular and Jergensen, 1982)

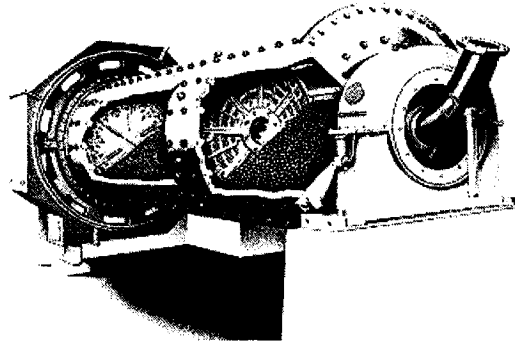


Figure 1.12: Ball Compartmented Mill
(Mular and Jergensen, 1982)

In the tumbling mill, due to the rotation and friction of the mill shell and liner, the grinding medium is lifted along the rising side of the mill until a position of dynamic equilibrium is reached, when the bodies cascade and cataract down the free surface of the other bodies, about a dead zone where little movement occurs, down to the toe of the mill charge (Figure 1.13.).

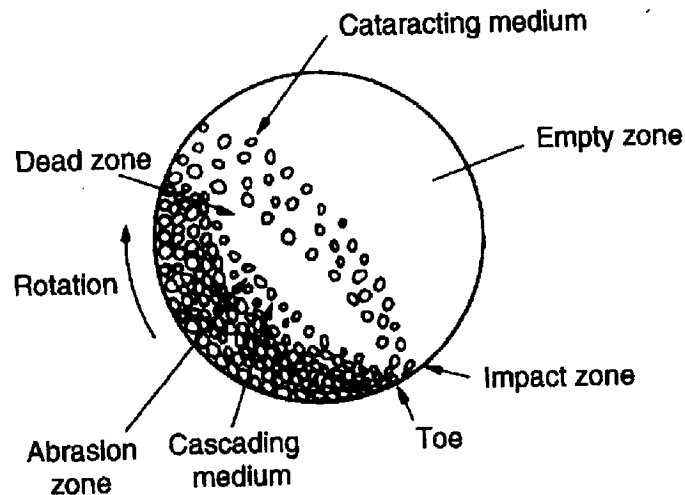


Figure 1.13: Motion of charge in a tumbling mill (Wills, 1997)

The speed at which a mill is run is important, since it governs the nature of the product and the amount of wear on the shell liners. On the other hand, the selection of driving system is constrained by available budget and mill size.

1.2. Review of the current drive systems

Tumbling mills can be driven by either chain and sprocket (lab mills), gear and pinion (pilot and industrial scale mills) or gearless drives in very large diameter mill (30 to 40 ft dia.).

1.2.1. Chain & Sprocket Drives

The lab tumbling mills are generally rotated by chain and sprocket. The design provides for some advantages that are unrestricted shaft distances, no creep or slip, a rolling action while roller chains engage the sprockets, a large reduction in speed if desired, and more practical for low speeds. The tolerances for a chain drive are greater than for gears, and the installation is relatively easy. Chains present no fire hazard and are unaffected by the relatively high temperatures and the presence of oil or grease. Unfortunately, the chain drives require lubrication and provide no overload protection because they cannot slip.

1.2.2. Geared Drives

There are also non-cylindrical gears used for transmitting motion and power from one rotating shaft to another by means of the contact of successive engaging teeth. Compared with the chain drives, gear drives are more compact, operate at high speeds, and provide precise timing of motion and positive engagement. However, gear drives require better lubrication and more cleanliness and are more affected by shaft misalignment. The design of gears must consider the type, material, quality, heat treatment, loading, efficiency, life,

surface durability and strength rating, temperature of operation, speed, alignment, adjustment, and lubrication and so on.

Tumbling mills are most commonly rotated by a pinion meshing with a girth ring bolted to one end of the machine (as shown in Figure 1.14). The pinion shaft is driven from the prime mover through vee-belts, for a small mill of less than about 180kw. For larger mills the shaft is coupled directly to the output shaft of a slow-speed synchronous motor, or to the output shaft of a motor-driven helical or double helical gear reducer. Very large mills driven by girth gears require two to four pinions, and complex load sharing systems must be incorporated. However, the gear driving system is not the best solution in terms of maintenance requirement, operation cost and availability.

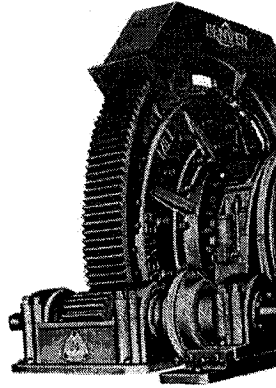


Figure 1.14: Gear/pinion on ball mill
(Mular and Jergensen, 1982)

1.2.3. Gearless Drives

The gearless drive system (Figure 1.15) is developed because of the limitations in the strength of ring gears on very large mills. The larger the mill, the greater are the stresses between the shells and heads and the trunnions and heads. Typically, a large mill uses a gearless ring or “wraparound” motor. The rotor of a driving motor is built into the shell, and the stator is mounted to surround it. The stator has a closed circuit cooling system for the windings, and the mill speed is infinitely variable by frequency control, allowing automatic adjustments to the mill throughput as ore grindability changes. Significant

reductions in energy consumption and operating costs can be achieved with the use of a gearless drive. Unfortunately, it is also significantly more expensive and technically sophisticated than a gear driving system.

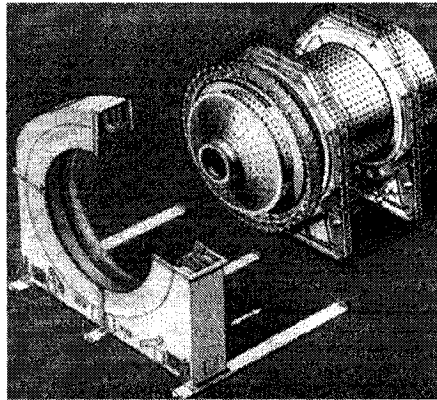


Figure 1.15: Ball mill with gearless ring motor
(Mular and Jergensen, 1982)

1.3. Objective of this work

As stated previously, all of these mill drives present advantages and limitations. In this work, an alternative drive system is designed and developed that uses a newly patented speed-o-cam technology (Angeles, et al, 2002) and applies it to a 5 ft diameter lab mill. The Figure 1.16 shows a typical prototype of a planar Speed-o-Cam.

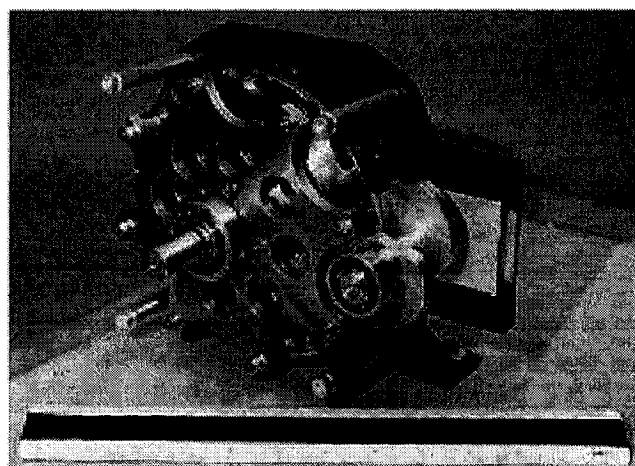


Figure 1.16: Prototype of planar Speed-o-Cam (Zhang, 2003)

The objective of this research project is to design and develop a cam drive for a laboratory ball mill set-up allowing testing for a 36'', 48'' & 60'' diameter 1' deep glass faced tumbling mill to be used for charge motion validation studies.

The major design constraints for the alternative cam-driven ball mill include:

- Compact size imposed by laboratory, that is, the final apparatus should be no taller in height than about 2m, no wider in width than about 1m as a result of satisfying the size of laboratory door, and no longer in length than about 2m in order to meet the need for laboratory space,
- Allow use of most current equipment, which is 5 Hp motor & controller,
- Low building & operation cost.

In the process of design and development the cam-driven ball mill, virtual prototype technology and computational finite element analyses (FEA) are used to optimize the apparatus before committing to expensive hardware prototypes.

CHAPTER 2

Design Parameters of Ball Mill

Over the years, a number of attempts have been made to validate different charge motion models using lab mill set-ups (Agrawala, 1997, Govender, 2001, and Hlungwani, 2003). All have studied the motion of small (< 1m diameter) glass faced mills. As stated, the objective of this project is to design a lab mill set-up that will allow the study of charge motion in mills greater than 1m diameter. In this case, it becomes important to specify the operating speed range of the mill and estimate the power consumption of the lab mill before selecting the mill drive.

2.1. Derivation for Speed

The speed at which a ball mill is run is a pivotal parameter when the ball mill is designed, since it dominates the nature of the product and the amount of wear on the shell liners. Critical speed, which is the speed at which the centrifugal force is sufficiently large to cause a small particle to adhere to the shell liners for the full revolution of the mill.

Critical speed is determined from the following equation:

$$N_c = 42.305 D^{-0.5} \quad (2.1a)$$

The notation used is described below:

N_c : critical speed in rpm;

D : mill diameter inside liners specified in meters.

or,

$$N_c = 76.63D^{-0.5} \quad (2.1b)$$

where the notation D is mill diameter inside liners specified in feet.

Peripheral speed, which doesn't influence mill power but is a factor in liner wear, has to be considered in mill design. It can be determined by the following either as meters per minute or as feet per minute (Wills, 1997).

$$N_p = \pi DN_m \quad (2.2)$$

where

N_p : peripheral speed in rpm;

D : mill diameter inside liners ;

N_m : mill speed in rpm.

As shown in table 2.1, the average recommended speed as percent of critical speed decreases when mill diameters increase.

Table 2.1 Average % of Critical Speed

Mill Diameter Inside Liners		% of Critical Speed	Mill Speed (rpm)
Meters	Feet	Ball Mills	
0.91~1.83	3~6	80~78	36~24
1.83~2.74	6~9	78~75	24~19
2.74~3.66	9~12	75~72	19~16

In the Comminution Dynamics Lab, the testing speed as percent of critical speed is from 60 to 90. D is 5 feet. These variables are put into the equation (2.1b) and are calculated

by this equation. According to the Table 2.1, We got the ball mill peripheral speed in rpm , i.e., N_p , from 26 to 42 rpm.

2.2. Power Prediction

Mill power consumption can be estimated using different models (Agrawala, 1997, Govender, 2001, and Hlungwani, 2003). Here, mill power will be estimated using a validated charge motion model, which has been described by Radziszewski and Morrell (1998). Quoting them, the mill charge is first discretized using a constant radial division. Only the elements that are found below the horizontal line defining the charge surface at rest are fitted with a cross that describes the center of mass of each discrete element in the charge.

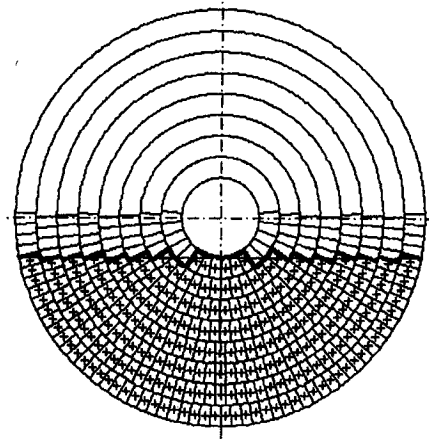


Figure 2.1: Discrete ball charge at rest

At this point, charge motion can be simulated by applying the relationships of motion (Radziszewski, Morrell, 1998) to the discrete element centres of mass. In this case, it is assumed that the principal of the conservation of momentum is applied, which states that the mean trajectory of the centre of mass of a system of particles before and after collision will not change. Thus single particle motion as described by the above

relationships can be applied to describe the mean trajectory of the system of particles which can be found in such a discrete element description of the ball charge.

In the rotate charge block, new charge element positions are determined by equations. Also, mill net power P_{net} is determined for each time step and is determined separately for the charge P_{charge} and the slurry pool $P_{slurry\ pool}$ if overflow discharge is present:

$$P_{net} = P_{charge} + P_{slurry\ pool} \quad (2.3)$$

Charge power is determined using the following relationship:

$$P_{charge} = \sum_{i=1}^n m_e g r_i \cos(\phi_i) \omega_o \quad (2.4)$$

The slurry pool contribution is determined for slurry elements outside of the charge with:

$$P_{slurry\ pool} = \sum_{i=1}^{n\ slurry} m_{slurry\ e} g r_i \cos(\phi_i) \omega_o \quad (2.5)$$

where

m_e : the mass of the charge [kg],

$m_{slurry\ e}$: the mass of the slurry elements [kg],

r_i : the element radial position [m],

ϕ_i : the element angular position [rad],

. ω_o : the mill rotation speed [rad/s].

Figures 2.2 and 2.3 show typical charge profiles for grate and overflow discharge mills.

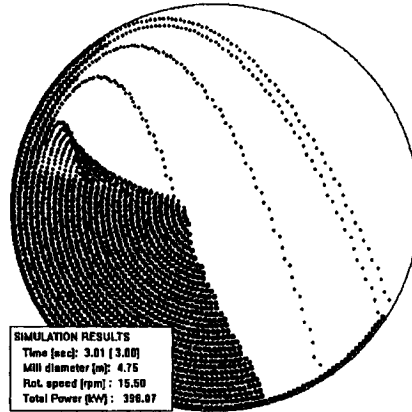


Figure 2.2: Charge profile simulation (4.75 m dia., 45% filling, 12.5 cm top size ball, 80% crit. Speed, 1 m length)

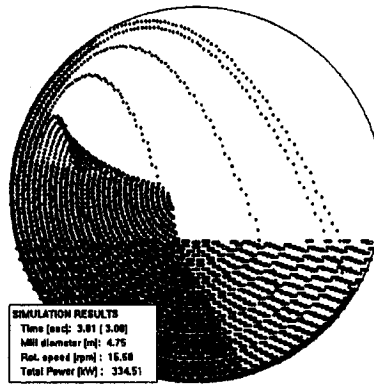


Figure 2.3: Slurry pool overlapping with ball charge (4.75 m dia., 45% filling, 12.5 cm top size ball, 80% crit. Speed, 1 m length)

The discrete ball charge model was used to simulate the power draw of each of the mills in the JKMRC data bank. Comparing the observed data with the simulated, a power draw calibration equation was determined:

$$P_{predicted} = P_{no\ load} + P_{simulated} * F_{power} \quad (2.6)$$

where

F_{power} : a constant which is 1.29,

$P_{no\ load}$: no load as described by Morrell[1996].

The resulting comparison with observed data for all 41 mills simulated from the JKMRC data bank can be found in figure 2.4 (Radziszewski, Morrell, 1998).

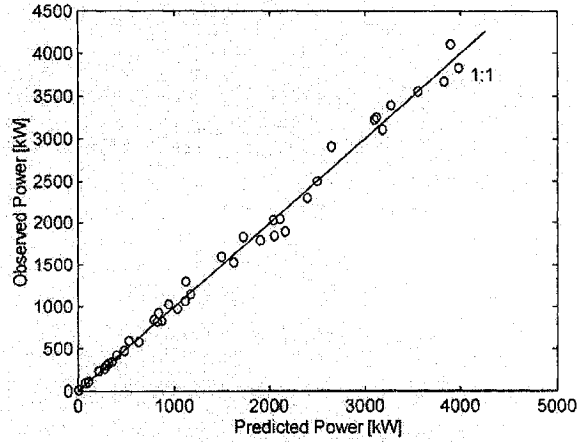


Figure 2.4: Combined data set: Observed vs predicted power

In the case of the lab mill, it will be run dry so the slurry power is not calculated.

The initial charge state is that 40% of mill volume is filled with ceramic media of an average density 2500kg/m³. The resulting net power estimates for these conditions can be found in Table 2.2.

Table 2.2: Net power estimates for the lab mill design

diameter	1m	1.5m
75% crit. (rpm)	32	36
Power (kW)	1.191352	1.424432
Power (HP)	1.620239	1.937228
85% crit. (rpm)	26	29
Power (kW)	3.061717	3.800061
Power (HP)	4.163935	5.168083

Based on the estimates found in Table 2.2, it is possible to run the mill with the 5HP electric motor provided that the mill charge volume maximum will be slightly less than the target volume or if the charge media can be changed for something lighter. In both the cases, this is acceptable.

2.3. Drive Selection

The speed-o-cam drive system is an innovative design concept with rolling friction, high stiffness and high machinability, and an alternative to gears in precision demanding mechanical systems. The table 2.1 is comparison of different drive systems.

Table 2.3: Estimated comparison of different drive systems

Drive systems	Cost	Manufacture	Efficiency	Precision	Maintainability
Gearless	↑↑↑	↓↓↓	↑↑	↑↑↑	↑↑↑
Gear	↑↑	↓↓	↑	↑↑	↓↓
Chain/sprocket	↓	↑↑↑	↓↓↓	↑	↓↓
Speed-o-Cam	↑	↑	↑	↑↑↑	↑↑↑

Based on this table, it is clear that the chain & sprocket is the lowest cost system and for the case of the lab mill; it would be very adequate. The geared and gearless drive would be quite cost prohibitive. While more expensive than the chain and sprocket, the cam drive system pose the added challenge of a new drive system as well as providing a more efficient alternative drive. So despite the added cost and risk, it is decided to design and fabricate a cam drive system for the lab mill, which raises a number of issues such as:

- Cam Profile Determination
- Pressure Angle Determination
- Cam Curvature
- Undercutting of the Cam Profile

CHAPTER 3

The Synthesis of Planar Speed-o-Cam

Generally speaking, the speed-o-cam mechanism, a planar four-link mechanism, comprises a cam that rotates about an axis, and a follower supplied with a roller, rotating about the follower centre at a fixed distance from the follower centre. The speed-o-cam theory is available in (Gonzalez-Palacios and Angeles, 1993) and the original design and undercutting methods can be found in (Lee,2001 and Zhang, 2003). The Figure 3.1. shows the typical palanar external speed-o-cam embodiments.

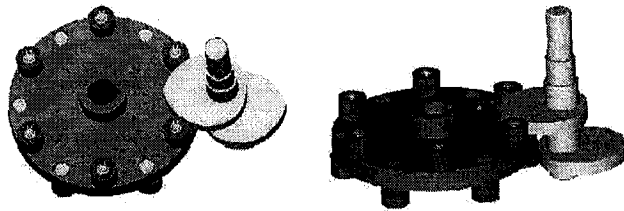


Figure 3.1: Two distinct views of external Speed-o-Cam

3.1. Geometry of the Cam-Profile

As shown in Figure 3.2, the $x-y$ frame is fixed and the $u-v$ frame is attached to the cam. The origin of the frames is defined by O , while O_1 is the centre of the follower, O_2 is the centre of the roller, P is the pitch point, and C is the contact point, respectively.

$$\delta = \arctan \left(\frac{a_3 \sin \tilde{\phi}}{a_3 \cos \tilde{\phi} + a_1 - b_2} \right) \quad (3.5)$$

The coordinates of C in the $x - y$ frame can be readily obtained:

$$x(\psi) = b_2 + (b_3 - a_4) \cos(\delta) \quad (3.6)$$

$$y(\psi) = (b_3 - a_4) \sin(\delta) \quad (3.7)$$

For the external planar speed-o-cam, the input-output relationship takes the form

$$\tilde{\phi} = - \left[\pi \left(1 - \frac{1}{N} \right) + \frac{\psi}{N} \right] \quad (3.8)$$

The notation used is described below:

a_1 : distance between input and output axes;

a_3 : distance between input and roller axes;

a_4 : radius of the roller;

ψ : angle of rotation of cam;

$\tilde{\phi}$: angular displacement of the follower;

$\tilde{\phi}'$: derivative of the angular displacement of the follower with respect to ψ , also known as the *velocity ratio*;

N : number of indexing steps, its reciprocal being the *velocity ratio*.

An extended angle Δ is introduced so that the cam profile can be closed with

$-\Delta \leq \psi \leq 2\pi + \Delta$. Angle Δ is obtained as a root of the equation:

$$v(-\Delta) = 0 \quad (3.9)$$

3.2. Pressure Angle Determination

The pressure angle is a matter of concern in cam design. The pressure angle, designated as α , is defined as the angle between the velocity of the contact point of the follower and the normal to the cam profile at the same point see Fig. 3.2 (Angeles, 1991).

In general, as a result of the rotation of the cam, when the point of contact changes, so does the pressure angle. Therefore, the pressure angle is a function of the cam angular displacement ψ , i.e., $\alpha = \alpha(\psi)$. The pressure angle directly influences the force transmission properties of the mechanism and determines how good the effectiveness of the force transmission is. In fact, force transmission is better for small pressure angles. The smaller the absolute value, the better the force transmission. That is because the higher the pressure angle, the smaller the component of the force transmitted to and used to drive the follower and a high pressure angle means a heavy load transmitted to the bearings, which impacts on their life. One way of keeping this value small is to increase the base circle.

Form the geometry in Figure 3.2, we obtain the equation:

$$\alpha = \pi/2 - \gamma = \tilde{\phi} - \delta - \pi/2 \quad (3.10)$$

γ : the transmission angle, which is that between vector $\overrightarrow{O_1O_2}$ and the normal vector \overrightarrow{CP} .

The pressure angle has a second form, as derived by means of statics. The contact force between cam and roller is denoted by F . The torque exerted on the follower is

$$T_f = Fa_3 \cos \alpha \quad (3.11)$$

The distance from the centre O to the normal \overrightarrow{CP} is $b_2 \sin \delta$ in Figure 3.2, and, hence, the torque exerted on the cam is

$$T_c = Fb_2 \sin \delta \quad (3.12)$$

Static equilibrium leads to the relationship between T_f and T_c , namely,

$$T_c = T_f \tilde{\phi}' \quad (3.13)$$

Substituting eqs. (3.11) and (3.12) into eq.(3.13), we obtain the second form of the pressure angle as

$$\cos \alpha = \left(\frac{a_1 - b_2}{a_3} \right) \sin \delta$$

i.e.

$$\alpha = \arccos \left[\left(\frac{a_1 - b_2}{a_3} \right) \sin \delta \right] \quad (3.14)$$

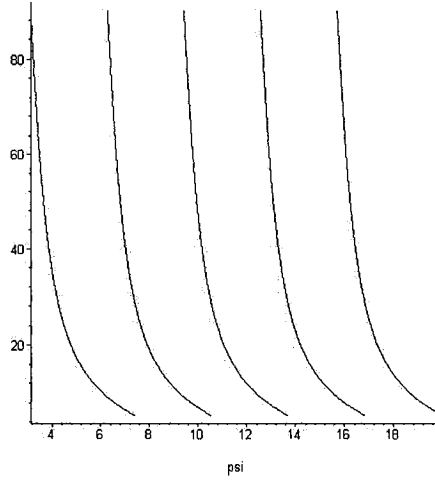


Figure 3.3: The pressure angle distribution

Figure 3.3 shows a typical plot of the pressure angle distribution. Two conjugate cams are used to ensure that there is a correct transmission at any time, i.e., the pressure angle is always as small as possible when transmission occurs.

3.3. Cam Curvature

The cam curvature plays an important role in the design of cam mechanisms, for it is directly related to the appearance of cusps and *undercutting*. This variable determines the shape of a planar curve which depends on the rate of change of the direction of its tangent with respect to the arc length, a measure which is called the *curvature* of planar curve and is designated as κ . The reciprocal of the radius of curvature, r , is the curvature, κ , i.e. (Angeles, 1991),

$$\kappa = \frac{1}{r}$$

The radius of a circle tangent at a point of the cam profile is the radius of curvature at that point to the cam profile. The curvature of the cam profile is the same as the curvature of the circle. The radius of curvature is positive if the center K of the circle is located between the center of rotation and the point of tangency; otherwise, the radius of curvature is negative.

The curvature of a contour in terms of a parameter ψ takes the form (Gonzalez-Palacios and Angeles, 1993)

$$\kappa = \frac{\nu'(\psi)\mu''(\psi) - \mu'(\psi)\nu''(\psi)}{((\nu'(\psi))^2 + (\mu'(\psi))^2)^{\frac{3}{2}}} \quad (3.15)$$

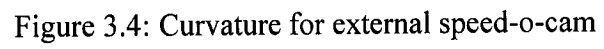
In order to avoid undercutting for an external speed-o-cam, a_3/a_1 has to satisfy (Lee, 2001)

$$\frac{a_3}{a_1} \leq \frac{1}{1 + 1/N}$$

The condition for a fully convex cam profile of an external speed-o-cam is

$$\frac{a_3}{a_1} \leq \frac{1}{(1 + 1/N)^2}$$

Figure 3.4. is a curvature distribution for external speed-o-cam, from which we find that the curvature attains one minimum and two maxima throughout the cam profile.



The diagram illustrates a circular cross-section of a body with a central hole. The outer boundary is a circle with center O . The inner boundary is a smaller circle with center O_1 . A horizontal line passes through both centers. Points $A, B, C, D, E, F, G, H, I$ are marked on the boundaries. Vectors ρ and u are shown originating from O . Vectors u_{BG} and u_{EC} are shown at points B and C respectively. Vectors u_0, u_A, u_E, u_C are shown as horizontal arrows. A vector v_A is shown at point A . Stress components $\sigma_A, \sigma_H, \sigma_F, \sigma_I$ are indicated at various points.

Figure 3.5: Cam profile

Undercutting is a function of merit in roller-follower cam mechanisms (Angeles, 1991). Whether the cam profile is convex or concave, undercutting may appear when the minimum absolute value of the radius of curvature of the pitch curve is less than or equal to the follower radius, a_4 . In the former case, the desired follower motion cannot be produced. In the latter case, cusp, as shown in Figure 3.5, the point C , is produced on the cam profile, can cause a high compressive stress at the instant of roller-contact at the cusp, and lead to poor dynamic performance.

The maximum compressive stress S_c is given by (Oberg, Jones, and Horton, 1988)

$$S_c = K \sqrt{\frac{F_n}{b} (\kappa_c + \kappa_r)} \quad (3.16)$$

The notation used is described below:

S_c : the maximum compressive stress;

K : constant, which depends on the materials and the treatments of the cam and the roller

F_n : the normal load;

b : the cam width;

κ_c : the curvatures of the cam at the contact point;

κ_r : the curvatures of the roller at the contact point.

From equation (3.16), an infinite value of the maximum compressive stress will be yielded if the value of κ_c or κ_r is infinite. Due to the curvature discontinuity at point C , stress concentration likely occurs. It is desired to smooth the cam profile around the cusp.

Meanwhile, the blunt point B , as shown in Fig. 3.6, corresponds to a toggle position. When point B is at a toggle position, in which the pressure angle is 90° (Norton, 2001), and touches the roller, the compressive stress will be high and the life expectancy of the mechanism will decrease. Consequently, blunt regions on a cam lead poor kinematic

performance. So, the curve around the blunt regions should be modified in order to avoid contact between cam and roller.

These situations end in wear and the eventual shortening of the life span of the mechanism. Undercutting is taken into account for cam mechanism optimization by properly introducing the Cubic spline, 2-4-6 Polynomial and 2-4-6-8 Polynomial (Zhang, 2003) for the cam profile which is symmetric with respect to the u axis.

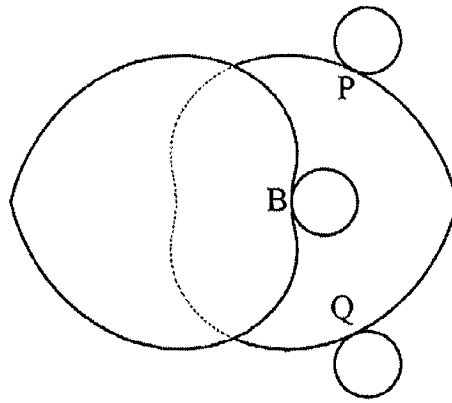


Figure 3.6 : Toggle position

In fact, when the cam profile is unsymmetrical, as in our case, with respect to the u axis, the fifth or sixth order polynomial offers a more flexible approach to curve synthesis. The advantage lies in that this polynomial leads themselves to optimization, constraints can be imposed, and the objective parameter can be chosen in an flexible way, as discussed in detail in next section and chapter 4.

3.5. Polynomial

The polynomial function is the most versatile and useful for cam design. In principle, the lower and upper dwells with a polynomial of degree n can be joined if there are $n + 1$

conditions on displacement, velocity, and acceleration to be met. That is, the normal motion $S(\tau)$, can be expressed as:

$$S(\tau) = a_0 + a_1\tau + a_2\tau^2 + a_3\tau^3 + \cdots + a_n\tau^n \quad (3.17)$$

The polar coordinates are introduced to use the polynomial function. As shown in Figure 3.5 the normal of the cam profile at point A and the u axis intersect at the point O_1 , which is denoted as the origin of the polar coordinate system. Point H is normal of the cam profile at point H , and the normal is by point O_1 . We denote the u coordinate of O_1 with u_{O_1} , which can be derived as

$$u_{O_1} = u(\psi_A) + tv(\psi_A) \quad (3.18)$$

where

$$t = \frac{dv(\psi)/d\psi}{du(\psi)/d\psi} \Big|_{\psi=\psi_A} \quad (3.19)$$

So, we can describe the cam profile in the polar coordinates as

$$\rho(\psi) = \sqrt{(u(\psi) - u_1)^2 + v(\psi)^2} \quad (3.20)$$

$$\sigma(\psi) = \arctan\left(\frac{v(\psi)}{u(\psi) - u_{O_1}}\right) \quad (3.21)$$

Now, we introduce the notation

$$\rho' = \frac{d\rho(\psi)}{d\psi} \quad \rho'' = \frac{d^2\rho(\psi)}{d\psi^2} \quad \rho''' = \frac{d^3\rho(\psi)}{d\psi^3} \quad (3.22)$$

$$\sigma' = \frac{d\sigma(\psi)}{d\psi} \quad \sigma'' = \frac{d^2\sigma(\psi)}{d\psi^2} \quad \sigma''' = \frac{d^3\sigma(\psi)}{d\psi^3} \quad (3.22)$$

$$\dot{\rho} \equiv \frac{d\rho}{d\sigma} = \frac{d\rho/d\psi}{d\sigma/d\psi} = \frac{\rho'}{\sigma'} \quad (3.23)$$

$$\ddot{\rho} \equiv \frac{d\dot{\rho}}{d\sigma} = \frac{d\dot{\rho}/d\psi}{d\sigma/d\psi} = \frac{\rho''\sigma' - \rho'\sigma''}{\sigma'^3} \quad (3.24)$$

$$\ddot{\rho} \equiv \frac{d\ddot{\rho}}{d\sigma} = \frac{d\ddot{\rho}/d\psi}{d\sigma/d\psi} = \frac{\rho'''\sigma'^2 - \rho'\sigma'\sigma''' - 3\rho''\sigma'\sigma'' + 3\rho'\sigma''^2}{\sigma'^5} \quad (3.25)$$

The coordinate ρ_E of E can be expressed as

$$\rho_E = u_c - u_{EC} - u_{O_1} \quad (3.26)$$

When the cam profile is unsymmetrical, i.e., the curve \hat{FA} and \hat{IH} are different, we can obtain the coordinates (ρ_A, σ_A) of point A and (ρ_H, σ_H) of point H in polar coordinate, respectively, as

$$\rho_A = \rho(\psi_A) = \sqrt{(u_1(\psi_A) - u_{O_1})^2 + v_1(\psi_A)^2} \quad (3.27a)$$

$$\sigma_A = \sigma(\psi_A) = \arctan\left(\frac{v_1(\psi_A)}{u_1(\psi_A) - u_{O_1}}\right) \quad (3.27b)$$

$$\rho_H = \rho(\psi_H) = \sqrt{(u_2(\psi_H) - u_{O_1})^2 + v_2(\psi_H)^2} \quad (3.28a)$$

$$\sigma_H = \sigma(\psi_H) = \arctan\left(\frac{v_2(\psi_H)}{u_2(\psi_H) - u_{O_1}}\right) \quad (3.28b)$$

The expression for angle γ that the tangent of a curve at a point makes with the radius vector at that point (Jeffrey, 1969) in polar coordinate, i.e.,

$$\tan \gamma = \frac{\rho}{\dot{\rho}} \quad (3.29)$$

The angles γ_A at the point A and γ_H at the point H are 90° . So,

$$\rho(\psi_A) = 0 \quad (3.30a)$$

$$\rho(\psi_H) = 0 \quad (3.30b)$$

Hence

$$\dot{\rho}'(\psi_A) = 0 \quad (3.31a)$$

$$\dot{\rho}'(\psi_H) = 0 \quad (3.31b)$$

We simplify the equations by substituted the equation (3.30a), (3.30b), (3.31a) and (3.31b) into equations (3.23), (3.24) and (3.25).

We get

$$\dot{\rho}_A = 0 \quad (3.32a)$$

$$\dot{\rho}_H = 0 \quad (3.32b)$$

$$\ddot{\rho}_A = \frac{\rho''(\psi_A)}{(\sigma'(\psi_A))^2} \quad (3.33a)$$

$$\ddot{\rho}_H = \frac{\rho''(\psi_H)}{(\sigma'(\psi_H))^2} \quad (3.33b)$$

$$\ddot{\rho}_A = \frac{\rho'''(\psi_A)\sigma'(\psi_A) - 3\rho''(\psi_A)\sigma''(\psi_A)}{(\sigma'(\psi_A))^4} \quad (3.34a)$$

$$\ddot{\rho}_H = \frac{\rho'''(\psi_H)\sigma'(\psi_H) - 3\rho''(\psi_H)\sigma''(\psi_H)}{(\sigma'(\psi_H))^4} \quad (3.34a)$$

3.5.1. The Fifth Order Polynomial

When the cam profile is unsymmetrical with respect to the u axis, the fifth or sixth order polynomial offers a more flexible approach to curve synthesis.

If we denote that the curve is of G2 continuity at the blending points, A and H , we should define the fifth order polynomial function $S(\tau)$ as

$$S(\tau) = a_0 + a_1\tau + a_2\tau^2 + a_3\tau^3 + a_4\tau^4 + a_5\tau^5 \quad (3.35)$$

where τ is a dimensionless variable, i.e.,

$$\tau = \frac{\sigma}{\sigma_A - \sigma_H} \quad (3.36)$$

and

$$0 \leq S(\tau) \leq 1 \quad \frac{\sigma_H}{\sigma_A - \sigma_H} \leq \sigma \leq \frac{\sigma_A}{\sigma_A - \sigma_H} \quad (3.37)$$

The derivatives of $S(\tau)$ are derived from equation (3.35), i.e.,

$$S'(\tau) = a_1 + 2a_2\tau + 3a_3\tau^2 + 4a_4\tau^3 + 5a_5\tau^4 \quad (3.38)$$

and

$$S''(\tau) = 2a_2 + 6a_3\tau + 12a_4\tau^2 + 20a_5\tau^3 \quad (3.39)$$

Also, we can express the curve as:

$$S(\tau) = \frac{\rho - \rho_H}{\rho_A - \rho_H} \quad (3.40a)$$

i.e.

$$\rho = \rho_H + (\rho_A - \rho_H)S(\tau) \quad (3.40b)$$

Hence,

$$\dot{\rho} = \frac{d\rho}{d\sigma} = \frac{d\rho}{d\tau} \frac{d\tau}{d\sigma} = \frac{1}{\sigma_A - \sigma_H} (\rho_A - \rho_H) S'(\tau) \quad (3.41)$$

and

$$\ddot{\rho} = \frac{d\dot{\rho}}{d\sigma} = \frac{d\dot{\rho}}{d\tau} \frac{d\tau}{d\sigma} = \frac{1}{(\sigma_A - \sigma_H)^2} (\rho_A - \rho_H) S''(\tau) \quad (3.42)$$

According to the equations (3.41) and (3.42), we get

$$S'(\tau) = \frac{\sigma_A - \sigma_H}{\rho_A - \rho_H} \dot{\rho} \quad (3.44)$$

$$S''(\tau) = \frac{(\sigma_A - \sigma_H)^2}{\rho_A - \rho_H} \ddot{\rho} \quad (3.45)$$

We recall that the curve sought is a planar, G2 continuity at the blending points, A and H , i.e.,

$$S(\tau_A) = \frac{\rho_A - \rho_H}{\rho_A - \rho_H} = 1 \quad (3.46a)$$

$$S(\tau_H) = \frac{\rho_H - \rho_H}{\rho_A - \rho_H} = 0 \quad (3.46b)$$

$$S'(\tau_A) = \frac{\sigma_A - \sigma_H}{\rho_A - \rho_H} \dot{\rho}_A \quad (3.46C)$$

$$S'(\tau_H) = \frac{\sigma_A - \sigma_H}{\rho_A - \rho_H} \dot{\rho}_H \quad (3.46D)$$

Upon substitution of equations (3.32a) and (3.32b) into equations (3.46C) and (3.46D), respectively, we obtain

$$S'(\tau_A) = 0 \quad (3.46d)$$

$$S'(\tau_H) = 0 \quad (3.46d)$$

$$S''(\tau_A) = \frac{(\sigma_A - \sigma_H)^2}{\rho_A - \rho_H} \ddot{\rho}_A \quad (3.46E)$$

$$S''(\tau_H) = \frac{(\sigma_A - \sigma_H)^2}{\rho_A - \rho_H} \ddot{\rho}_H \quad (3.46F)$$

Upon substitution of equations (3.33a) and (3.33b) into equations (3.46E) and (3.46F), respectively, we obtain

$$S''(\tau_A) = \frac{(\sigma_A - \sigma_H)^2}{\rho_A - \rho_H} \frac{\rho''(\psi_A)}{(\sigma'(\psi_A))^2} \quad (3.46f)$$

$$S''(\tau_H) = \frac{(\sigma_A - \sigma_H)^2}{\rho_A - \rho_H} \frac{\rho''(\psi_H)}{(\sigma'(\psi_H))^2} \quad (3.46g)$$

Upon substitution of equations (3.38) and (3.39) into equations (3.46a), (3.46b), (3.46c), (3.46d), (3.46e), and (3.46f), respectively, we obtain

$$a_0 + a_1\tau_A + a_2\tau_A^2 + a_3\tau_A^3 + a_4\tau_A^4 + a_5\tau_A^5 = 1 \quad (3.47a)$$

$$a_0 + a_1\tau_H + a_2\tau_H^2 + a_3\tau_H^3 + a_4\tau_H^4 + a_5\tau_H^5 = 0 \quad (3.47b)$$

$$a_1 + 2a_2\tau_A + 3a_3\tau_A^2 + 4a_4\tau_A^3 + 5a_5\tau_A^4 = 0 \quad (3.47c)$$

$$a_1 + 2a_2\tau_H + 3a_3\tau_H^2 + 4a_4\tau_H^3 + 5a_5\tau_H^4 = 0 \quad (3.47d)$$

$$2a_2 + 6a_3\tau_A + 12a_4\tau_A^2 + 20a_5\tau_A^3 = \frac{(\sigma_A - \sigma_H)^2}{\rho_A - \rho_H} \frac{\rho''(\psi_A)}{(\rho'(\psi_A))^2} \quad (3.47e)$$

$$2a_2 + 6a_3\tau_H + 12a_4\tau_H^2 + 20a_5\tau_H^3 = \frac{(\sigma_A - \sigma_H)^2}{\rho_A - \rho_H} \frac{\rho''(\psi_H)}{(\rho'(\psi_H))^2} \quad (3.47f)$$

Upon solving the equations (3.47), we obtain the value of $a_0 \dots a_5$. The example of this polynomial is presented in detail in chapter 4.

3.5.2 The Sixth Order Polynomial

If we denote that the end conditions of the curve sought is not only a planar, second-order geometric continuity at the blending points, A and H , and but also by the point E , we should define the sixth order polynomial function $S(\tau)$ as

$$S(\tau) = a_0 + a_1\tau + a_2\tau^2 + a_3\tau^3 + a_4\tau^4 + a_5\tau^5 + a_6\tau^6 \quad (3.48)$$

where τ is a dimensionless variable, i.e.,

$$\tau = \frac{\sigma}{\sigma_A - \sigma_H} \quad (3.49)$$

and

$$0 \leq S(\tau) \leq 1 \quad \frac{\sigma_H}{\sigma_A - \sigma_H} \leq \sigma \leq \frac{\sigma_A}{\sigma_A - \sigma_H} \quad (3.50)$$

The derivatives of $S(\tau)$ are derived from equation (3.48), i.e.,

$$S'(\tau) = a_1 + 2a_2\tau + 3a_3\tau^2 + 4a_4\tau^3 + 5a_5\tau^4 + 6a_6\tau^5 \quad (3.51)$$

and

$$S''(\tau) = 2a_2 + 6a_3\tau + 12a_4\tau^2 + 20a_5\tau^3 + 30a_6\tau^4 \quad (3.52)$$

Also, we can express the curve sought as the same as that in fifth order polynomial, i.e.,

$$S(\tau) = \frac{\rho - \rho_H}{\rho_A - \rho_H} \quad (3.53a)$$

i.e.

$$\rho = \rho_H + (\rho_A - \rho_H)S(\tau) \quad (3.53b)$$

The difference of the sixth and fifth order polynomial is the end conditions. We increase an end condition that is the curve sought is by the point E , i.e.,

$$S(0) = \frac{\rho_E - \rho_H}{\rho_A - \rho_H} \quad (3.54)$$

Hence, we obtain

$$a_0 = \frac{\rho_E - \rho_H}{\rho_A - \rho_H} \quad (3.55a)$$

$$a_0 + a_1\tau_A + a_2\tau_A^2 + a_3\tau_A^3 + a_4\tau_A^4 + a_5\tau_A^5 + a_6\tau_A^6 = 1 \quad (3.55b)$$

$$a_0 + a_1\tau_H + a_2\tau_H^2 + a_3\tau_H^3 + a_4\tau_H^4 + a_5\tau_H^5 + a_6\tau_H^6 = 0 \quad (3.55c)$$

$$a_1 + 2a_2\tau_A + 3a_3\tau_A^2 + 4a_4\tau_A^3 + 5a_5\tau_A^4 + 6a_6\tau_A^5 = 0 \quad (3.55d)$$

$$a_1 + 2a_2\tau_H + 3a_3\tau_H^2 + 4a_4\tau_H^3 + 5a_5\tau_H^4 + 6a_6\tau_H^5 = 0 \quad (3.55e)$$

$$2a_2 + 6a_3\tau_A + 12a_4\tau_A^2 + 20a_5\tau_A^3 + 30a_6\tau_A^4 = \frac{(\sigma_A - \sigma_H)^2}{\rho_A - \rho_H} \frac{\rho''(\psi_A)}{(\sigma'(\psi_A))^2} \quad (3.55f)$$

$$2a_2 + 6a_3\tau_H + 12a_4\tau_H^2 + 20a_5\tau_H^3 + 30a_6\tau_H^4 = \frac{(\sigma_A - \sigma_H)^2}{\rho_A - \rho_H} \frac{\rho''(\psi_H)}{(\sigma'(\psi_H))^2} \quad (3.55g)$$

Upon solving the equations (3.55), we obtain the value of $a_0 \cdots a_6$. The example of this polynomial is presented in detail in chapter 4.

CHAPTER 4

Design and Development

Based on the theory and parameters that discussed in the previous chapters, we design and develop a mill that is driven by a speed-o-cam. The mill is compact in size, versatile enough to provide different operating conditions such as speed, charge volume and lifter configuration to test and analyse the lifter signal measurements as well as provide the possibility to install a signal filtering system that determines charge shoulder and toe positions of mill from signal data. To achieve the desired level of operation flexibility, the design and manufacture incorporate state-of-the-art technologies such as dynamics analysis.

4.1. Virtual Prototyping Technology

In this work, the basic objective of using virtual prototyping technology is to get the optimum cam profile. ADAMS (Automatic Dynamic Analysis of Mechanical Systems) was used for the purpose in order to simulate, understand and quantify the performance of the mechanical systems before committing to expensive hardware prototypes or conduct numerous physical tests and to develop consistent virtual prototypes that guide in making critical design decisions.

The ADAMS software package was developed by Mechanical Dynamics Inc., is brand owned by MSC-Software, and the world's widely used mechanical system simulation software. ADAMS enables building of virtual prototypes, i.e., the simulation of the behaviour of mechanical systems as well as the 3D visualization without using a physical

prototype (ADAMS/View 12.0 Help, 2001). Distances and component dimensions of model are taken from the physical prototype. All the motion constraints are defined in the forms of joints and contacts between two moving components.

The steps that are used in ADAMS/View to create a virtual prototype of any mechanical system mirror the same steps that are used to build a physical prototype, which would be built by creating parts, connecting them with joints, assembling the system, and driving it with experiment-verified forces and motions. And, the entire behavior of the virtual prototype can be simulated. Springs, dampers, contacts, and friction were applied in order to improve the fidelity of the simulation.

ADAMS/View can also be used to quickly analyze multiple design variations until the optimal design is found. To evaluate multiple design ideas, ADAMS/View supports parametric modeling so that model can be easily modified and used in designed experiments. During simulations, or when they are complete, ADAMS/View provides the ability to animate models movement and view key physical measures of specific simulation data. This data emulates the data that would be normally produced physically.

While using ADAMS for the simulation purposes, it was assumed that in the simulation the component is modelled as a rigid body (ADAMS/View 12.0 Help, 2001). But in real practice, the components will engender distortion because the forces act on them.

The benefits of using ADAMS/View software package is as follow (ADAMS/View 12.0,2001):

- Quickly build and review models for simulation;
- Rapidly change design parameters and compare iterations in order to answer "what-if" questions about design;
- Visually share design ideas with product development teammates.

The sequence of the design process, which is followed according to the requirements, is shown in the figure 4.1.

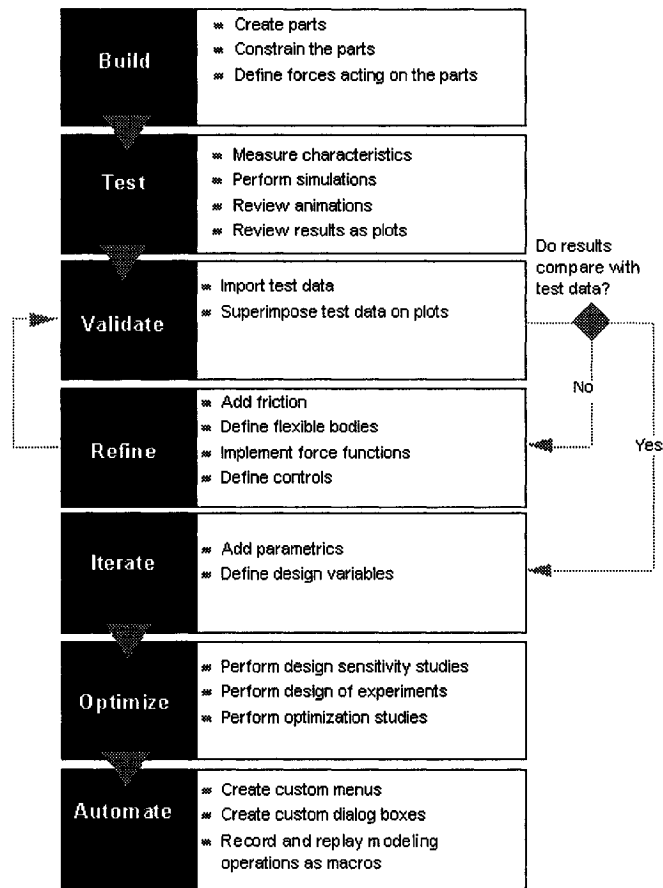


Figure 4.1: Design process steps (ADAMS/View 12.0, 2001)

4.2. Design and Optimization of Speed-o-Cam

In the Speed-o-Cam design, the virtual prototype of Speed-o-Cam drive system was built creating parts, connecting them with joints, defining the contacts, and driving them with accurate motions in order to optimize the design before the cam driven mill was manufactured. Several simulation runs, in which the design parameters were changed and iterations were compared to answer what-if question about the design, were executed for ascertaining and updating the cam profiles. By comparison these simulation results, the cam profiles were determined because the effects of cam profile on forces that are acted

on the rollers and cam were shown on the aforementioned testing conditions. Based on the simulation, the cam-driving mill was built on the appropriate the cam profiles that have had a signification impact on the product quality.

4.2.1. Version I of Speed-o-Cam

In the first step of this design, the velocity ratio will be determined, which is affected by the critical speed and the speed range of motor. In the Comminution Dynamics Lab, the testing speed as percent of critical speed is from 60 to 90 and the speed range of motor is from 1000 to 1800 rpm. After calculations, which are based on the chapters 2 & 3, have been completed, the velocity ratio is known as $1/40$, i.e., N is determined 40. Subsequently, a_1 , a_3 , and a_4 are determined 906mm, 870mm, and 11mm, respectively, in order that the final mechanism should be no longer in length than about 2m, no taller in height than about 2m, and no wider in width than about 1m as a result of satisfying the constraints imposed by laboratory. In the last step of this design, these variables are put into the equations, (3.1) and (3.2), and are calculated by Maple. We got the cam profile points shown in Table 4.1.

The cam and the speed-o-cam were designed as shown in Figure 4.2 and 4.3.

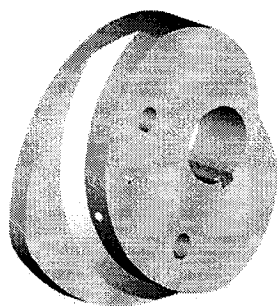


Figure 4.2: Cam

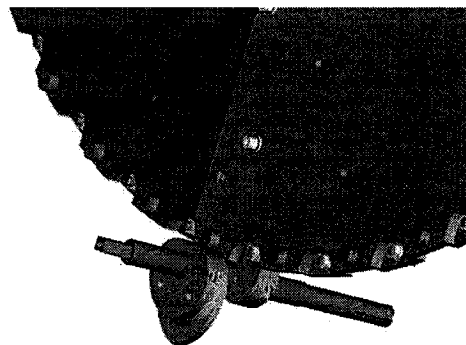


Figure 4.3: Speed-O-Cam

Table 4.1 Cam Profile Points with $a_1 = 906mm$,
 $a_3 = 870mm$, $a_4 = 11mm$, and $N = 40$.

	x (mm)	y (mm)	z (mm)
1	90.63	.00	0.0
2	90.18	-1.78	0.0
3	89.69	-3.54	0.0
4	89.16	-5.27	0.0
5	88.60	-6.99	0.0
6	88.01	-8.69	0.0
7	87.39	-10.36	0.0
8	86.74	-12.01	0.0
\vdots	\vdots	\vdots	\vdots

The cam profile, the cam pressure angle, and the cam curvature are shown in figure 4.4.

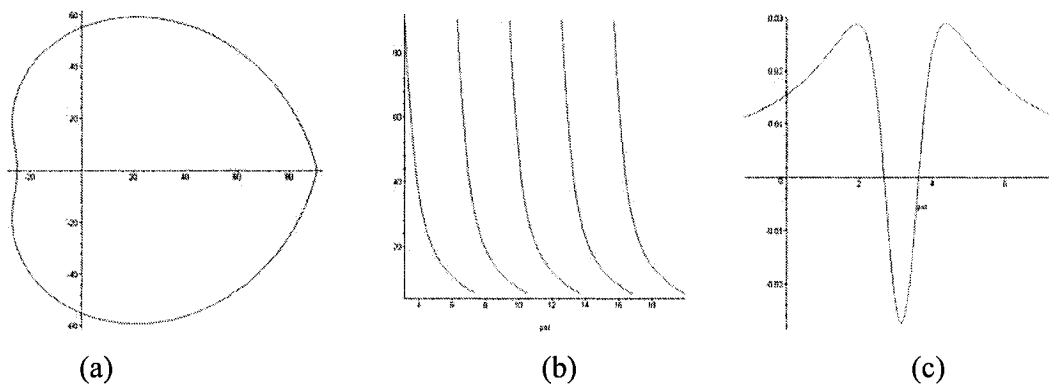
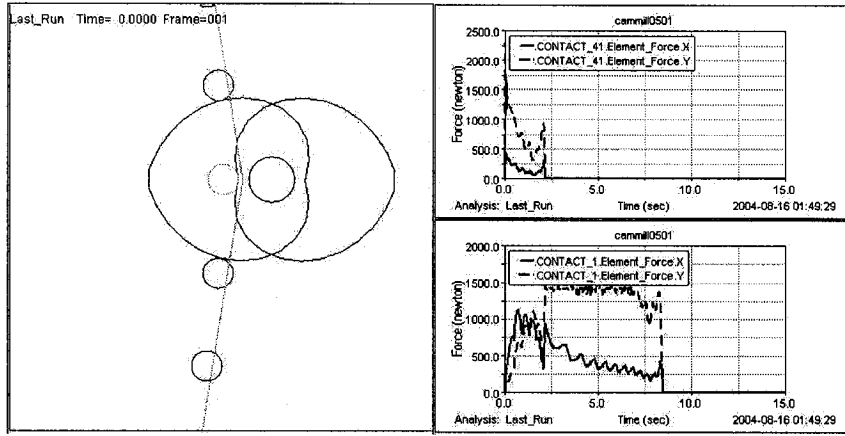
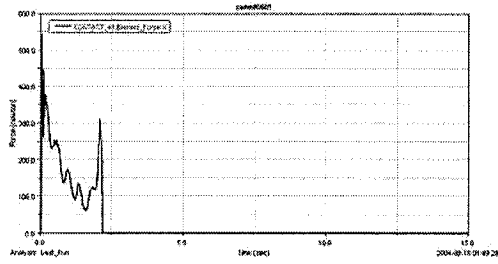


Figure 4.4: Plotting of cam kinematics: (a) cam profile; (b) pressure angle; (c) curvature:

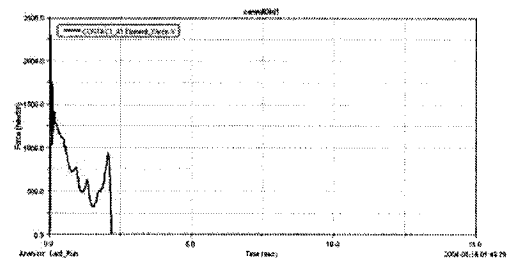
$a_1 = 906mm$, $a_3 = 870mm$, $a_4 = 11mm$, and $N = 40$.



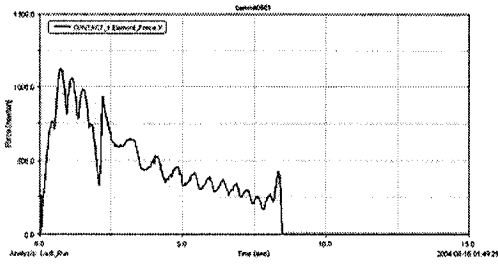
(a)



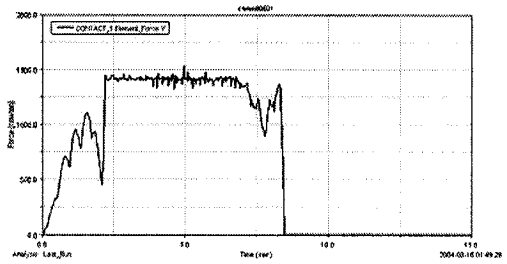
(b)



(c)



(d)



(e)

Figure 4.5: version I of Speed-o-Cam simulation: (a) model and result; (b) detail about component of contact force on x axis at contact 1; (c) detail about component of contact force on y axis at contact 1; (d) detail about component of contact force on x axis at contact 41; (e) detail about component of contact force on y axis at contact 41:

$$a_1 = 906\text{mm}, a_3 = 870\text{mm}, a_4 = 11\text{mm}, \text{ and } N = 40.$$

In order to determine the effect of theoretical dynamics and to determine the effect of different cam profile of the cam driven system, the virtual prototype of Speed-o-Cam drive system was built on the steps shown in the figure 4.1, i.e., in the first phase parts were created, constraints were applied and forces were defined using ADAMS/View's libraries.

Since the mode is cyclic loading, we only need to research the contact 1, which is the first contact between cam and roll, and the contact 41, which is the second contact between cam and roll. We obtain the curve of forces that acted on cams as shown in figure 4.5, respectively.

4.2.2. Version II of Speed-o-Cam

As mentioned in the chapter 3.4, the curve around cusp and the blunt point regions should be undercutting in order to improve the system kinematic performance.

Undercutting is taken into account for cam mechanism optimization by properly introducing 2-4-6-8 Polynomial (Zhang, 2003), in which the new variables ε and λ are 0.1 and 2/3, respectively, for the cam profile.

All variables are put into the equations and are calculated by Maple. We got the cam profile points shown in Table 4.2.

We modify the cam profile according to the aforementioned data in the virtual prototype of Speed-o-Cam drive system and obtain the curves of forces that acted on cams as shown in figure 4.7.

Table 4.2 Cam Profile Points with $a_1 = 906mm$, $a_3 = 870mm$, $a_4 = 11mm$, $N = 40$,
 $\varepsilon = 0.1$, and $\lambda = \frac{2}{3}$

	x (mm)	y (mm)	z (mm)
1	87.83	-9.17	0.0
2	87.32	-10.53	0.0
3	86.78	-11.88	0.0
4	86.23	-13.21	0.0
5	85.65	-14.53	0.0
6	85.06	-15.83	0.0
7	84.45	-17.12	0.0
8	83.81	-18.39	0.0
\vdots	\vdots	\vdots	\vdots

The cam corresponding profile, the cam pressure angle, and the cam curvature are shown in figure 4.6, respectively.

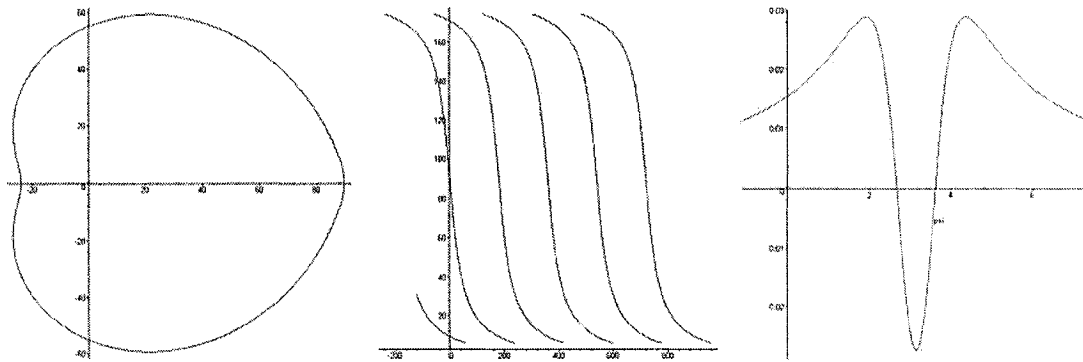


Figure 4.6: Plotting of cam kinematics: (a) cam profile; (b) pressure angle; (c) curvature:

$$a_1 = 906mm, a_3 = 870mm, a_4 = 11mm, N = 40, \varepsilon = 0.1, \text{ and } \lambda = \frac{2}{3}$$

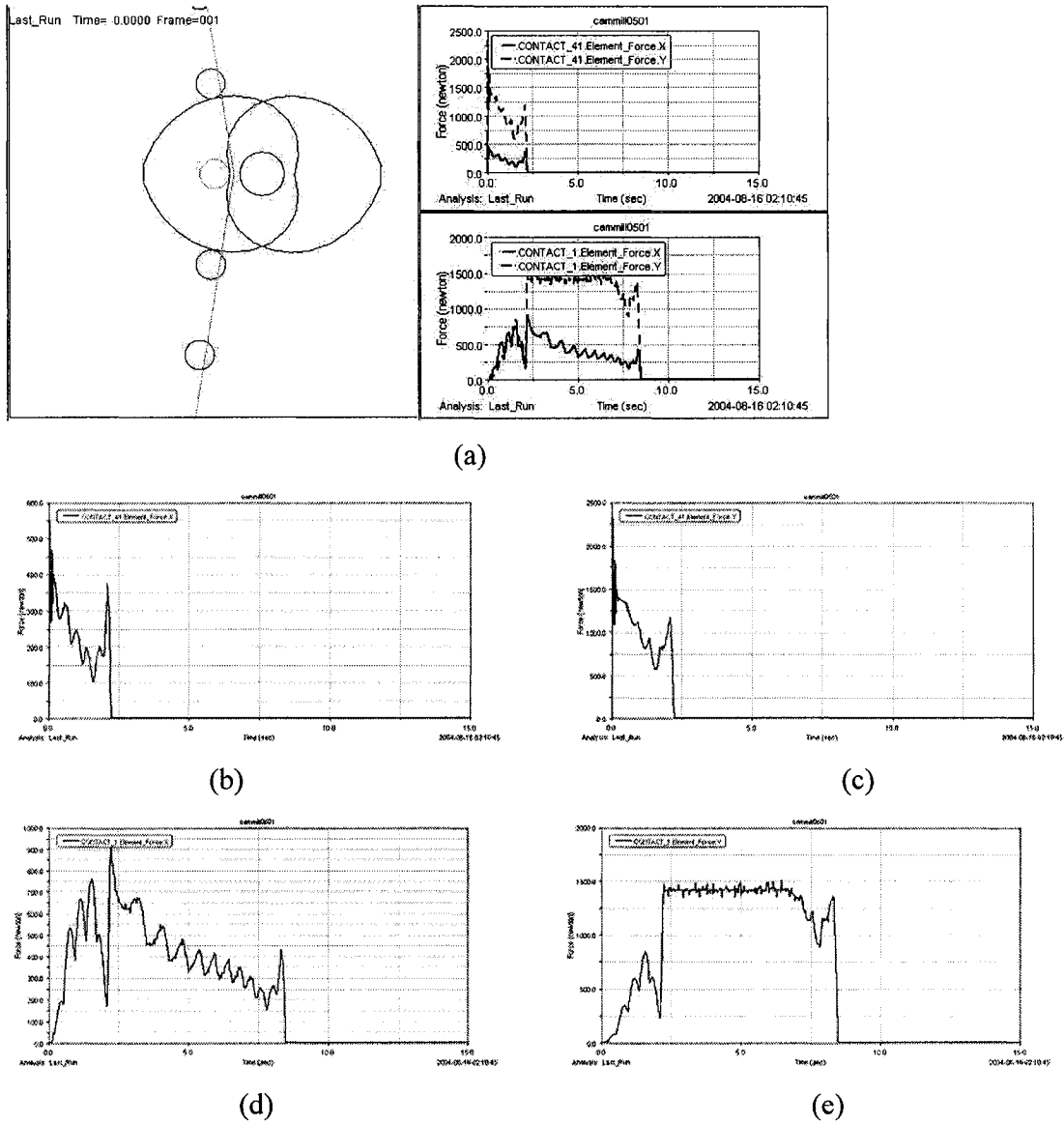


Figure 4.7: version II of Speed-o-Cam simulation: (a) model and result; (b) detail about component of contact force on x axis at contact 1; (c) detail about component of contact force on y axis at contact 1; (d) detail about component of contact force on x axis at contact 41; (e) detail about component of contact force on y axis at contact 41:

$$a_1 = 906\text{mm}, a_3 = 870\text{mm}, a_4 = 11\text{mm}, N = 40, \varepsilon = 0.1, \text{ and } \lambda = \frac{2}{3}$$

The force curves of I and II version Speed-o-Cam are compared as shown in figure 4.8.

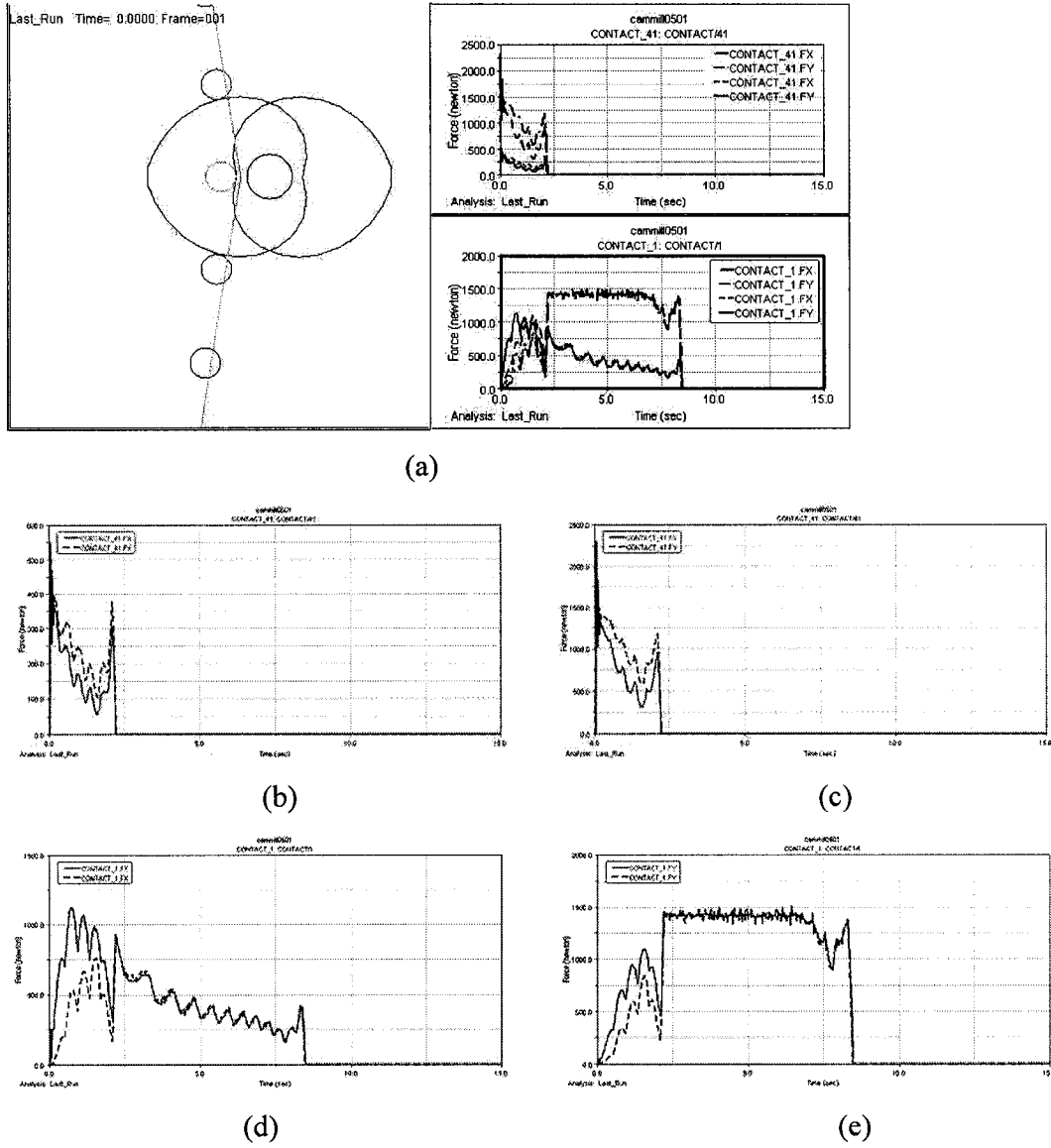


Figure 4.8: Comparison between version I and II of the Speed-o-Cam simulation:
 (a) model and result; (b) detail about component of contact force on x axis at contact 1;
 (c) detail about component of contact force on y axis at contact 1; (d) detail about
 component of contact force on x axis at contact 41; (e) detail about component of
 contact force on y axis at contact 41.

It is obvious that the undercutting improve the system performance.

4.2.3. Version III of Speed-o-Cam

In the Speed-o-Cam driving system, the function of cam is to deliver, following a prescribed motion, a vibrationless and smooth movement. Actually, it is impossible to manufacture a dimension to an exact value. Vibration, noise, wear and indeed binding may be instigated by a break in the cam profile curve or/and imprecise position of roller. For example, as shown in figure 4.9, the cam will be bind if the actual distance of two rolls is smaller than the theoretical distance. The simulation result is shown in figure 4.10.

The curve under negative action is undercut 0.25mm, i.e., $a'_4 = a_4 + 0.25$, in order that the probability of occurrence of these disadvantageous factors will be kept as small as possible. That is, the cam profile is unsymmetrical with respect to the u axis.

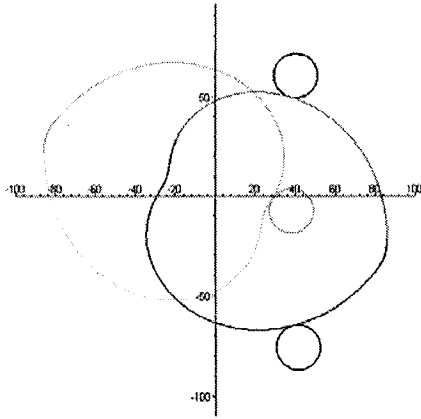


Figure 4.9: A toggle position

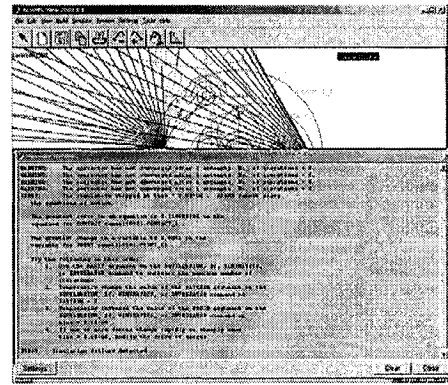


Figure 4.10: Simulation failure

As mentioned in the chapter 3.5., the fifth order polynomial is introduced to get a smooth cam profile. We denote $a_1 = 906mm$, $a_3 = 870mm$, $a_4 = 11mm$, $a'_4 = a_4 + 0.25mm$, $N = 40$, $\sigma_A = 0.1$, and $\sigma_F = 0.2$ and put other variable into the equations, and are calculated by Maple. We got the cam profile points shown in Table 4.3.

Table 4.3 Cam Profile Points with $a_1 = 906mm$, $a_3 = 870mm$, $a_4 = 11mm$, $a'_4 = a_4 + 0.25mm$, $N = 40$, $\sigma_A = 0.1$, and $\sigma_F = 0.2$.

	x (mm)	y (mm)	z (mm)
1	88.20	-8.15	0.0
2	87.57	-9.89	0.0
3	86.90	-11.60	0.0
4	86.20	-13.29	0.0
5	85.47	-14.95	0.0
6	84.71	-16.58	0.0
7	83.92	-18.19	0.0
8	83.10	-19.78	0.0
\vdots	\vdots	\vdots	\vdots

The cam corresponding profile, the cam pressure angle, and the cam curvature are shown in figure 4.11, respectively.

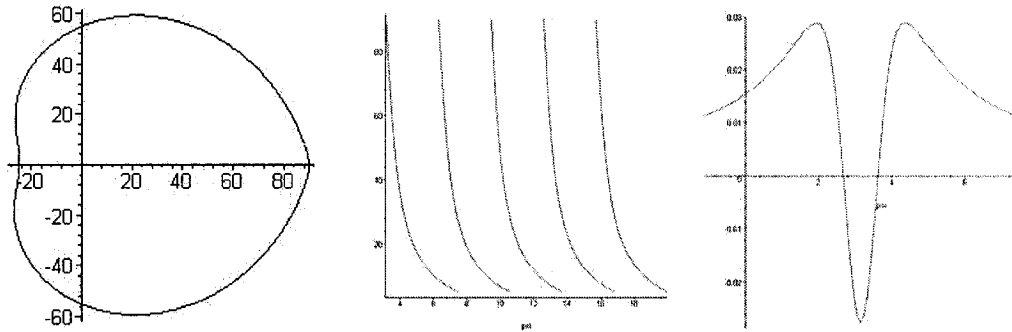
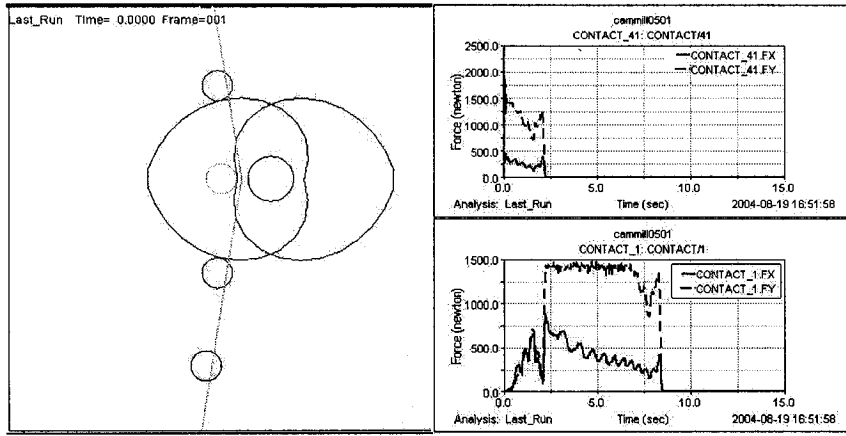
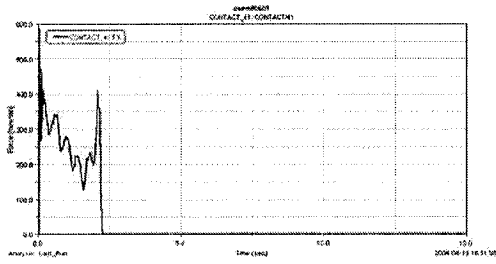


Figure 4.11: Plotting of cam kinematics: (a) cam profile; (b) pressure angle; (c) curvature: $a_1 = 906mm$, $a_3 = 870mm$, $a_4 = 11mm$, $a'_4 = a_4 + 0.25mm$, $N = 40$, $\sigma_A = 0.1$, and $\sigma_F = 0.2$.

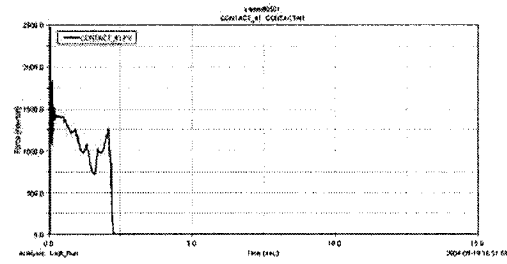
The curves of forces, which acted on cams as shown in figure 4.12, respectively, are obtained when the cam profile is modified according to the aforementioned data in the virtual prototype of Speed-o-Cam drive system.



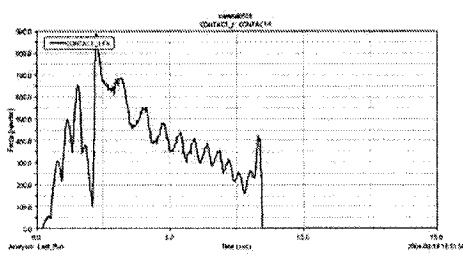
(a)



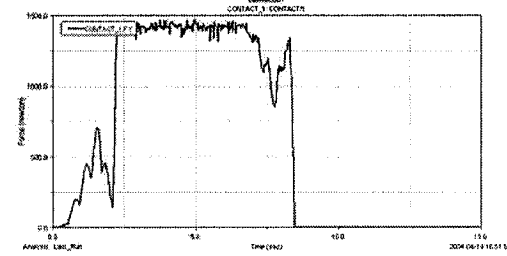
(b)



(c)



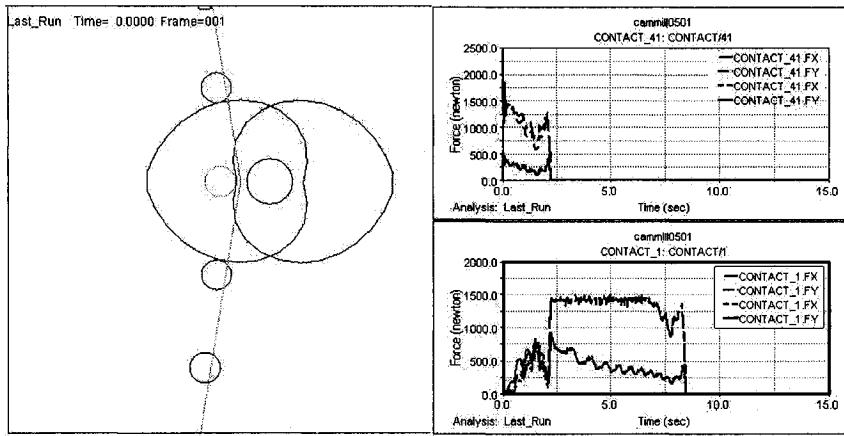
(d)



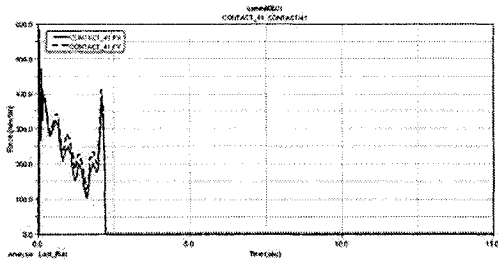
(e)

Figure 4.12: version III of Speed-o-Cam simulation: (a) model and result; (b) detail about component of contact force on x axis at contact 1; (c) detail about component of contact force on y axis at contact 1; (d) detail about component of contact force on x axis at contact 41; (e) detail about component of contact force on y axis at contact 41: $a_1 = 906\text{mm}$, $a_3 = 870\text{mm}$, $a_4 = 11\text{mm}$, $a'_4 = a_4 + 0.25\text{mm}$, $N = 40$, $\sigma_A = 0.1$, and $\sigma_F = 0.2$.

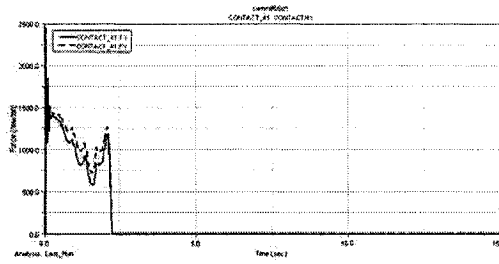
The two curves, which are in undercutting by the 2-4-6-8 (Zhang, 2003) and fifth order polynomial, are compared as shown in figure 4.13.



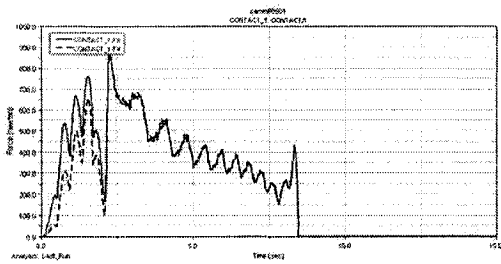
(a)



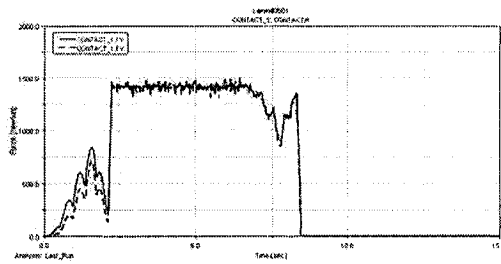
(b)



(c)



(d)



(e)

Figure 4.13: Comparison between version II and III of the Speed-o-Cam simulation: (a) model and result; (b) detail about component of contact force on x axis at contact 1; (c) detail about component of contact force on y axis at contact 1; (d) detail about component of contact force on x axis at contact 41; (e) detail about component of contact force on y axis at contact 41.

It is obvious that the system performance is better by undercutting with the fifth order polynomial than the 2-4-6-8 polynomial.

4.2.4. Version IV of Speed-o-Cam

The disadvantage of the fifth order polynomial lies in that the cam profile in the cusp and blunt point regions is not easily controlled. That is, the curves may be out of the original cam profile if the parameters, σ_A , and σ_F , are not selected correctly. So, the sixth order polynomial is introduced.

As mentioned in the chapter 3.5., we denote the new parameter u_{EC} and u_{BG} , which is 0.5mm and 0.8mm, respectively, and put them with other variable into the equations and are calculated by Maple. We got the cam profile points shown in Table 4.4.

Table 4.4 Cam Profile Points with $a_1 = 906mm$, $a_3 = 870mm$, $a_4 = 11mm$, $a'_4 = a_4 + 0.25mm$, $N = 40$, $\sigma_A = 0.1$, $\sigma_F = 0.5$, $u_{EC} = 0.5$ and $u_{BG} = 0.8$.

	x (mm)	y (mm)	z (mm)
1	88.20	-8.15	0.0
2	87.62	-9.76	0.0
3	87.00	-11.34	0.0
4	86.36	-12.91	0.0
5	85.70	-14.45	0.0
6	85.00	-15.97	0.0
7	84.28	-17.47	0.0
8	83.53	-18.94	0.0
\vdots	\vdots	\vdots	\vdots

The cam corresponding profile, the cam pressure angle, and the cam curvature are shown in figure 4.14, respectively.

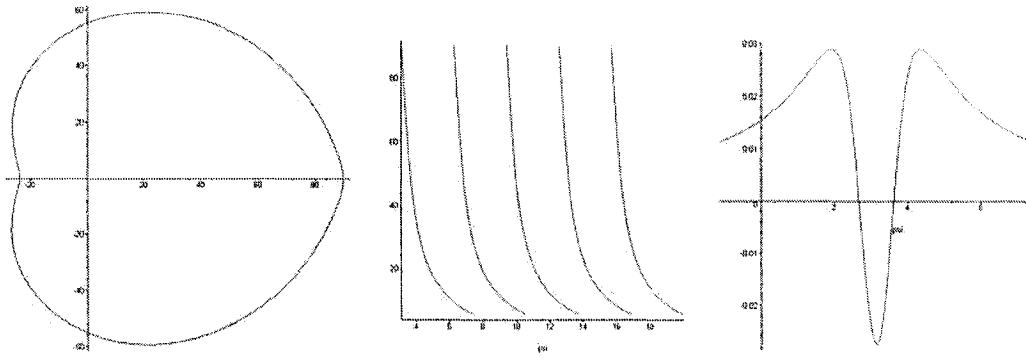
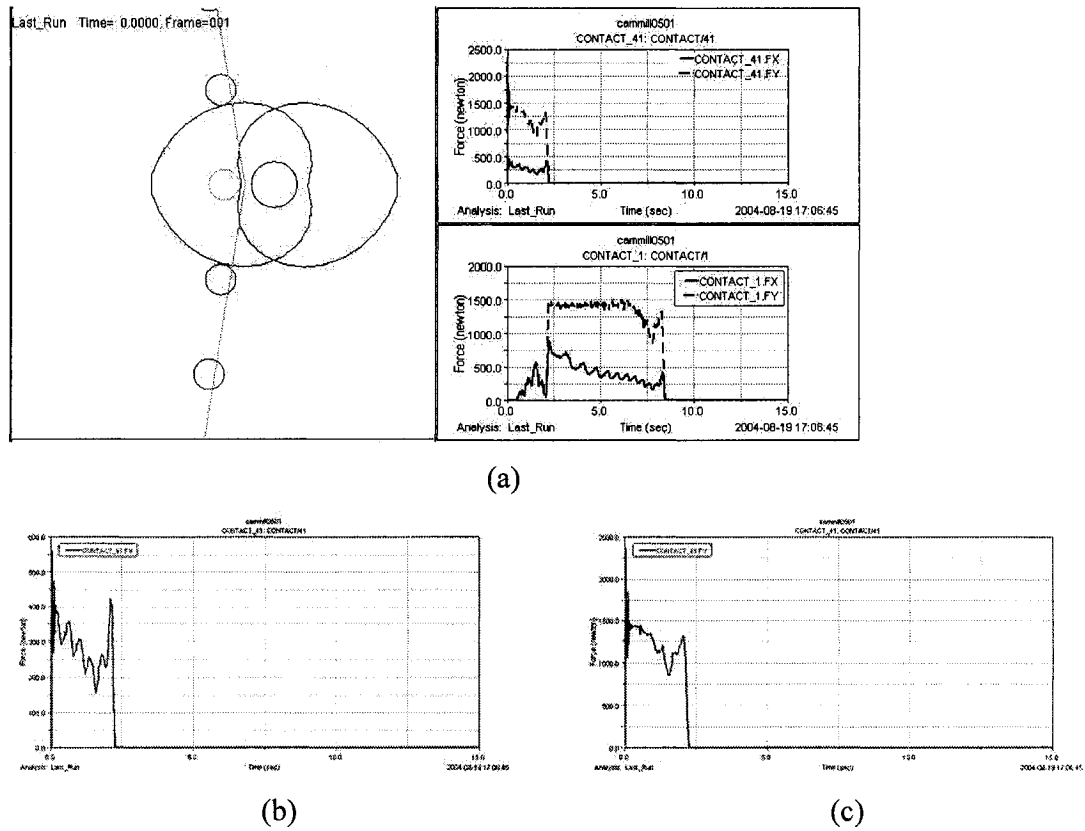
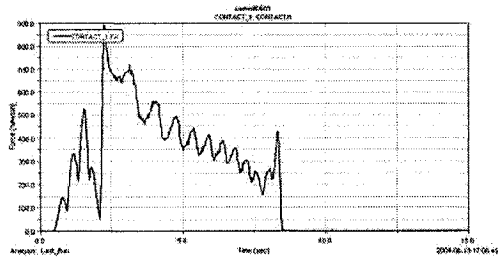


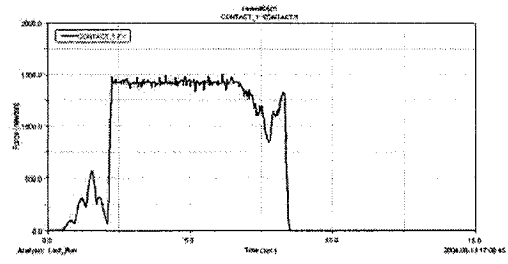
Figure 4.14: Plotting of cam kinematics: (a) cam profile; (b) pressure angle; (c) curvature:
 $a_1 = 906mm$, $a_3 = 870mm$, $a_4 = 11mm$, $a'_4 = a_4 + 0.25mm$, $N = 40$, $\sigma_A = 0.1$,
 $\sigma_F = 0.5$, $u_{EC} = 0.5$ and $u_{BG} = 0.8$.

After the cam profile is modified according to data in table 4.4, the curve of forces in the virtual prototype of Speed-o-Cam drive system is shown in figure 4.15, respectively.





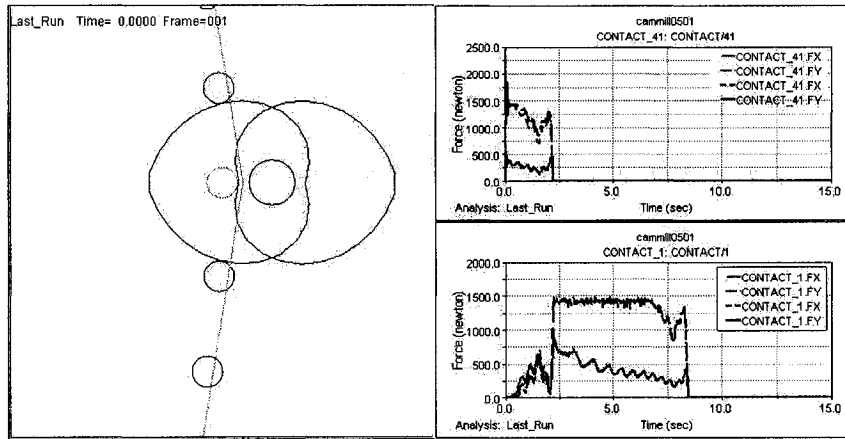
(d)



(e)

Figure 4.15: version IV of Speed-o-Cam simulation: (a) model and result; (b) detail about component of contact force on x axis at contact 1; (c) detail about component of contact force on y axis at contact 1; (d) detail about component of contact force on x axis at contact 41; (e) detail about component of contact force on y axis at contact 41: $a_1 = 906mm$, $a_3 = 870mm$, $a_4 = 11mm$, $a'_4 = a_4 + 0.25mm$, $N = 40$, $\sigma_A = 0.1$, $\sigma_F = 0.5$, $u_{EC} = 0.5$ and $u_{BG} = 0.8$.

The two curves, which are in undercutting by the fifth and sixth order polynomial, are compared as shown in figure 4.16.



(a)

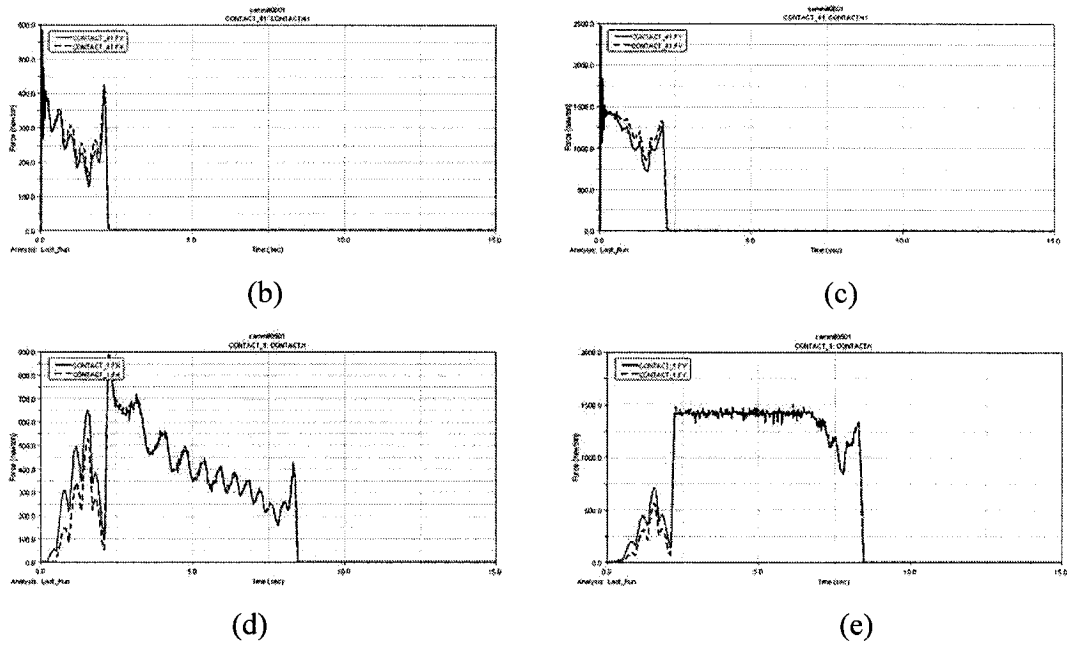


Figure 4.16: Comparison between version III and IV of the Speed-o-Cam simulation: (a) model and result; (b) detail about component of contact force on x axis at contact 1; (c) detail about component of contact force on y axis at contact 1; (d) detail about component of contact force on x axis at contact 41; (e) detail about component of contact force on y axis at contact 41.

It is obvious that the system performance is better by undercutting with the sixth order polynomial than the fifth order polynomial.

The four curves are compared as shown in figure 4.17.

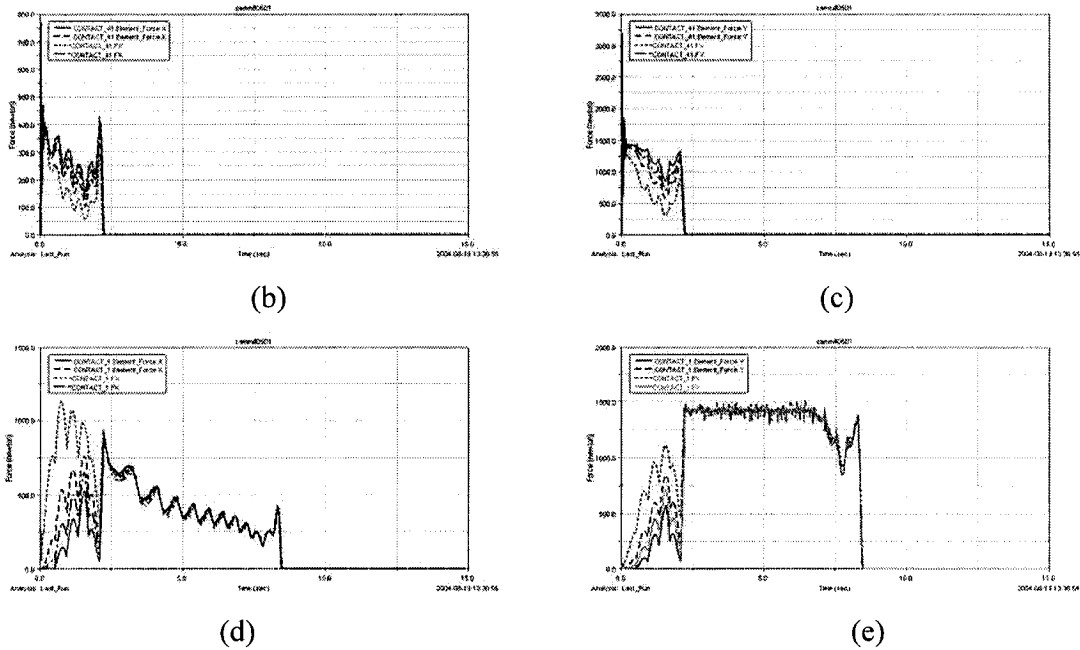
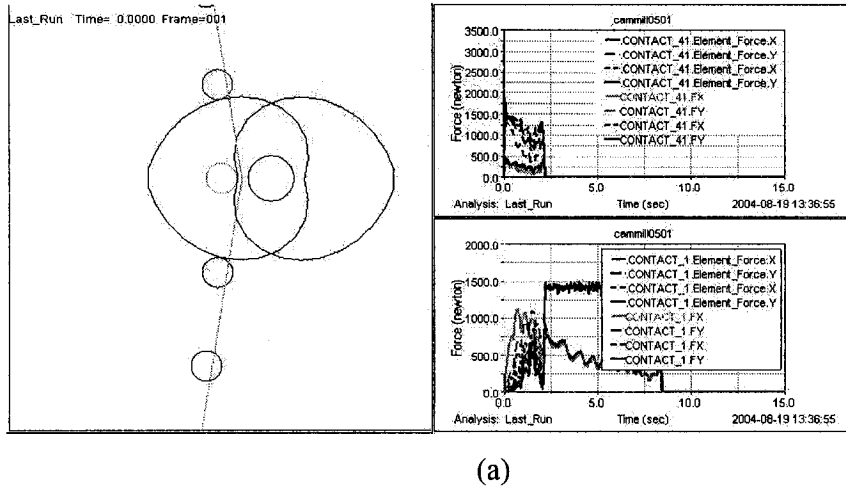


Figure 4.17: Comparison between version I, II, III and IV of the Speed-o-Cam simulation: (a) model and result; (b) detail about component of contact force on x axis at contact 1; (c) detail about component of contact force on y axis at contact 1; (d) detail about component of contact force on x axis at contact 41; (e) detail about component of contact force on y axis at contact 41.

Also, we found that the simulation result is not obviously changed when the tolerances are adopted as shown in Table 4.5

Table 4.5 Accepted tolerance limits for cam & disc manufacture

Name	Dimension (mm)	Tolerance (mm)
Cam Profile	23.90~89.00	+0.01 -0.01
The Basic Circle of Rollers	ϕ 1740	+0.01 -0.25
The Hole for Rollers	ϕ 10	+0.001 -0.001
⋮	⋮	⋮

With these details, the cam profile was determined and engineering drawings were produces as shown in appendix A.

4.3. Design and Optimization of other components

4.3.1. Design and Optimization of Disc

The disc has been designed to make it as a cam follower as well as a ball mill back cover, as shown in figure 4.18. To reduce the material cost, the disc is composed of two pieces and was manufactured after patched up as a whole.

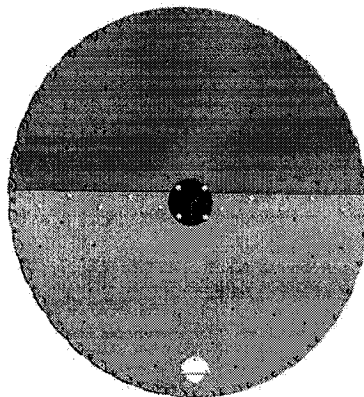


Figure 4.18: The cam follower disc

4.3.2. Design and Optimization of Supports

There are two supports with the similar U frame, as shown in figure 4.19 and 4.20. Mounted on them, pillow blocks were used to fix the shafts that provide the sustainment for the cams and disc. And, power and motion are transmitted from one rotating shaft to another by cams and disc that are attached to the shafts by set screws and key.

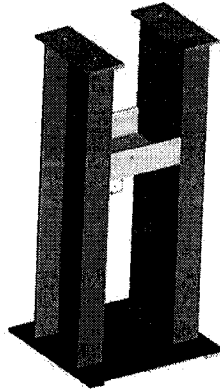


Figure 4.19: The support for disc shaft

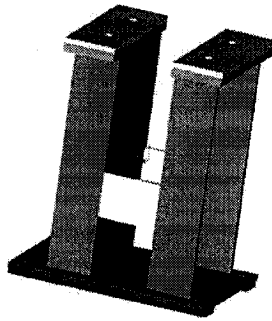


Figure 4.20: The support for cam shaft

4.3.3. Design and Optimization of Base

The base is designed as a plate as shown in figure 4.21. The slots are produced to adjust the position of motor and other components. In order to convey the equipment conveniently, the four wheels were fixed on the base.



Figure 4.21: The base of cam driven ball mill

With these details, the cam driven ball mill shell was determined, as shown in figure 22 and engineering drawings were produced as shown in appendix A.

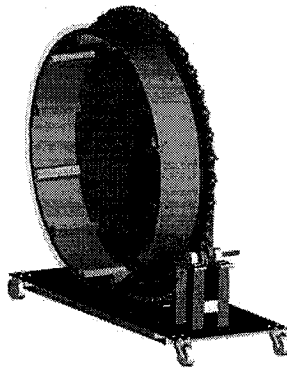


Figure 4.22: The cam driven ball mill

CHAPTER 5

Finite Element Analyses of Cam Profile

In the later stages of this design, finite element analyses (FEA) were used in order to determine if a cam was safe to transmit loads acting upon it. ANSYS 7.0 was used comprehensively for this purpose. ANSYS is a finite element modeling and analysis tool. ANSYS finite element analysis software (ANSYS 7.0 Help, 2002) can be used to perform the following tasks:

- Build computer models or transfer CAD models of structures, products, components, or systems.
- Apply operating loads or other design performance conditions.
- Study physical responses, such as stress levels, temperature distributions, or electromagnetic fields.
- Optimize a design early in the development process to reduce production costs.
- Do prototype testing in environments where it otherwise would be undesirable or impossible (for example, biomedical applications).

Structural analysis is probably the most common application of the finite element method. The term structural (or structure) implies not only civil engineering structures such as bridges and buildings, but also naval, aeronautical, and mechanical structures such as ship hulls, aircraft bodies, and machine housings, as well as mechanical components such as pistons, machine parts, and tools.

There are the seven types of structural analyses available in the ANSYS family of products. They are Static Analysis, Modal Analysis, Harmonic Analysis, Transient Dynamic Analysis, Spectrum Analysis, Buckling Analysis, and Explicit Dynamic Analysis. Static Analysis can be used to determine displacements, stresses, etc. under static loading conditions (ANSYS 7.0 Help, 2002). Nonlinearities can include plasticity, stress stiffening, large deflection, large strain, hyperelasticity, contact surfaces, and creep. The primary unknowns (nodal degrees of freedom) calculated in a structural analysis are *displacements*. Other quantities, such as strains, stresses, and reaction forces, are then derived from the nodal displacements.

5.1. The static analysis

A typical static analysis has three distinct steps:

1. Build the model.
2. Apply loads and obtain the solution.
3. Review the results.

Following these steps, we built a finite element model required by defining the element types, element real constants, material properties, and the model geometry, which is based on the points as shown in table 4.4. Once material properties were defined, the next step in an analysis is generating a finite element model - nodes and elements - that adequately describes the model geometry.

Then, we used the ANSYS 7.0 processor to define the analysis type and analysis options, apply loads, specify load step options, and initiate the finite element solution. When we applied the loads, we used the *function* command. That is, the equations (3.1), (3.2), (3.3), (3.4), (3.5), and (3.6) was used to define the boundary condition as shown in figure 5.1. Applying these loads on the different nodes that corresponds to the points in table 4.4, we use the *solve* command. The ANSYS program takes the model and loading information from the database and calculates the results. Results are written to the results file and also to the database.

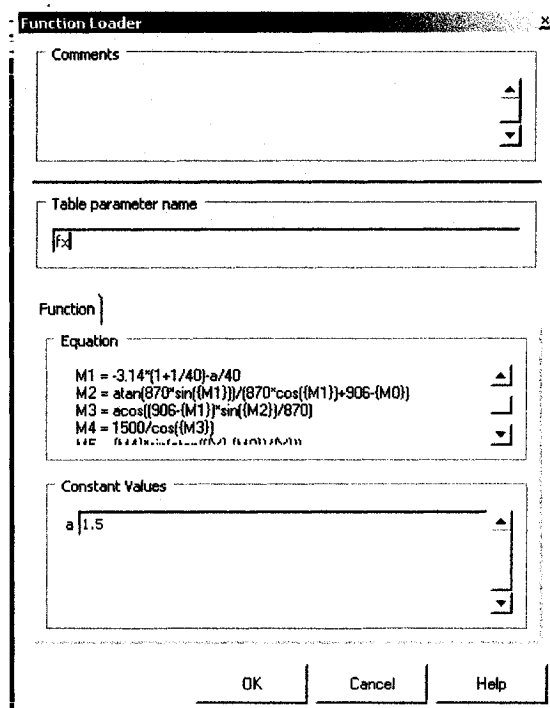


Figure5.1: the function command

Once the solution has been calculated, the ANSYS postprocessors is used to review the results. There are different results corresponding to different points. One of them is shown in figure 5.2.

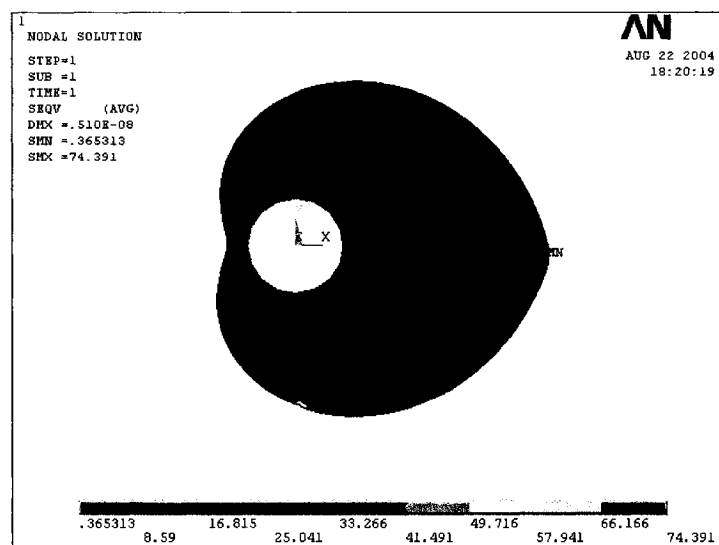


Figure 5.2: Simulation results obtained from the FEA

From the static analysis, we found that the cams were safe to transmit loads acting upon it, i.e., the design stress was large enough to prevent failure in static case loads in this design.

5.2. The dynamic forces analysis

Explicit Dynamic Analysis is only available in the ANSYS LS-DYNA program (ANSYS 7.0 Help, 2002). ANSYS LS-DYNA provides an interface to the LS-DYNA explicit finite element program. Explicit dynamic analysis is used to calculate fast solutions for large deformation dynamics and complex contact problems.

ANSYS LS-DYNA combines the LS-DYNA explicit finite element program with the powerful preprocessing and postprocessing capabilities of the ANSYS program. The explicit method of solution used by LS-DYNA provides fast solutions for short-time, large deformation dynamics, quasi-static problems with large deformations and multiple nonlinearities, and complex contact/impact problems. Using this integrated product, structure can be modeled in ANSYS, the explicit dynamic solution can be obtained via LS-DYNA, and results can be reviewed by using the standard ANSYS postprocessing tools. The geometry and results information can be transferred between ANSYS and ANSYS LS-DYNA to perform sequential implicit-explicit / explicit-implicit analyses, such as those required for droptest, springback and other applications.

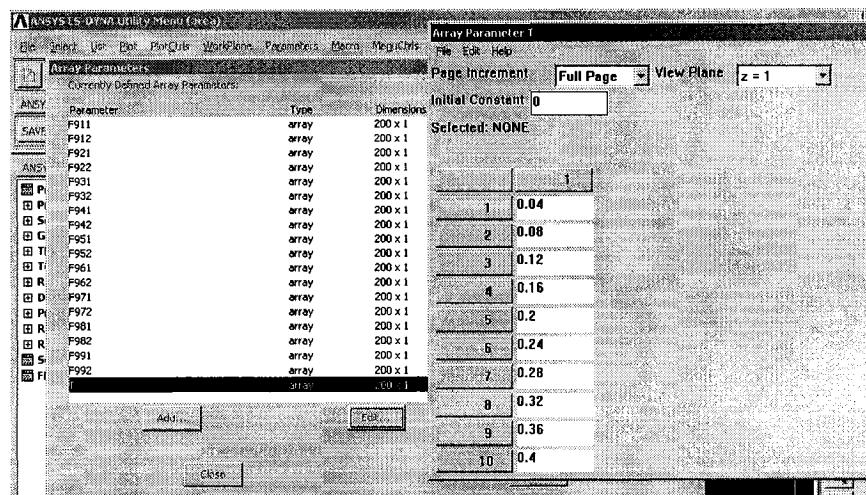
The procedure for an explicit dynamic analysis is similar to any other analysis that is available in the ANSYS program. The three main steps are:

1. Build the model (with the PREP7 preprocessor)
2. Apply loads and obtain the solution (with the SOLUTION processor)
3. Review the results (with the POST1 and POST26 postprocessors)

In the first step, we built the model by the method that is mentioned in last section.

Table 5.1 Force on the cam

	F_x (N)	F_y (N)
1	-1495.99	184.49
2	-1491.03	222.05
3	-1485.12	259.52
4	-1478.26	296.88
5	-1470.46	334.08
6	-1461.72	371.09
7	-1452.05	407.90
8	-1441.45	444.46
\vdots	\vdots	\vdots



62

In the last step, the ANSYS postprocessors is used to review the results. The figure 5.4 is one of results.

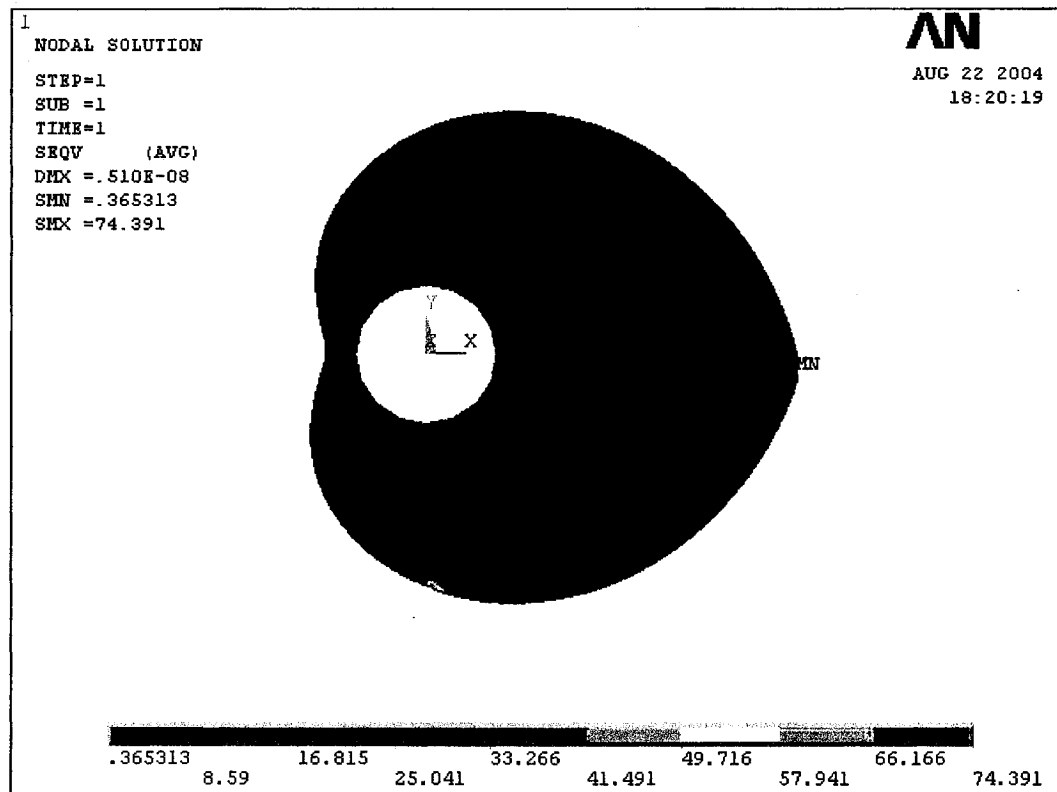


Figure 5.2: Simulation results obtained from the FEA

From the dynamic analysis, we drew a conclusion that capacity was greater than load and strength should be greater than stress. That is, the allowable stress on the cams is large enough to prevent failure in case loads exceed expected values, or other uncertainties react, such as short-time, large deformation dynamics and complex contact/impact problems, in this design.

CHAPTER 6

The Cam Driven Mill Fabrication & Assessment

6.1. The Cam Driven Mill Fabrication

The cam drive fabrication leading to a successful initial operation was completed in two steps. The first step was initiated once all the parts were manufactured and delivered. In this first step, all the parts for the base, cam and cam follower disc were assembled and adjusted (Figure 6.1 and 6.2). The cam shaft support, however was only attached temporarily. This allowed the hand cranking of the cam in order to determine how the drive operated before attaching the motor.

As a result, a number of improvements were suggested by the Departmental technicians and completed. This leads to the second step in the fabrication process. The motor was installed (as shown in Figure 6.3) and Prony brake (Figure 6.4) was completed to simulate a load on the cam follower disc.

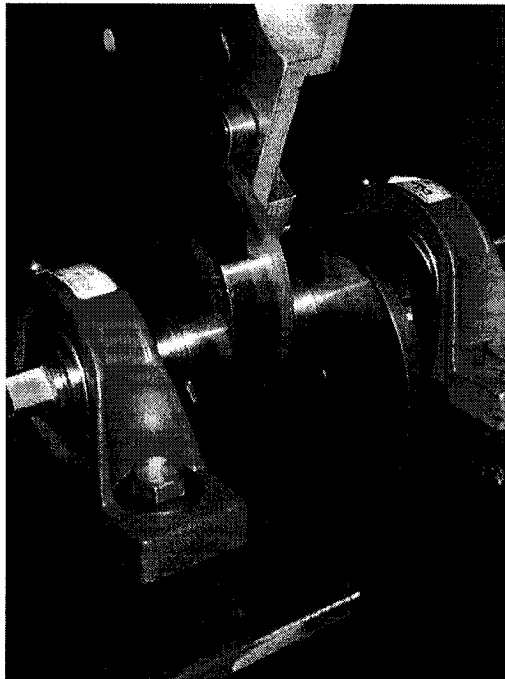


Figure 6.1: Cam Assembly

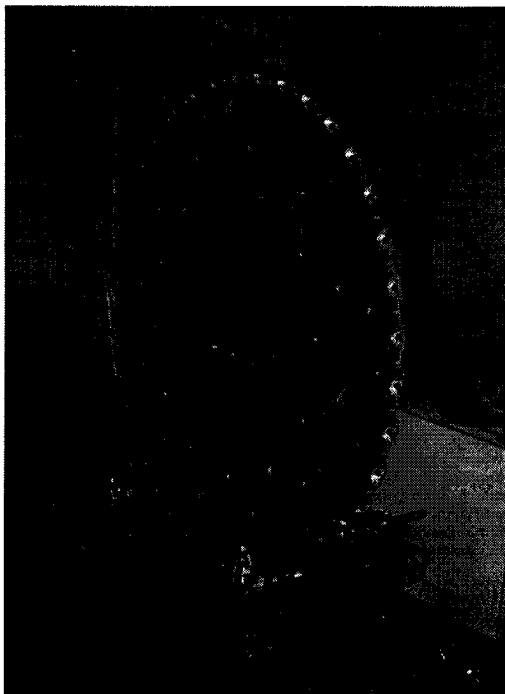


Figure 6.2: Cam rollers disk

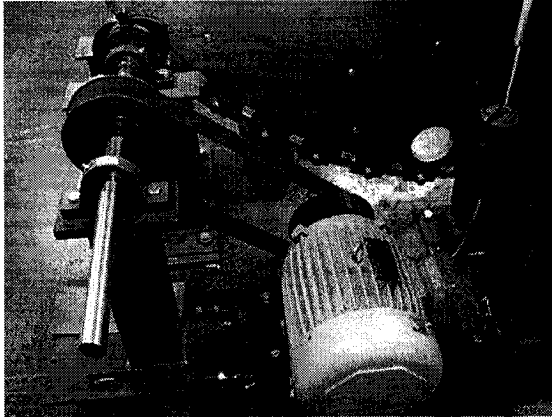


Figure 6.3: Cam shaft and motor modification

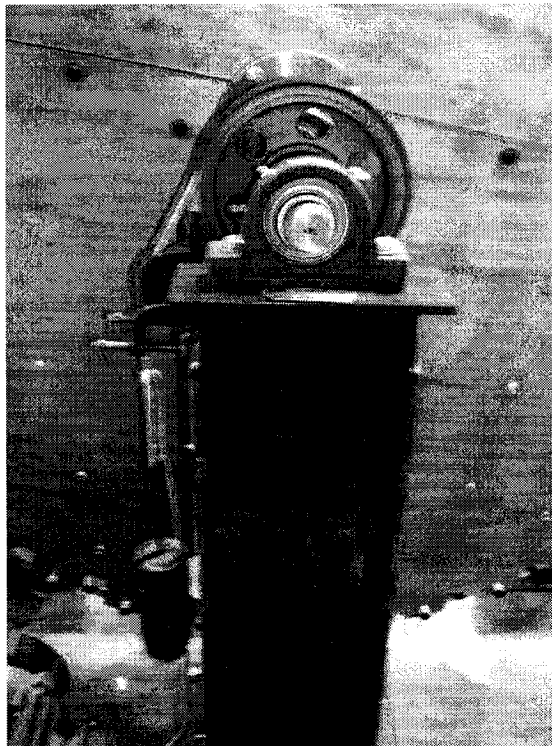


Figure 6.4 Prony brake

6.2. Cam Drive Initial Assessment

The criterion for the initial cam drive assessment was related to confirming operating speed range. This criterion was assessed by turning the electric motor on, ramping slowly up the speed and listening particularly to major impacting noise. Such noise would indicate possible shock problems between cam followers and the cam. The initial assessment showed that an operating speed of 30⁺ rpm can be reached and maintained without the envisioned possible problem binding. The result allows the set-up and preparation of a commissioning test to determine the efficiency of the drive over a range of operating loads and speeds.

CHAPTER 7

Conclusions and Recommendations for Future Work

7.1. Conclusions

The new cam driven tumbling mill that uses a newly patented speed-o-cam technology was designed and built to meet the specific demands of test operation at Comminution Dynamics Lab of Department of Mechanical Engineering of McGill University. Version IV of the Speed-o-Cam driven system has been designed and developed in this research thesis work.

The literature survey and the study of modern driven systems helped to understand the inherent importance of the driven system for the tumbling mills.

Cam-profile modifications around the cusp and the blunt point of the cam profile of Speed-o-Cam reducers are introduced to optimize the cam profile. Undercutting of the original profile by using polynomials was proposed here. The performance of the polynomials is quite good and takes simple forms. These are thus suitable polynomials to cope with the problems of interest to this thesis. We also derived geometrically and statically the pressure-angles distributions. The pressure angle directly influences the force transmission properties of the mechanism and determines how good the force transmission of the mechanism is.

Dynamic analyses helped to determine design, state and objective variables, which were used in optimizing the Speed-O-Cam design. It is successful that the new driven system for mill can transfer smoothly the power from one shaft to another on these simulations. And, it will be proved by the successful operation of the cam mill over the next few months in the Comminution Dynamics lab.

Finite element analysis (ANSYS) was used comprehensively for calibrating the stress on the cam with the maximum allowable stress in the components, after final design of the Speed-o-Cam driven system was reached after proposing evolutionary designs on the cam profile. That is because ANSYS is widely used for structural analyses in the field of engineering and its very powerful postprocessor & graphical capabilities.

The version VI of the Speed-o-Cam driven system has the following important features:

- Rolling action between the cam and cam follower as opposed to sliding in gear driven system,
- Ease of configuration to achieve the desired level of operation flexibility,
- Lower maintenance requirement and greater reliability,
- Allows the use of most current or future equipment,
- Flexibility of operating speeds,
- Greater machinability, performance, and efficiency,
- Low building & operation cost.

7.2. Recommendations for Future Work

In this work, a cam-driven laboratory ball mill was designed and developed, in which the friction of mill driving system is changed from the sliding to pure rolling. Future work could look into the prospect of building this driven system as very large to match the industry mills. It will be possible to see how the Speed-o-Cam technology is adopted in design driving system of large industry mills over the next few years.

An extension to the present work is recommended as follows:

- (i) Preparation of a commission test campaign to determine the efficiency of the driving system is recommended. Comparing the results of tests with the results of simulation by ADAMS should be conducted.
- (ii) The sensors should be used for measuring the force on the cam.
- (iii) The life expectancy of Speed-o-Cam should be determined. The modes of failure for primarily cyclic loading based on the endurance limit rather than on yield or tensile strength should be researched.
- (iv) The application of the appropriate Geometric Dimensioning and Tolerancing (GD&T) of the Speed-o-Cam should be researched. The sensitivity of the performance of Speed-o-Cam to machining errors should be tested.
- (v) More prototypes of Speed-o-Cam should be designed, manufactured and tested before it is adopted in design driving system of large industry mills.

REFERENCE

ADAMS/View 12.0 Help, 2001, Intranet HTML Help On Using ADAMS/View 12.0, Automatic Dynamic Analysis of Mechanical Systems, MSC Software, Santa Ana, CA.

AGRAWALA S., RAJAMANI R.K., SONGFACK P. and MISHRA B.K., 1997, “Mechanics of Media Motion in Tumbling Mills with 3D Discrete Element Method”, Minerals Engineering, Vol. 10, No. 2, pp. 215–227.

ANGELES, et al, 2002, Transmission Device, United States Patent No. 6,382,038.

ANGELES, J. and LOPEZ-CAJUN Bernad,C.S., 1991, *Optimization of Cam Mechanisms*, Kluwer Academic Publishers, Dordrecht, Boston.

ANSYS 7.0 Help, 2002, Intranet HTML Documentation for ANSYS 7.0 Help, ANSYS Inc., Canonsburg, PA.

BURR A.H., 1981, *Mechanical Analysis and Design*, ELSEVIER, New York, New York.

CUMMINS, A.B., 1973, *SME Mining Engineering Handbook*, Society of Mining Engineers of The American Institute of Mining, Metallurgical, and Petroleum Engineers, Inc., New York, New York.

DRAKE P.J., 1999, *Dimensioning and Tolerancing Handbook*, McGraw-Hill, New York.

EDWARDS K.S. and MCKEE R.B., 1991, *Fundamentals of Mechanical Component Design*, McGraw-Hill, Inc., Montreal.

GERE J.M. and TIMOSHENKO S.P., 1997, *Mechanics of Materials*, Pws Publishing Company, Toronto

GONZALEZ-PALACIOS, M. A. and ANGELES, J., 1993, *Cam Synthesis*, Kluwer Academic Publishers, Dordrecht.

GOGU G., COUTELLIER D., CHEDMAIL P. and RAY P., 2002, *Recent Advances in Integrated Design and Manufacturing in Mechanical Engineering*, KLUWER ACADEMIC PUBLISHER, DORDRECHT.

GOVENDER I., POWELL M.S., and NURICK G.N., 2001, "3D Particle Tracking in a Mill: a Rigorous Technique for Verifying DEM Predictions", *Minerals Engineering*, Vol. 14, No. 10, pp. 1329–1340.

HIBBELER R.C., 2000, *Mechanics of Materials*, Prentic Hall, Upper Saddle River, New Jersey.

HILL R. and JENSEN C.H., 1976, *Modern Engineering Tolerancing*, McGRAW-HILL RYERSON LIMITED, Toronto.

HLUNGWANI O., RIKHOTSO J., DONG H., and MOYS M.H., 2003, "Further Validation of Dem Modeling of Mill: Effects of Liner Profile and Mill Speed", *Minerals Engineering*, 16 (2003) 993-998.

JUVINALL R.C., 1983, *Fundamentals of Machine Component Design*, John Wiley & Sons, Toronto.

KING R.P., 2001, *Modeling & Simulation of Mineral Processing Systems*, Butterworth-Heinmann, Boston.

KNECHT, J and PATZELT N., "Growing Mill Sizes, a Challenge for the Design of Large Diameter SAG Mills", *Paper presented at the SAG 1996 Conference*, Vancouver.

KUTZ M., 2002, *Handbook of Materials Selection*, John Wiley & Sons, New York.

LEE, M.K., 2001, *Design for Manufacturability of Speed-Reduction Cam Mechanisms*, M.Eng., Thesis, McGill University, Canada.

MEADOWS J.D., 1998, *Measurement of Geometric Tolerances in Manufacturing*, Marcel Dekker, Inc., New York.

MORRELL, S., Power draw of wet tumbling mills and its relationship to charge dynamics- Part 1: a continuum approach to mathematical modelling of mill power draw, *Transaction of the Institution of Mining and Metallurgy*, Sec. C, no.105, C43-45.

MULAR A.L. and JERGENSEN G.V., 1982, *Design and Intallation of Comminution Circuits*, Society of Mining Engineers of the American Institute of Mining, Metallurgical, and Petroleum Engineers, Inc., New York, New York.

NORTON R.L., 2002, *CAM DESIGN and Manufacturing Handbook*, Industrial Press, Inc., New York.

PRYOR E.J., 1955, *AN Introduction to Mineral Dressing*, MINING PUBLICATIONS, LTD., London.

PRYOR E.J., 1965, *Mineral Processing*, ELSEVIER PUBLISHING GO LTD, Ameterdam.

RADZISZEWSKI P. and TARASIEWICZ S., "Grinding Process Simulation in a Ball mill", *7th Intl Conf. Math. & Comp. Modeling Proceedings*, Chicago.

RADZISZEWSKI P. and Morrell, S., 1998, "Fundamental Discrete Element Charge Motion Model Validation", *Minerals Engineering*, Vol. 11, No. 12, pp. 1161–1178.

RADZISZEWSKI P., 1999, "Comparing Three DEM Charge Motion Models", Minerals Engineering, Vol. 12, No. 12, pp. 809–826.

RADZISZEWSKI P. and VALERY W., 1999, "Candia SAG Mill Simulated Charge Behavior, CMP, Ottawa, Ontario, pp. 267–283.

RADZISZEWSKI P., 2000, An Update on Mill Media Impact Test Improvement, JKMRC/AMIRA P9L Technical Project Report, Queensland, Australia.

RADZISZEWSKI P., 2001, Exploring Total Media Wear, Mechanical Engineering Department Technical Report, McGill University, Montreal, Quebec.

ROCHARDS R.H. and LOCKE C.E., 1940, *Textbook of Ore Dressing*, McGRAW-HILL BOOK COMPANY, INC., NEW YORK AND LONDON.

SPOTTS M.F., 1983, *Dimensioning and Tolerancing for Quantity Production*, Prentice-Hall, Inc., Englewood Cliffs, New Jersey.

TAGGART, A.F., 1945, *Handbook of Mineral Dressing*, JOHN WILEY & SONS, Inc., NEW YORK

WILLS B.A., 1997, *Mineral Processing Technology*, Butterworth-Heinmann, Boston.

YALCIN T., 1994, *Innovations in Mineral Processing*, ACME PRINTERS, Subdury, Ontario.

ZHANG H.C., 1997, *Advanced Tolerancing Techniques*, JOHN WILEY & SONS, INC., New York.

ZHANG W.M., 2003, *Cam-Profile Optimization by Means of Undercutting in Cam Roller Speed Reducers*, M.Eng., Thesis, McGill University, Canada.

APPENDIX A

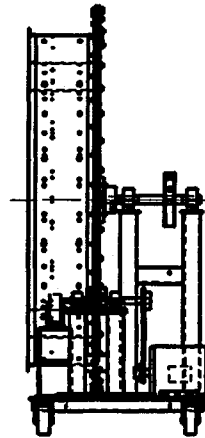
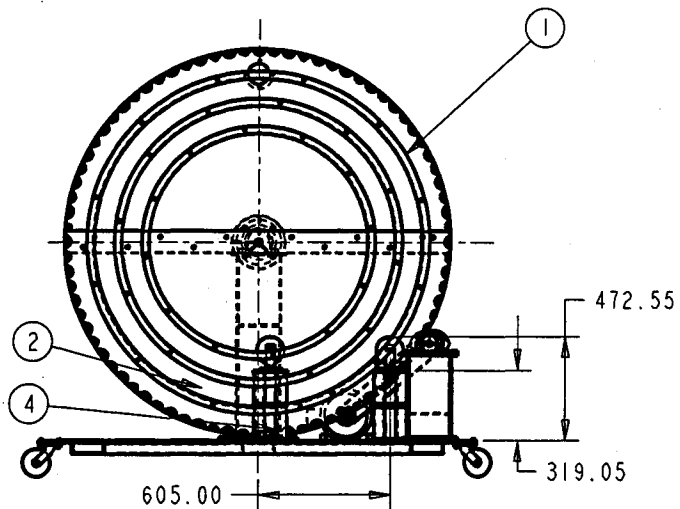
Engineering Drawings of the Cam-Driven Laboratory Ball Mill and its Components


A.1. Drawings of the Cam-Driven Laboratory Ball Mill and Components

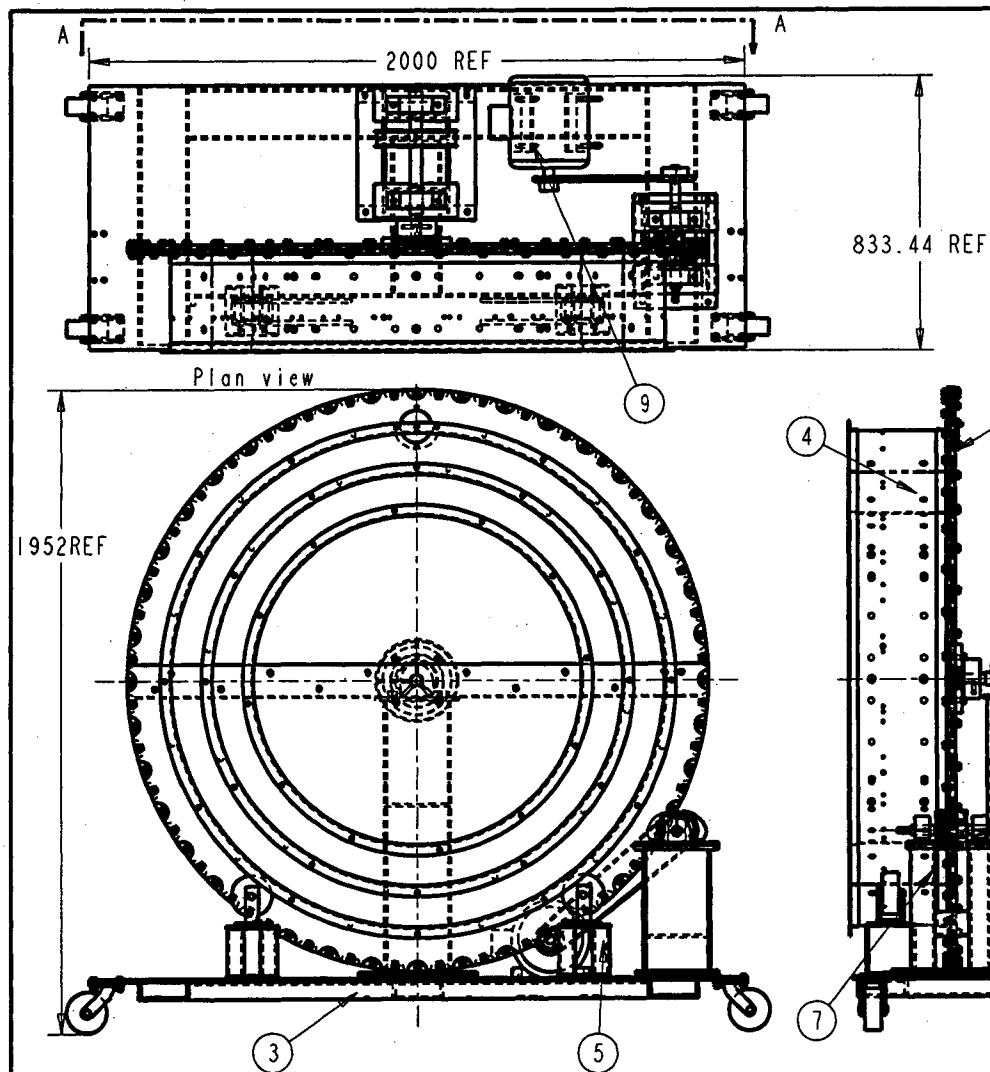
The summary of component names, codes and figure numbers is given in table A.1.

Page	PART NAME	DWG No.
A 1	*General assembly	CD01-000
A 2	*General assembly	CD01-001
A 3	*General assembly	CD01-001
A 4	*Disc and supports	CD01-002
A 5	*Supports elements	CD01-003
A 6	*Disc subassembly	CD01-100
A 7	Disc half, back detail	CD01-101
A 8	Disc half, front	CD01-102
A 9	Hub, detail	CD01-103
A10	Cover	CD01-104
A 11	*Cams & sensor subassembly	CD01-200
A 12	Cams subassembly	CD01-201
A 13	Cam, detail	CD01-202
A 14	Shaft	CD01-203
A 15	*Base subassembly & weldment	CD01-300
A16	C-Channels	CD01-301
A17	C-Channel 3	CD01-303
A18	C-Channel 4	CD01-304
A19	Base plate	CD01-305
A20	*Drum	CD01-400
A21	Plexiglass cover	CD01-402
A22	Drum unfolded	CD01-403
A23	Angle unfolded	CD01-404
A24	*Support for rollers	CD01-500
A25	Top plate	CD01-501

A26	C-Channel	CD01-502
A27	Bottom plate	CD01-503
A28	*Brake support	CD01-600
A29	C channel vertical	CD01-601
A30	Top plate	CD01-602
A31	C-Channel horizontal	CD01-603
A32	Bottom plate	CD01-604
A33	Contact plate	CD01-605
A34	*Cam support	CD01-700
A35	Top plate	CD01-702
A36	C channel horizontal	CD01-703
A37	Bottom plate	CD01-704
A38	Support plate	CD01-705
A39	Spacer (cam support)	CD01-706
A40	*Brake shaft subassembly	CD01-800
A41	Brake shaft	CD01-801
A42	Brake drum	CD01-802
A43	*Support spacer	CD01-900
A44	Cam & support subassembly	CD01-1100
A45	Cam & support subassembly	CD01-1100
A46	Tension brake & support subassembly	CD01-1200
A47	Brake & support subassembly	CD01-1300

[illegible]

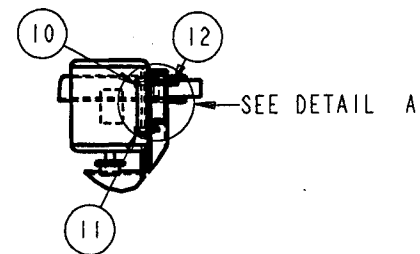
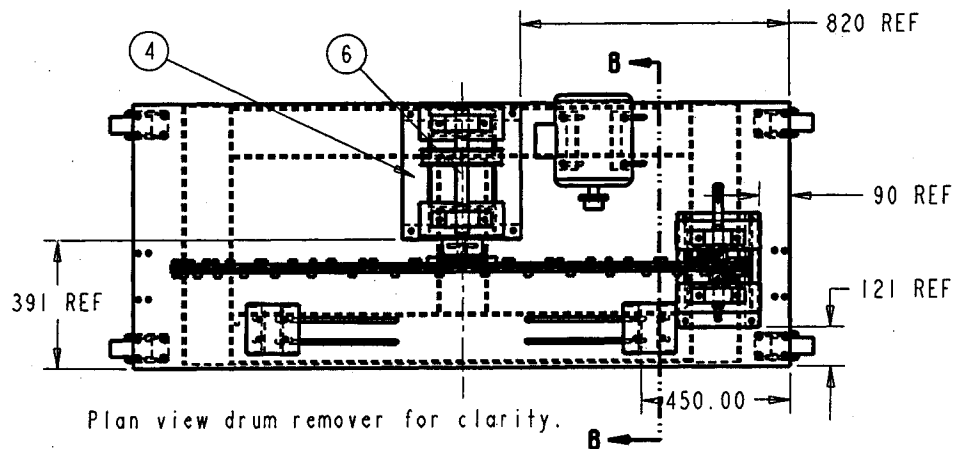
SUBASSEMBLY NAME: General assembly				NO.		REVISION		DATE		BY	
Unless otherwise specified 1. TOLERANCE ON: X, Y is ± 0.2 X.X is ± 0.2 X.XX is ± 0.05 2. ANGULAR TOLERANCE: ± 0.5 3. LAST REVISION INDICATED BY: <input type="checkbox"/> 4. SURFACE FINISH : 32						1		Final DWG.		02/12/03 Lei Geng	
						2					
DRAWN BY: L. GENG				DESIGNED BY: L. GENG				McGILL UNIVERSITY COMMUNITION DYNAMICS LABORATORY			
CHECKED BY: R. PERLIN				APPROVED BY: P. RADZISZEWSKI							
PROJECTION 		DIMENSION IN:		SIZE:		SCALE:		SHEET:		DWG NO CD01-000	
										REV	



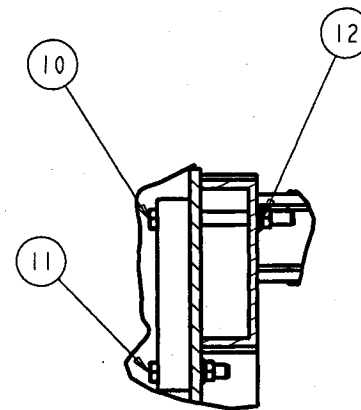
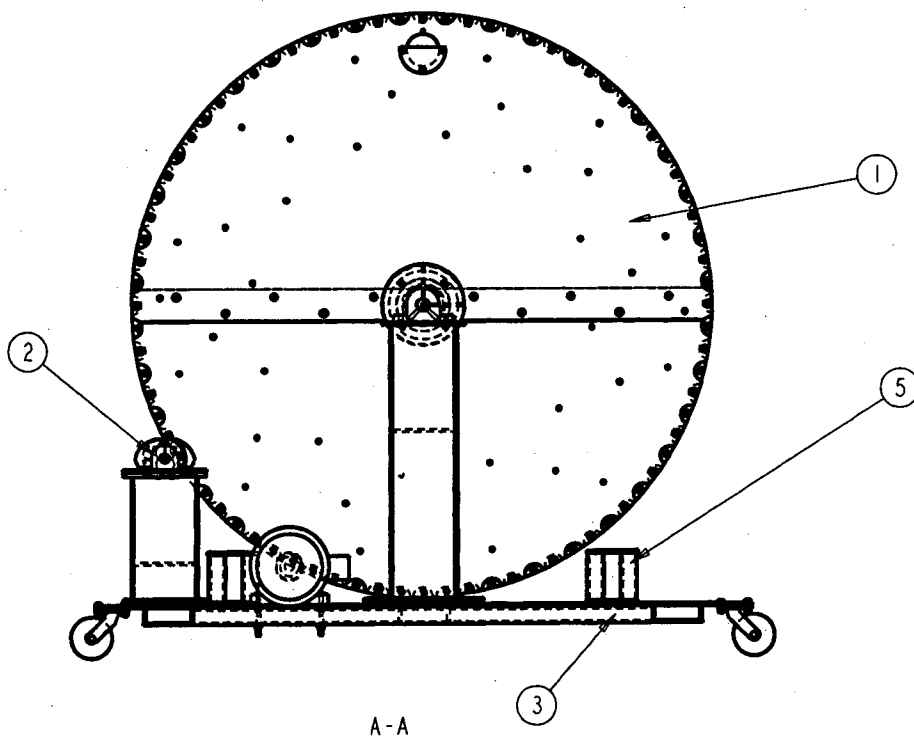
NO	PART NAME	PART CODE	QTY	MAT.
1	Disc assembly	CD01-100	1	
2	Cam subassembly	CD01-200	1	
3	Base subassembly	CD01-300	1	
4	Drum	CD01-400	1	
5	Support	CD01-500	2	
6	Brake support	CD01-600	1	
7	Cam support	CD01-700	1	
8	Brake shaft	CD01-800	1	
9	Motor		1	
10	1/2-UNC x 4" HEX HD BOLT		13	
11	1/2-UNCX 2" HEX HD BOLT		7	
12	1/2-UNC NUT & WASHER		20	

Note: 1. For view A-A see sheet 2 of 2
2. The disc rotate CW.

SUBASSEMBLY NAME:		NO.	REVISION	DATE	BY
General Assembly		1			
		2			
Unless otherwise specified: 1. TOLERANCE ON: X is ± 0.5 X.X is ± 0.2 X.XX is ± 0.05 2. ANGULAR TOLERANCE: ± 0.5 3. LAST REVISION INDICATED BY: <input type="checkbox"/> 4. SURFACE FINISH: 32		MATERIAL DESIGNED BY: L. GENG CHECKED BY: R. PERLIN APPROVED BY: P. RADZISZEWSKI			
PROJECTION DIMENSION		SIZE:	SCALE: 1:300	SHEET: 1 of 2	DWG NO. CD01-001 REV 0

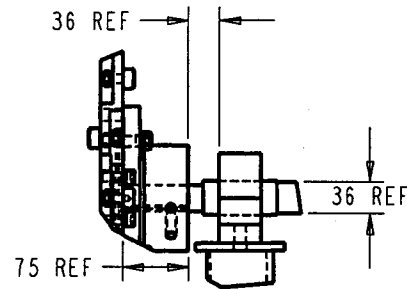
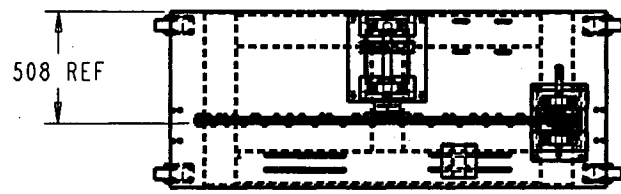


SECTION B-B
Rotated 90°

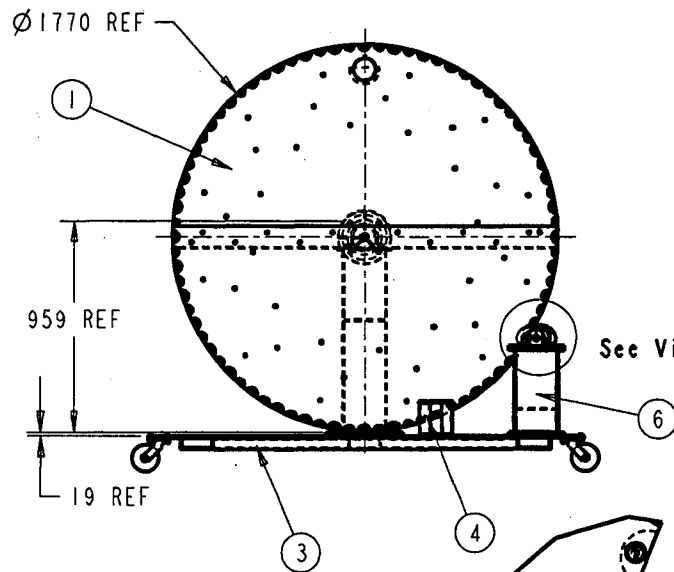


DETAIL A

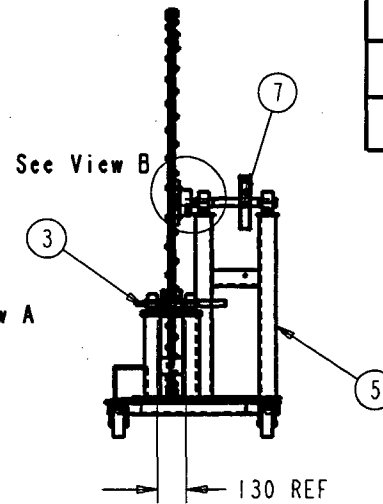
SUBASSEMBLY NAME:		NO.	REVISION	DATE	BY
General assembly		1			
		2			
Unless otherwise specified 1. TOLERANCE ON: X. is ± 0.5 X.X is ± 0.2 X.XX is ± 0.05 2. ANGULAR TOLERANCE: ± 0.5 3. LAST REVISION INDICATED BY: <input type="checkbox"/> 4. SURFACE FINISH: 32		MATERIAL: L. GENG R. PERFIN		DESIGNED BY: L. GENG APPROVED BY: P. RADZISZEWSKI	
PROJECTION: DIMENSION: mm SIZE: SCALE: SHEET: 2 of 2		MCGILL UNIVERSITY COMMINUTION DYNAMICS LABORATORY DWG NO. CD01-001 REV			



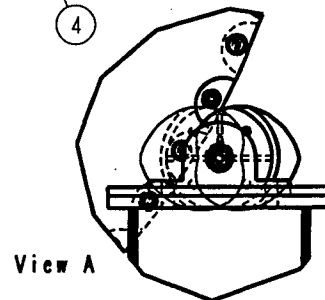
View B



See View A




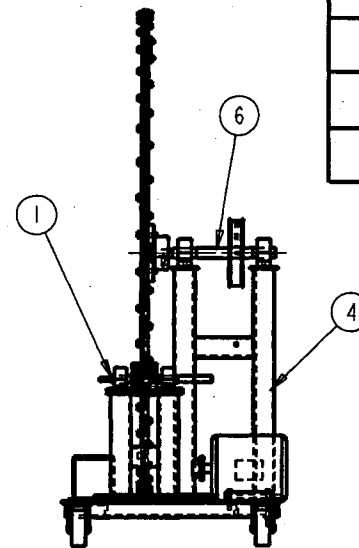
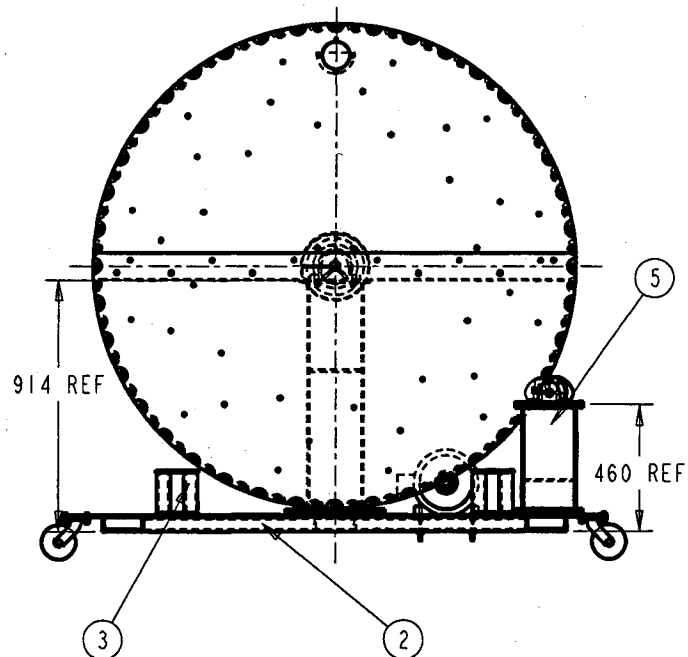
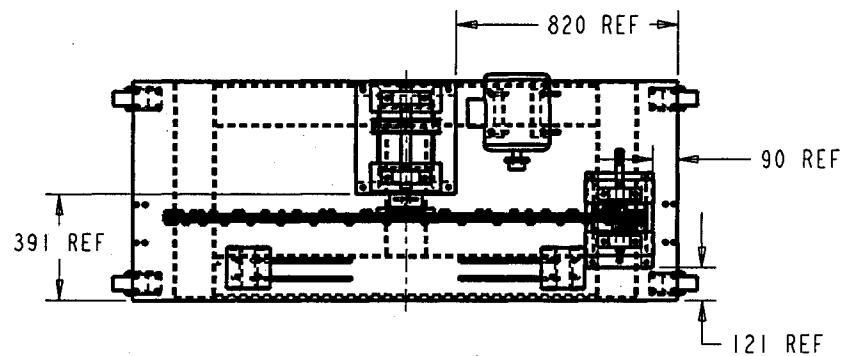
See View B



View A

NO	PART NAME	PART CODE	QTY	MAT.
1	Disc	CD01-100		
2	Cams shaft	CD01-200		
3	Frame	CD01-300		
4	Mill support	CD01-500		
5	Brake Support	CD01-600		
6	Cam support	CD01-700		
7	Brake shaft	CD01-800		

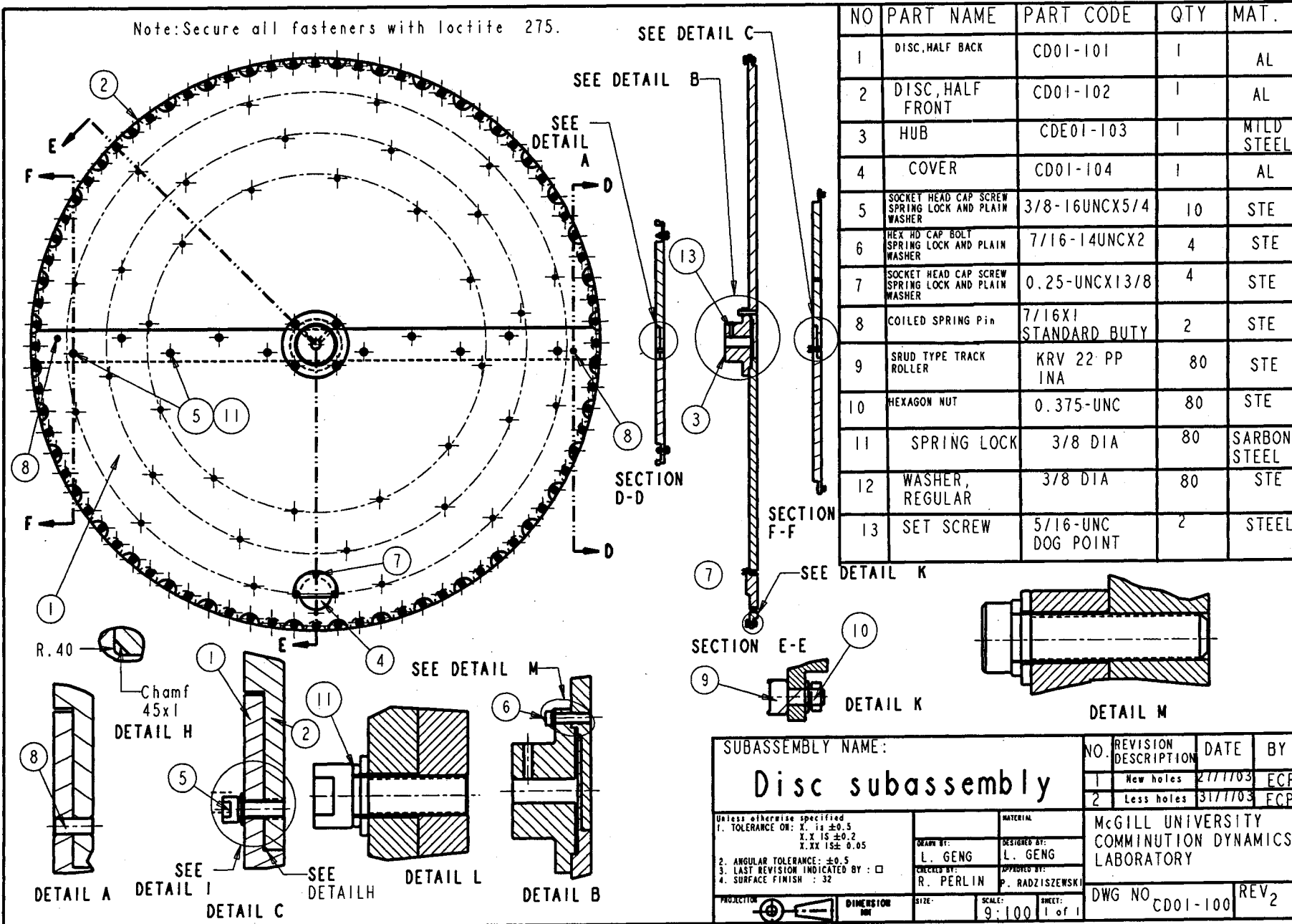
SUBASSEMBLY NAME:				NO.		REVISION		DATE		BY	
Disc and Supports				1							
				2							
Unless otherwise specified 1. TOLERANCE ON: X. is ± 0.5 X.X is ± 0.2 X.XX is ± 0.05 2. ANGULAR TOLERANCE: ± 0.5 3. LAST REVISION INDICATED BY: <input type="checkbox"/> 4. SURFACE FINISH : 32						MATERIAL		MCGILL UNIVERSITY COMMINUTION DYNAMICS LABORATORY			
DRAWN BY: L. GENG		DESIGNED BY: L. GENG									
CHECKED BY: R. PERLIN		APPROVED BY: P. RADZISZEWSKI									
PROJECTION				DIMENSION		SIZE:		SCALE:		SHEET:	
				mm				1:300		1 of 1	
				DWG NO				CD01-002		REV 0	



NO	PART NAME	PART CODE	QTY	MAT.
1	Cams shaft	CD01-200		
2	Frame	CD01-300		
3	Mill support	CD01-500		
4	Brake support	CD01-600		
5	Cam support	CD01-700		
6	Brake and shaft	CD01-800		

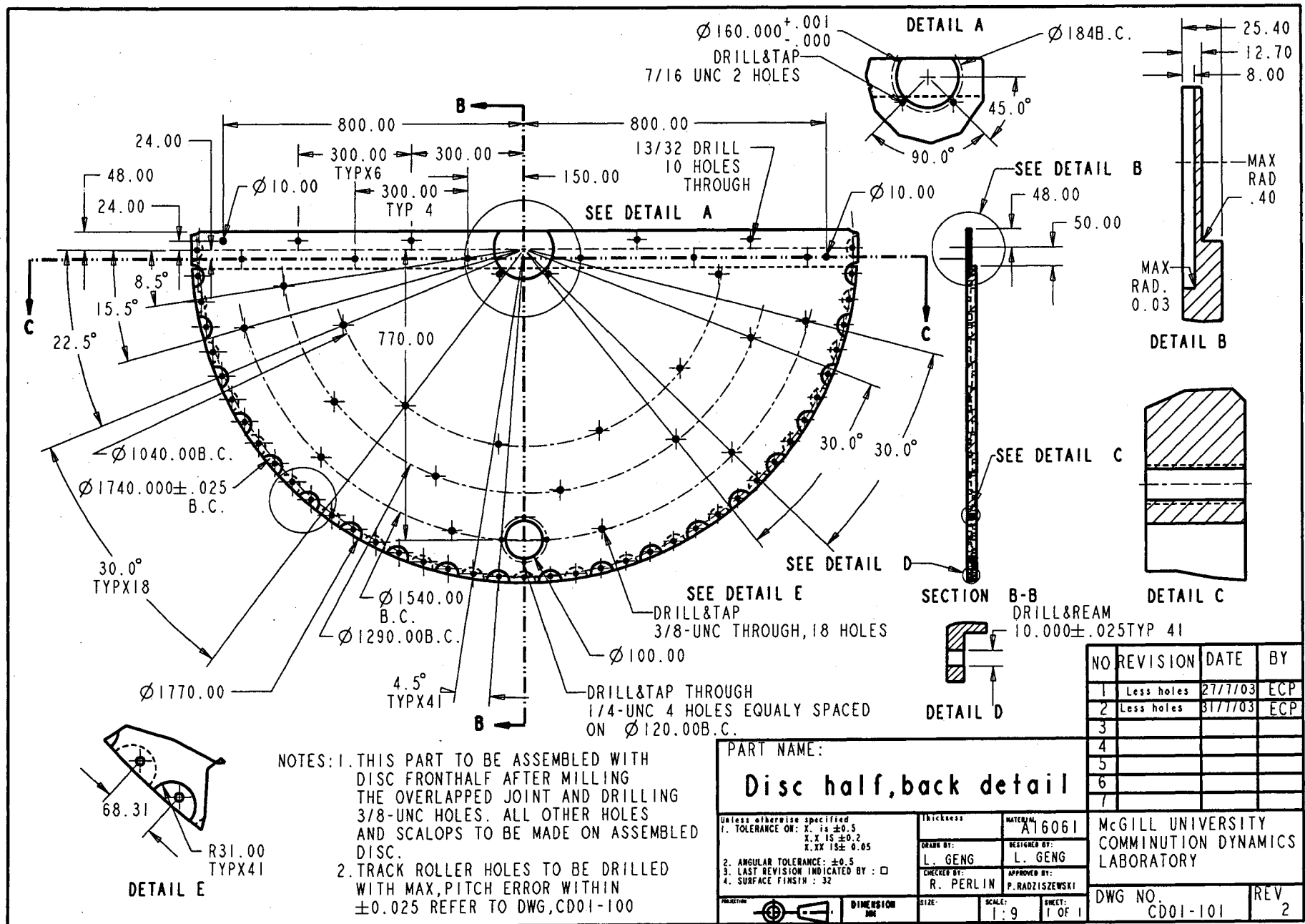
SUBASSEMBLY NAME:		NO.	REVISION	DATE	BY
Supports elements		1			
		2			
<small>Unless otherwise specified</small> 1. TOLERANCE ON: X: ± 0.5 Y: ± 0.2 Z: ± 0.05 2. ANGULAR TOLERANCE: ± 0.5 3. LAST REVISION INDICATED BY: <input type="checkbox"/> 4. SURFACE FINISH: 32		MATERIAL: DESIGNED BY: L. GENG CHECKED BY: R. PERLIN APPROVED BY: P. RADZISZEWSKI		MCGILL UNIVERSITY COMMUNION DYNAMICS LABORATORY	
PROJECTION: DIMENSION: mm		SIZE:	SCALE: 1:20	DWG NO: CD01-003 REV: 0	

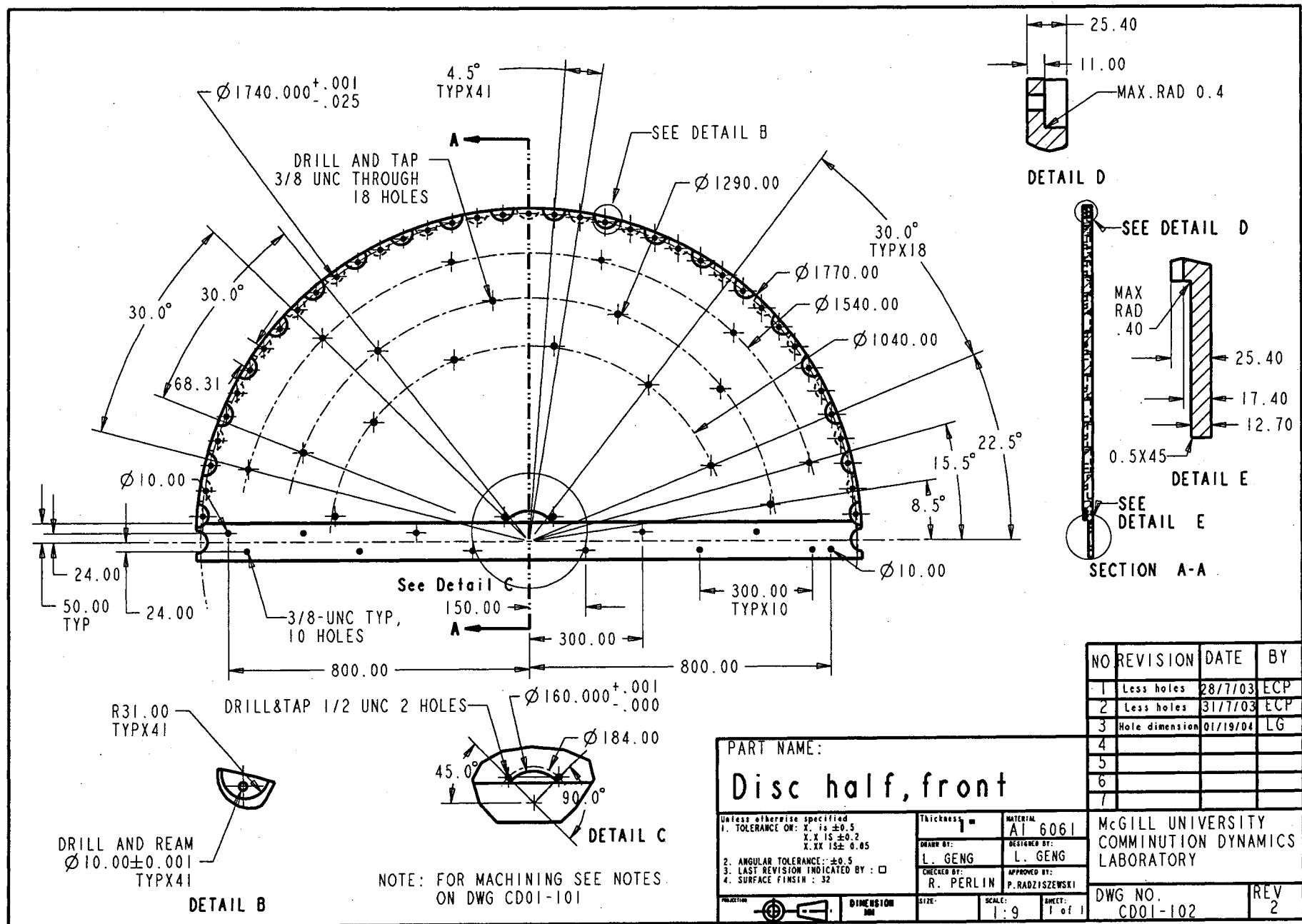
Note: Secure all fasteners with loctite 275.



NO	PART NAME	PART CODE	QTY	MAT.
1	DISC, HALF BACK	CD01-101	1	AL
2	DISC, HALF FRONT	CD01-102	1	AL
3	HUB	CDE01-103	1	MILD STEEL
4	COVER	CD01-104	1	AL
5	SOCKET HEAD CAP SCREW SPRING LOCK AND PLAIN WASHER	3/8-16UNCX5/4	10	STE
6	HEX HD CAP BOLT SPRING LOCK AND PLAIN WASHER	7/16-14UNCX2	4	STE
7	SOCKET HEAD CAP SCREW SPRING LOCK AND PLAIN WASHER	0.25-UNCX13/8	4	STE
8	COILED SPRING Pin	7/16X1 STANDARD BUTY	2	STE
9	SRUD TYPE TRACK ROLLER	KRV 22 PP INA	80	STE
10	HEXAGON NUT	0.375-UNC	80	STE
11	SPRING LOCK	3/8 DIA	80	SARBON STEEL
12	WASHER, REGULAR	3/8 DIA	80	STE
13	SET SCREW	5/16-UNC DOG POINT	2	STEEL

SUBASSEMBLY NAME:		NO.	REVISION DESCRIPTION	DATE	BY
Disc subassembly		1	New holes	2/7/703	ECP
		2	Less holes	3/7/703	ECP
Unless otherwise specified 1. TOLERANCE ON: X is ± 0.5 X.X is ± 0.2 X.XX is ± 0.05 2. ANGULAR TOLERANCE: ± 0.5 3. LAST REVISION INDICATED BY: <input type="checkbox"/> 4. SURFACE FINISH: 32		MATERIAL L. GENG R. PERLIN P. RADZISZEWSKI		McGill UNIVERSITY COMMUNION DYNAMICS LABORATORY	
PROJECTION DIMENSION		SIZE:	SCALE:	SHEET:	DWG NO
			9:100	1 of 1	CD01-100
					REV 2





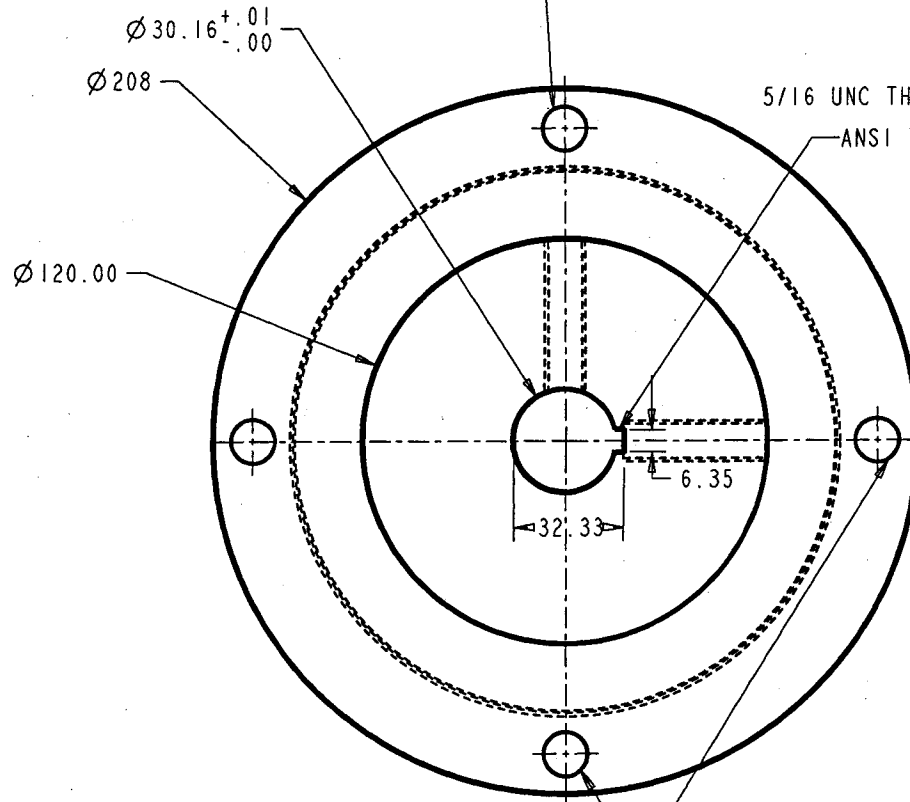
NO	REVISION	DATE	BY
1	Less holes	28/7/03	ECP
2	Less holes	31/7/03	ECP
3	Hole dimension	01/19/04	LG
4			
5			
6			
7			

PART NAME:
Disc half, front

1. TOLERANCE ON: X: IS ± 0.5 X: X IS ± 0.2 X: XX IS ± 0.05 2. ANGULAR TOLERANCE: ± 0.5 3. LAST REVISION INDICATED BY: <input type="checkbox"/> 4. SURFACE FINISH: 32	Thickness: 1 DRAWN BY: L. GENG CHECKED BY: R. PERLIN APPROVED BY: P. RADZISZEWSKI	MATERIAL: A1 6061 DESIGNED BY: L. GENG P. RADZISZEWSKI
DIMENSION: 300 SCALE: 1:9 SHEET: 1 of 1		

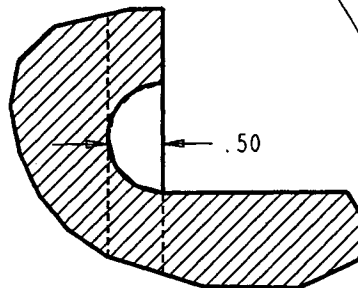
McGill University COMMINUTION DYNAMICS LABORATORY	DWG NO. CD01-102	REV 2
---	---------------------	----------

15/32, 2 HOLES ON 184 B.C. EQUALLY SPACED.

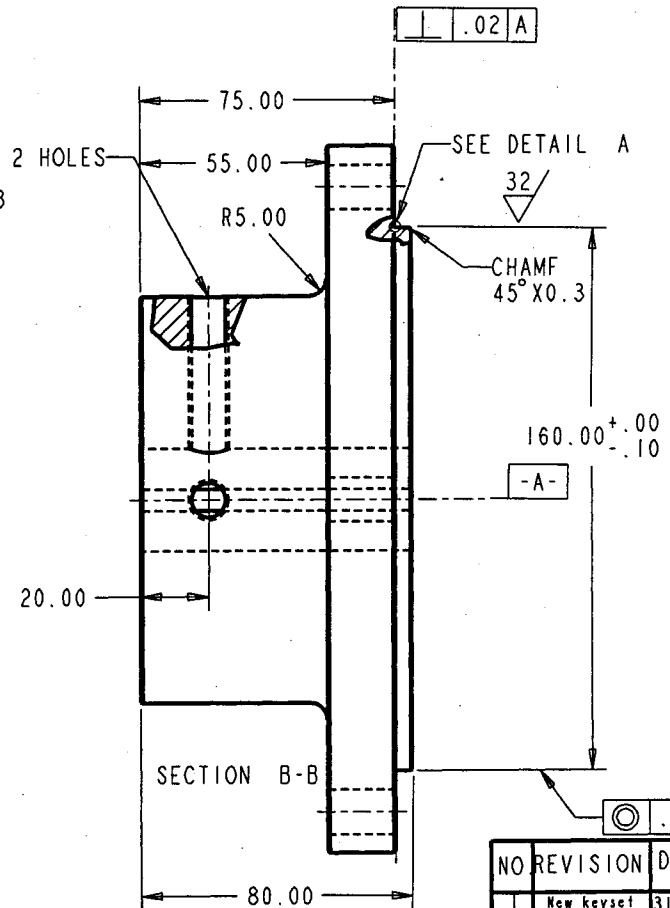


5/16 UNC THROUGH 2 HOLES
ANSI TI.273

17/32, 2 HOLES ON
184 B.C. EQUALLY SPACED.



DETAIL A



SECTION B-B

NO	REVISION	DATE	BY
1	New keyset	31/7/03	ECP
2	Hole dimension	18/01/04	LG
3			
4			
5			
6			
7			

PART NAME:

Hub, detail

Unless otherwise specified
1. TOLERANCE ON:
A. IS ± 0.5
X.X 16 ± 0.2
X.XX 16 ± 0.05
2. ANGULAR TOLERANCE: ± 0.5
3. LAST REVISION INDICATED BY: ☐
4. SURFACE FINISH: 32

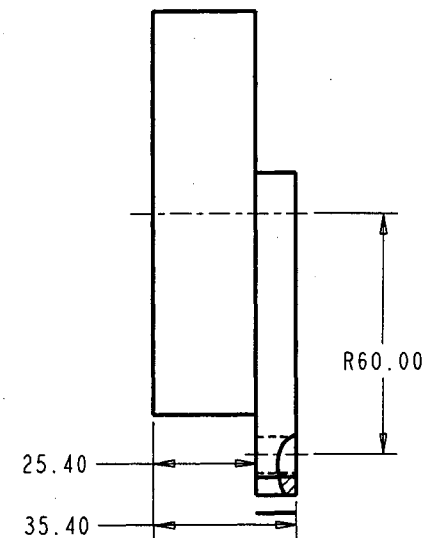
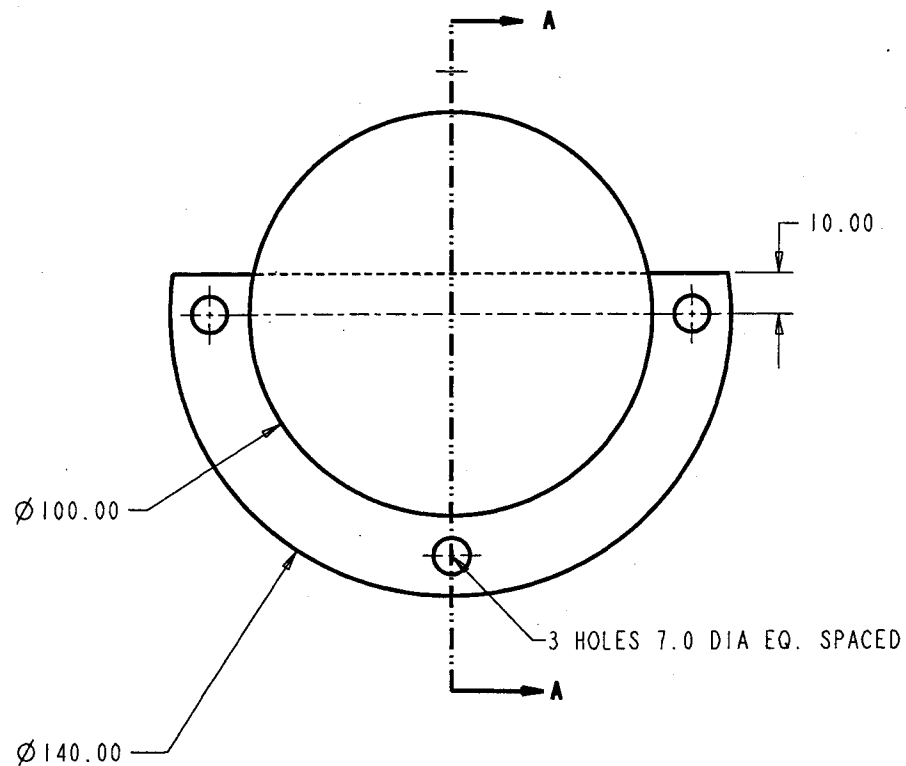
MATERIAL: Steel
DRAWN BY: L. GENG
DESIGNED BY: L. GENG
CHECKED BY: R. PERLIN
APPROVED BY: P. RADZISZEWSKI

McGILL UNIVERSITY
COMMINUTION DYNAMICS
LABORATORY

DWG NO CD01-103 REV 1

PROJECTION: DIMENSION: mm

SIZE: SCALE: 1:1.5 SHEET: 1 of 1

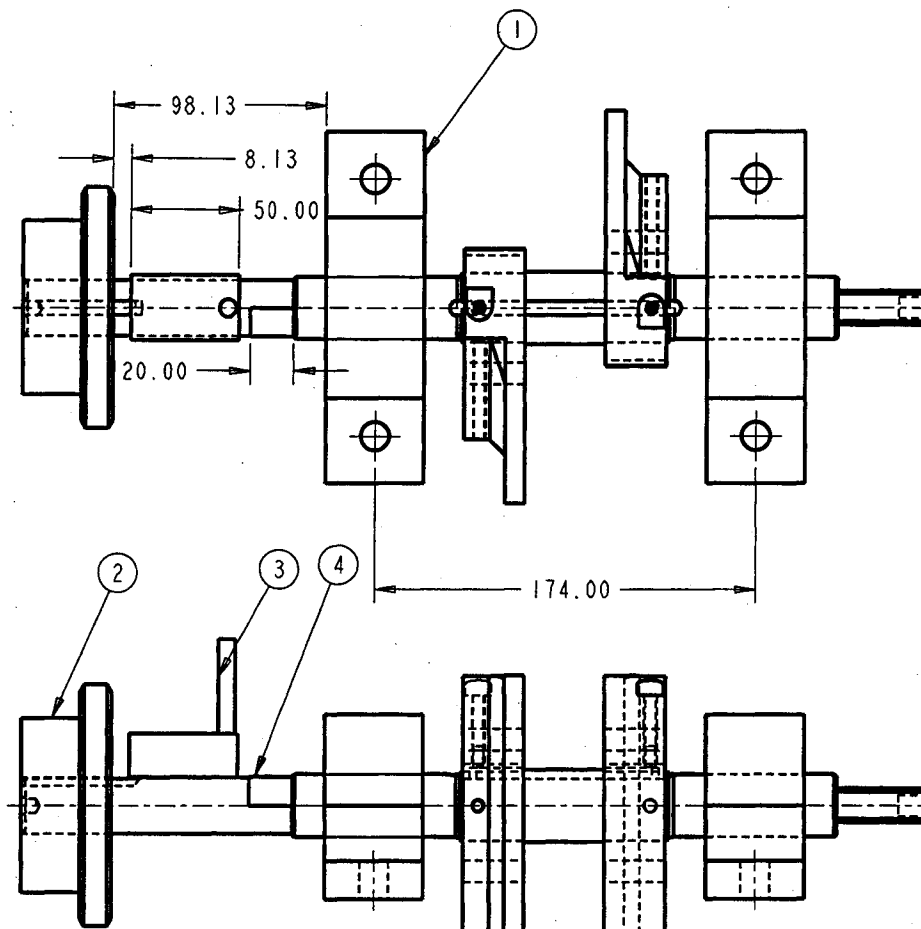


SECTION A-A

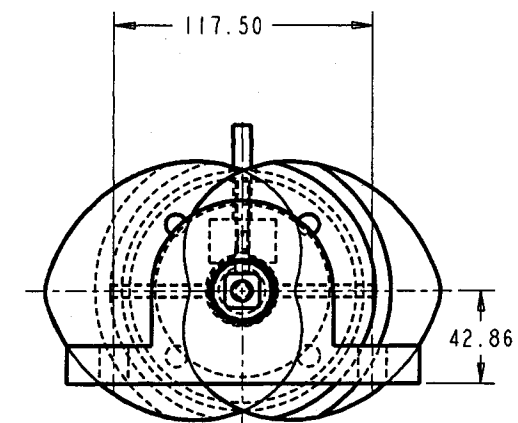
PART NAME:		NO	REVISION	DATE	BY
Cover		1	Smaller holes	31/7/03	ECP
		2			
		3			
		4			
		5			
		6			
		7			

Unless otherwise specified 1. TOLERANCE ON: X. is ± 0.5 X.X is ± 0.2 X.XX is ± 0.05 2. ANGULAR TOLERANCE: ± 0.5 3. LAST REVISION INDICATED BY: <input type="checkbox"/> 4. SURFACE FINISH: 32		MATERIAL 45	MCGILL UNIVERSITY COMMINUTION DYNAMICS LABORATORY
DRAWN BY: L. GENG	DESIGNED BY: L. GENG		
CHECKED BY: R. PERLIN	APPROVED BY: P. RADZISZEWSKI	DWG NO CD01-104	REV 1

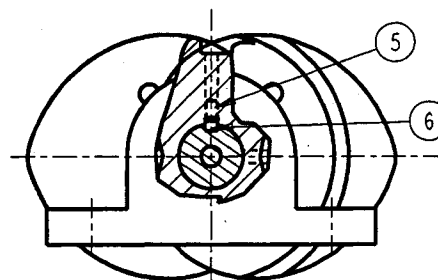
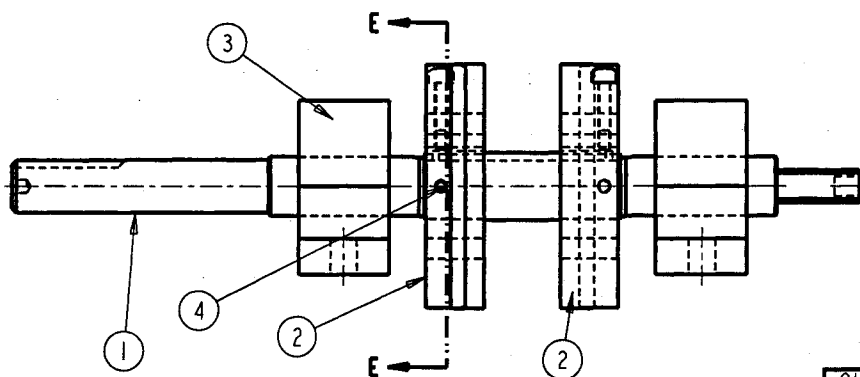
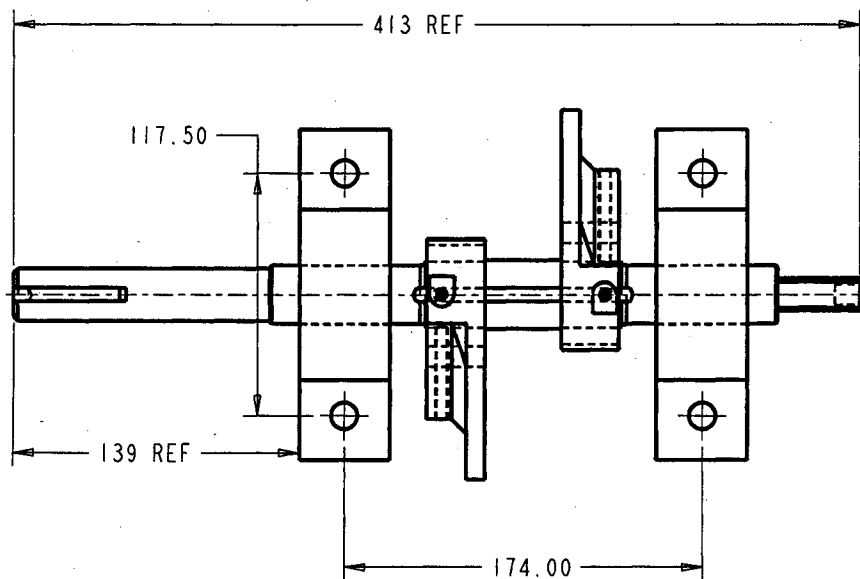
PROJECTION	DIMENSION	SIZE	SCALE	SHEET
	mm		1:1	1 of 1



NO	PART NAME	PART CODE	QTY	MAT.
1	Cams subassembly	CD01-201	1	
2	Sprocket	80B9	1	
3	Sensor		1	
4	Telemetry		1	



SUBASSEMBLY NAME:		NO.	REVISION	DATE	BY
Cam & sensor subassembly		1			
		2			
Unless otherwise specified 1. TOLERANCE ON: X.X is ± 0.5 X.X is ± 0.2 X.XX is ± 0.05 2. ANGULAR TOLERANCE: ± 0.5 3. LAST REVISION INDICATED BY: <input type="checkbox"/> 4. SURFACE FINISH: 32		MATERIAL: DESIGNED BY: L. GENG CHECKED BY: R. PERLIN APPROVED BY: P. RADZISZEWSKI		MCGILL UNIVERSITY COMMUNION DYNAMICS LABORATORY	
PROJECTION 	DIMENSION MM	SIZE: 1:2	SCALE: 1:2	SHEET: 1 of 1	DWG NO. CD01-200 REV 0

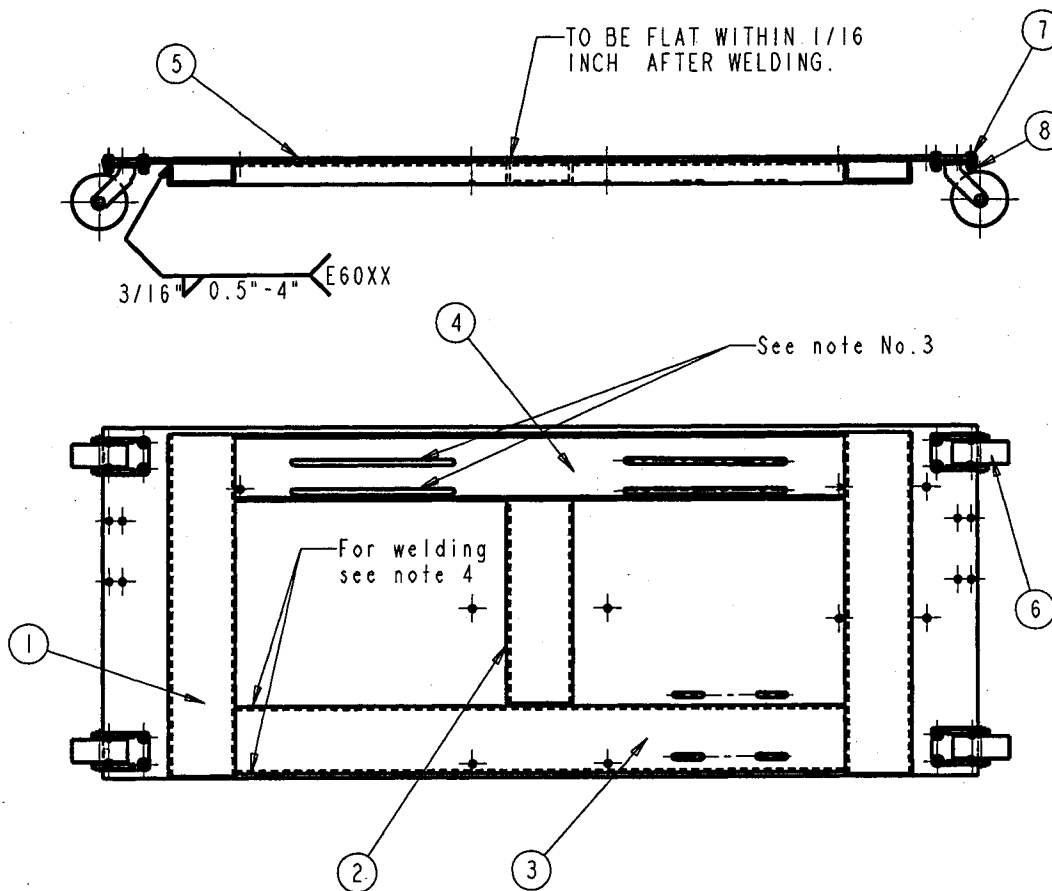


SECTION E-E

NOTE: The shape of cam is described on the CD disc.

NO	PART NAME	PART CODE	QTY	MAT.
1	Shaft	CD01-203	1	STE
2	Cam	CD01-202	2	STE
3	Pillow block		2	STE
4	SET SCREW	1/4-UNCX3/8	4	STE
5	KEY	1/4X1/4	2	STE

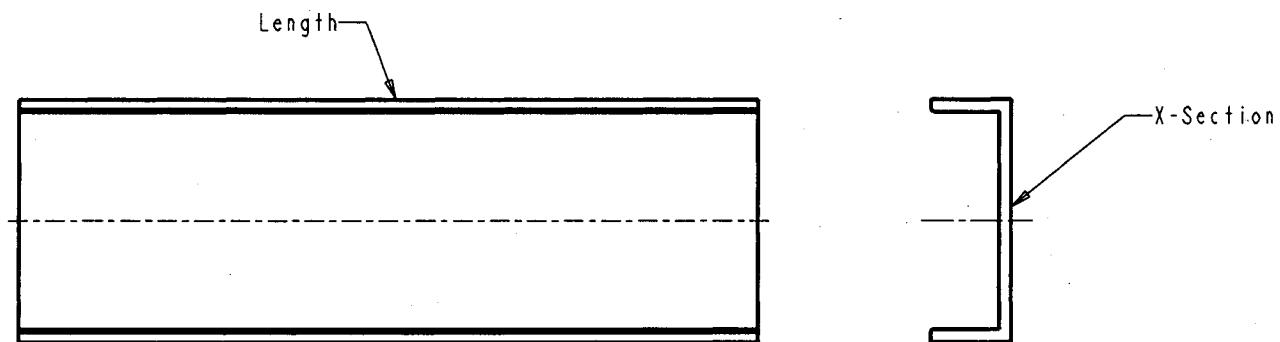
SUBASSEMBLY NAME: Cams subassembly		NO.	REVISION	DATE	BY
		1	Square shape	28/7/0	ECP
		2	Shorter	31/7/0	ECP
<small>Unless otherwise specified</small> 1. TOLERANCE ON: X is ± 0.5 X.Y is ± 0.2 X.XX is ± 0.05 2. ANGULAR TOLERANCE: ± 0.5 3. LAST REVISION INDICATED BY: <input type="checkbox"/> 4. SURFACE FINISH: 32		MATERIAL L.GENG R. PERLIN		DESIGNED BY: L. GENG APPROVED BY: P. RADZISZEWSKI	
PROJECTION DIMENSION		SIZE:	SCALE:	SHEET:	DWG NO CD01-201
			1:2	1 of 1	REV 2



NO	PART NAME	PART CODE	QTY	MAT.
1	C Channel 1	CD01-301	2	STE.
2	C Channel 2	CD01-302	1	STE.
3	C Channel 3	CD01-303	1	STE.
4	C Channel 4	CD01-304	1	STE.
5	Base Plate	CD01-305	1	STE.
6	Caster wheel, swivel	MDED 5 PEB	4	
7	3/8 UNC BOLT		16	STE.
8	3/8 UNC NUTS, SPRING & FLAT WASHER		16	STE.

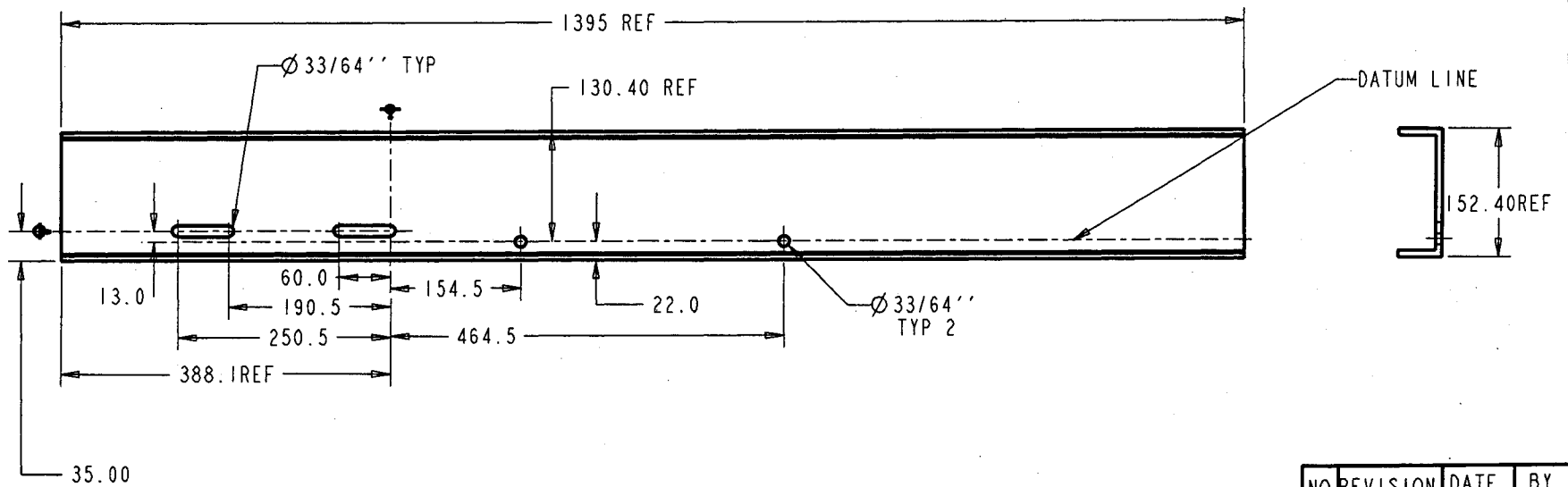
- Notes: 1. All T-joints and corner joints must be welded.
 2. Machining before welding.
 3. Slots on base plate item No. 5 and on channel item No. 4 to be aligned during welding.
 4. Weld with alternative technique to minimize distortion, seams to be 3/8 fillet x 1 1/2 long at 6 inch center to center, typ
 3/8 (1 1/2--6)

SUBASSEMBLY NAME:		NO.	REVISION	DATE	BY
Base subassembly & weldment		1	Notes	10/03	LG
		2			
<small>Unless otherwise specified</small> 1. TOLERANCE ON: X: is ± 0.5 X.X is ± 0.2 X.XX is ± 0.05 2. ANGULAR TOLERANCE: ± 0.5 3. LAST REVISION INDICATED BY: <input type="checkbox"/> 4. SURFACE FINISH: 32		MATERIAL DRAWN BY: L. GENG DESIGNED BY: L. GENG CHECKED BY: R. PERLIN APPROVED BY: P. RADZISZEWSKI		MCGILL UNIVERSITY COMMINUTION DYNAMICS LABORATORY	
PROJECTION DIMENSION		SIZE:	SCALE: 1:250	SHEET: 1 of 1	DWG NO. CD01-300 REV 1



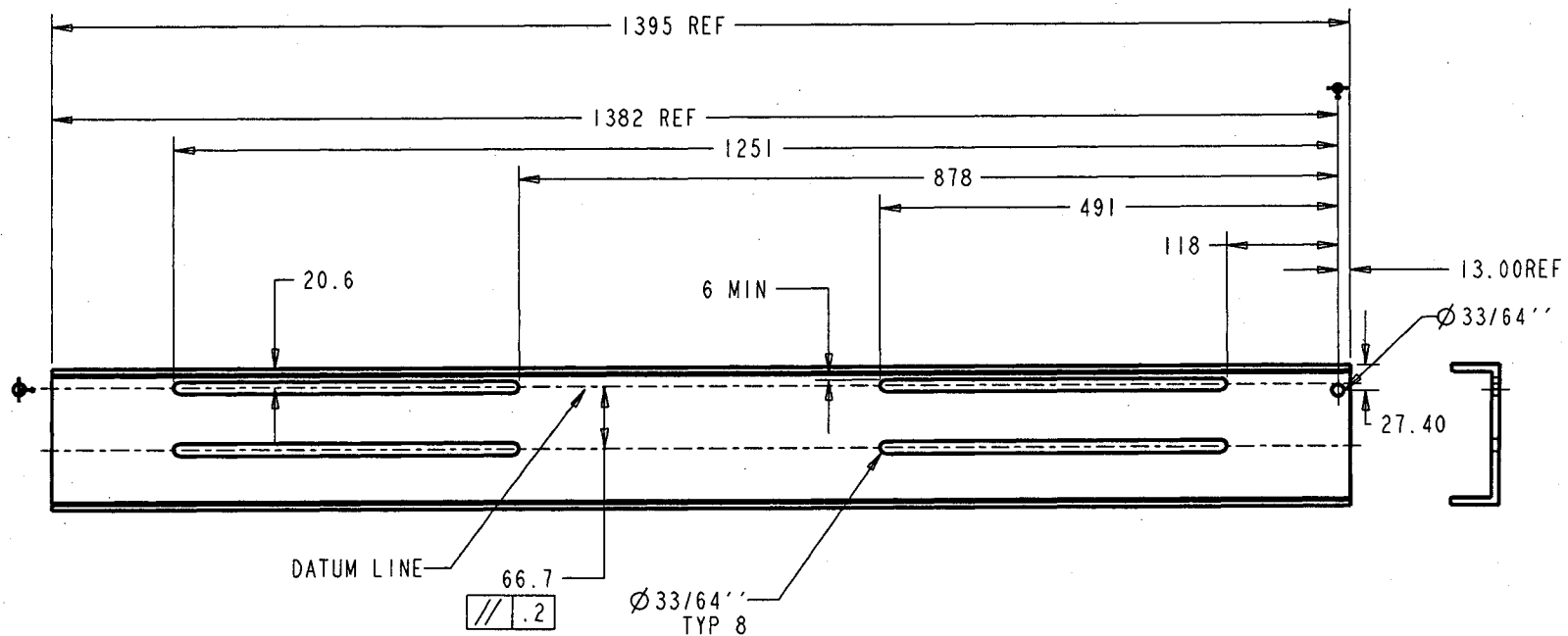
Part code	Length	X-section
CD01-301	780	C6
CD01-302	465	C6
CD01-601	824.68	C8
CD01-603	237.34	C8
CD01-701	416.68	C8
CD01-703	99.31	C8

PART NAME:		NO		REVISION	DATE	BY
C Channels		1	New length	5/8/03	ECP	
		2				
		3				
		4				
		5				
		6				
		7				
<small>Unless otherwise specified</small> 1. TOLERANCE ON: L. is ± 0.5 X.X is ± 0.2 X.XX is ± 0.05 2. ANGULAR TOLERANCE: ± 0.5 3. LAST REVISION INDICATED BY: <input type="checkbox"/> 4. SURFACE FINISH: 32		MATERIAL: DRAWN BY: L. GENG CHECKED BY: R. PERLIN		DESIGNED BY: L. GENG APPROVED BY: P. RADZISZEWSKI		MCGILL UNIVERSITY COMMINUTION DYNAMICS LABORATORY
DWG NO CD01-301		REV I				



NO	REVISION	DATE	BY
1	New shape	31/7/03	ECP
2			
3			
4			
5			
6			
7			

PART NAME:		C CHANNEL 3	
Unless otherwise specified 1. TOLERANCE ON: X is ± 0.5 X.X is ± 0.2 X.XX is ± 0.05 2. ANGULAR TOLERANCE: ± 0.5 3. LAST REVISION INDICATED BY: <input type="checkbox"/> 4. SURFACE FINISH: 32		MATERIAL: C6x8.20 DRAWN BY: L. GENG CHECKED BY: R. PERLIN DESIGNED BY: L. GENG APPROVED BY: P. RADZISZEWSKI	
DWG NO. CD01-303 SCALE: 1:5 SHEET: 1 of 1		MCGILL UNIVERSITY COMMINUTION DYNAMICS LABORATORY REV 1	



NO	REVISION	DATE	BY
1	Adpt to new drw	15/7/03	ECP
2	Move slots	31/7/03	ECP
3			
4			
5			
6			
7			

PART NAME:
C-Channel 4

Unless otherwise specified
1. TOLERANCE ON: X. is ± 0.5
X.X is ± 0.2
X.XX is ± 0.05
2. ANGULAR TOLERANCE: ± 0.5
3. LAST REVISION INDICATED BY: ☐
4. SURFACE FINISH: 32

DESIGNED BY:
L. GENG
CHECKED BY:
R. PERLIN
APPROVED BY:
P. RADZISZEWSKI

MATERIAL:
C6x8.20

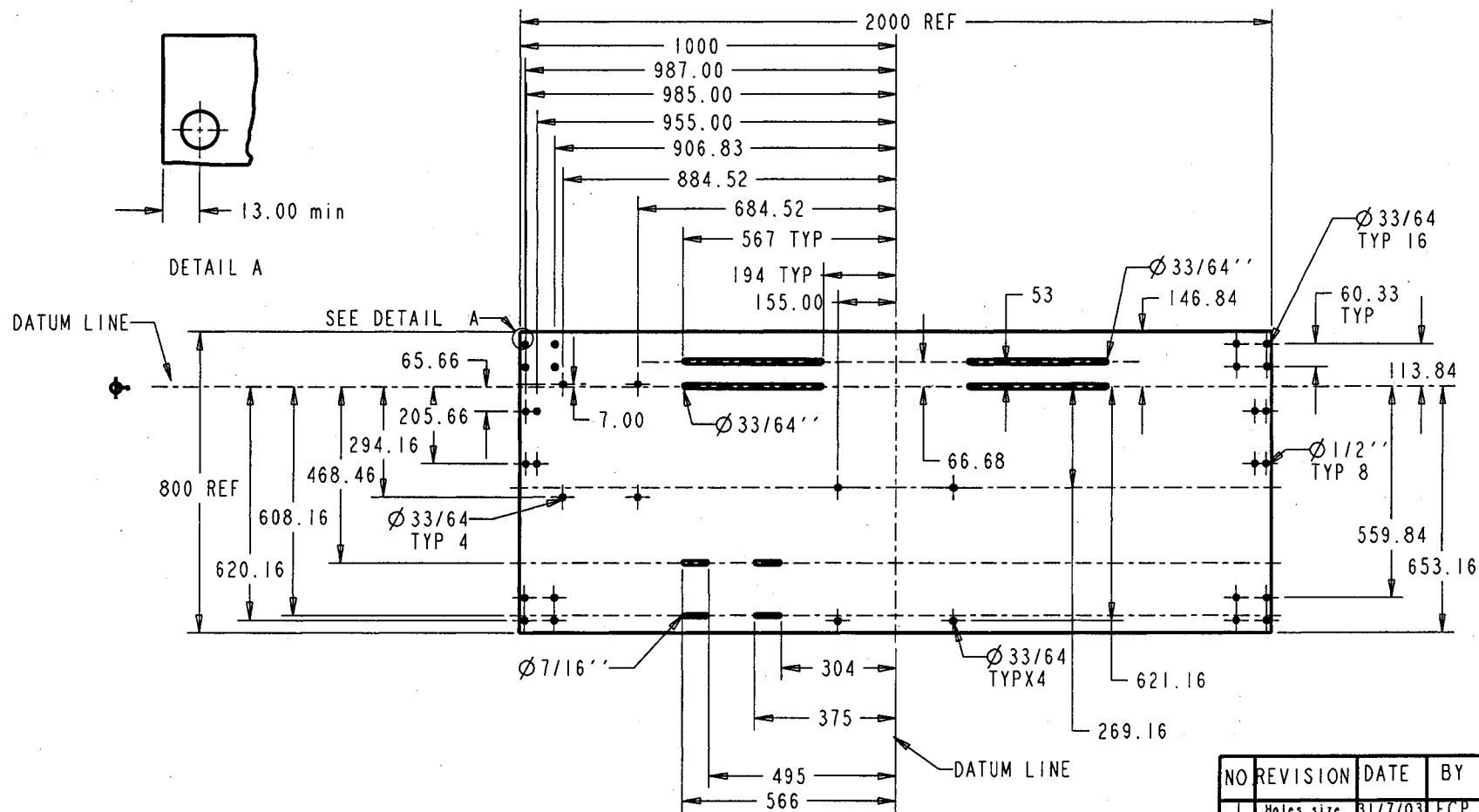
McGILL UNIVERSITY
COMMINUTION DYNAMICS
LABORATORY

DWG NO. CD01-304 REV 2



DIMENSION
mm

SIZE: SCALE: 1:5 SHEET: 1 of 1



- Notes:
1. The 4 groups of corner holes are equally spaced and symmetrical to the datum line.
 2. The 2 groups of small holes near the edge are equally spaced and symmetrical to the datum line.
 3. The 4 long slots are equally spaced and symmetrical to the datum line.
 4. All holes and slots are through the plate.

PART NAME:
BASE PLATE

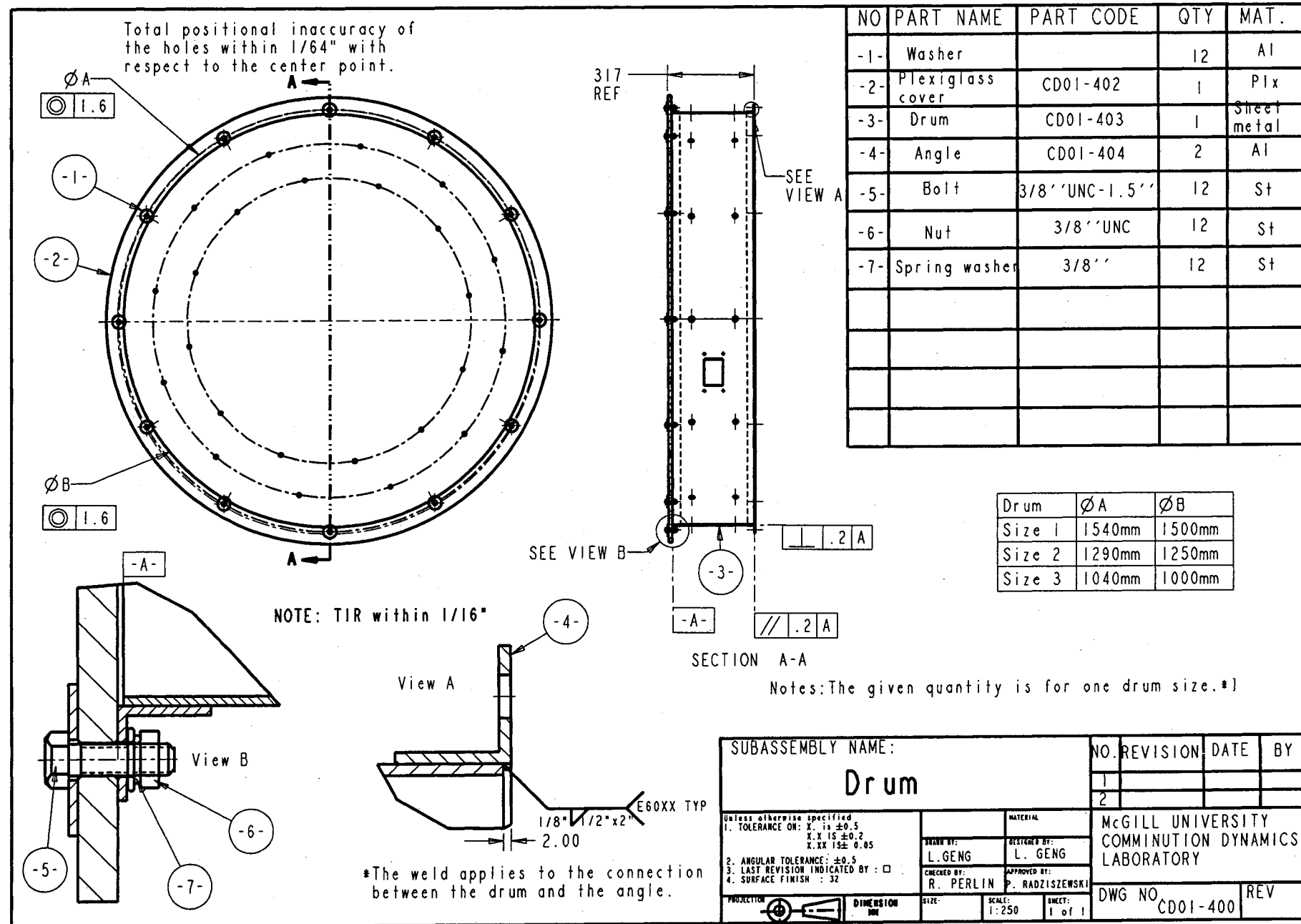
Unless otherwise specified
1. TOLERANCE ON: X: is ± 0.5
X.X IS ± 0.2
X.XX IS ± 0.05
2. ANGULAR TOLERANCE: ± 0.5
3. LAST REVISION INDICATED BY: ☐
4. SURFACE FINISH: 32

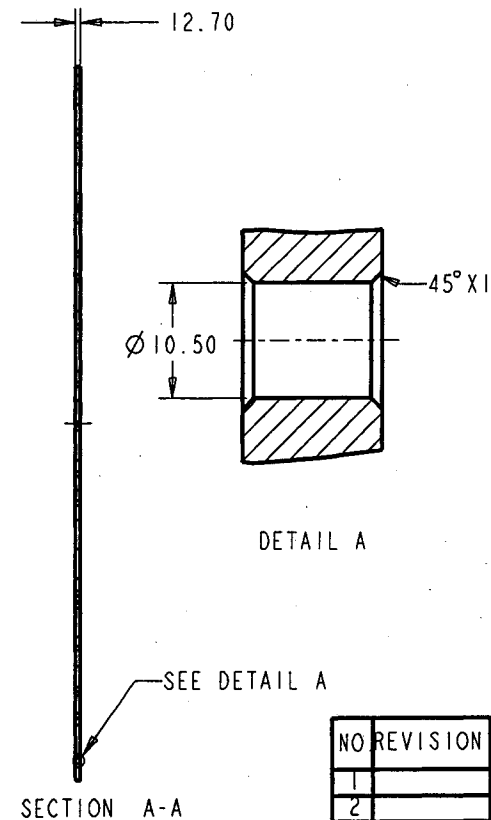
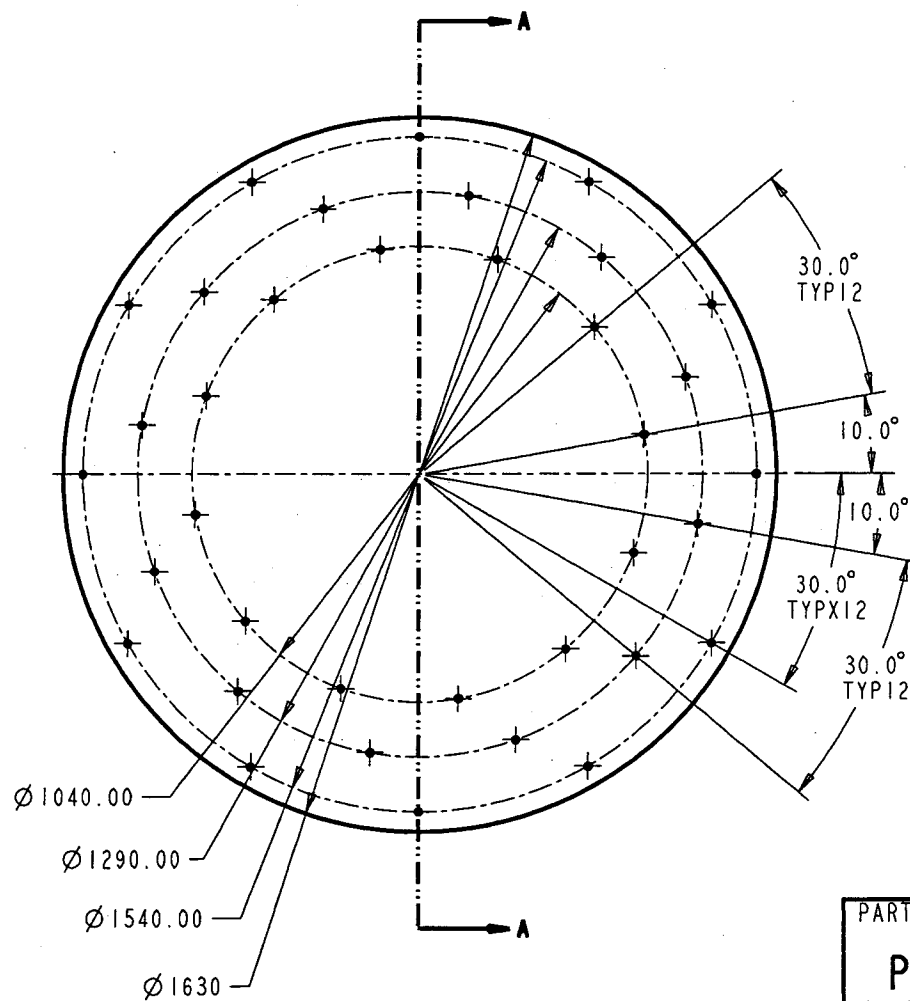
Thickness: **3/8"**
MATERIAL: Not Polished ASTM A36 OR EQUAL
DESIGNED BY: L. GENG
CHECKED BY: R. PERLIN
APPROVED BY: P. RADZISZEWSKI

NO	REVISION	DATE	BY
1	Holes size	3/17/03	ECP
2			
3			
4			
5			
6			
7			

McGILL UNIVERSITY
COMMINUTION DYNAMICS
LABORATORY

DWG NO CD01-305 REV 1





PART NAME:
PLEXIGLASS COVER

Unless otherwise specified
1. TOLERANCE ON: X is ± 0.5
X.Y is ± 0.2
X.XX is ± 0.05
2. ANGULAR TOLERANCE: ± 0.5
3. LAST REVISION INDICATED BY: ☐
4. SURFACE FINISH: 32

DRAWN BY:
L. GENG
CHECKED BY:
R. PERLIN

DESIGNED BY:
L. GENG
APPROVED BY:
P. RADZISZEWSKI

McGILL UNIVERSITY
COMMUNION DYNAMICS
LABORATORY

DWG NO.
CD01-402

REV
0



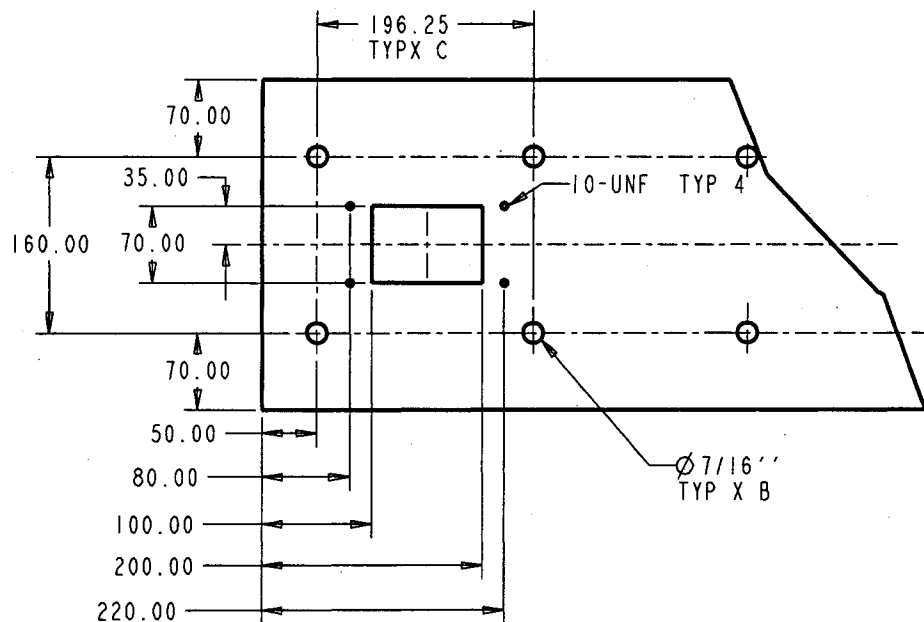
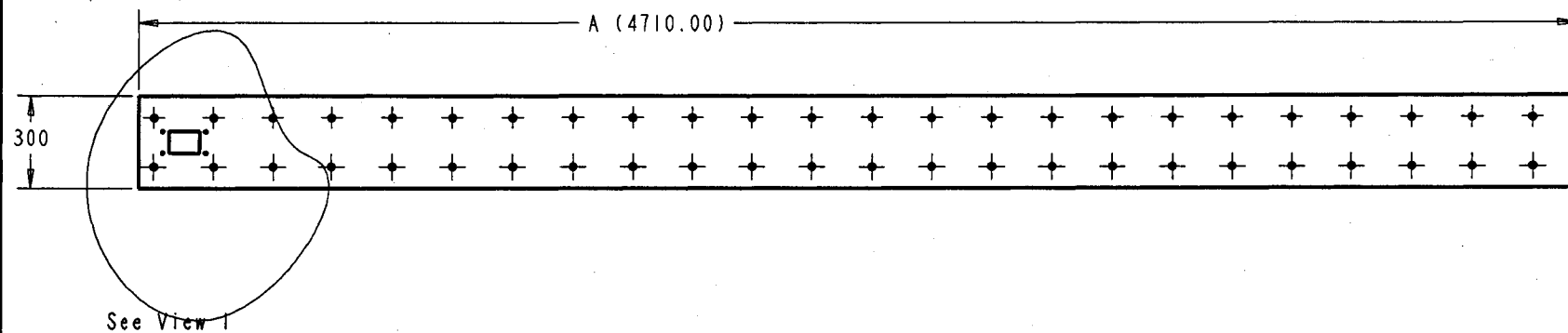
DIMENSION
IN

SIZE

SCALE:
1:250

SHEET:
1 of 1

A21



Drum	A	B	C
1500mm	4710mm	48	23
1250mm	3925mm	36	17
1000mm	3140mm	24	11

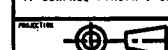
NO	REVISION	DATE	BY
1	Table	12/10	L.G.
2			
3			
4			
5			
6			
7			

PART NAME:
Drum unfolded

Unless otherwise specified
1. TOLERANCE ON: X is ± 0.5
X.X IS ± 0.2
X.XX IS ± 0.05
2. ANGULAR TOLERANCE: ± 0.5
3. LAST REVISION INDICATED BY: ☐
4. SURFACE FINISH: 32

DRAWN BY:
L. GENG
CHECKED BY:
R. PERLIN
DESIGNED BY:
L. GENG
APPROVED BY:
P. RADZISZEWSKI

MATERIAL
Sheet Metal 1/8"
McGILL UNIVERSITY
COMMINUTION DYNAMICS
LABORATORY



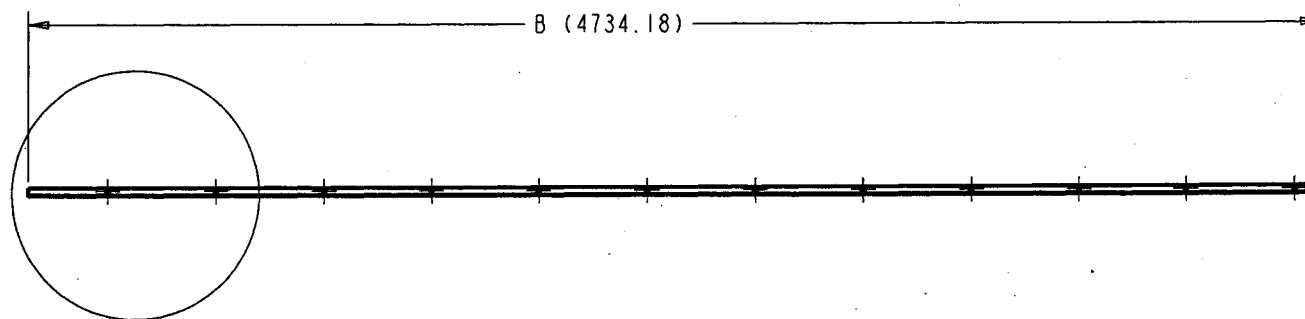
DIMENSION
mm

SIZE:
SCALE:
1:300
SHEET:
1 of 1

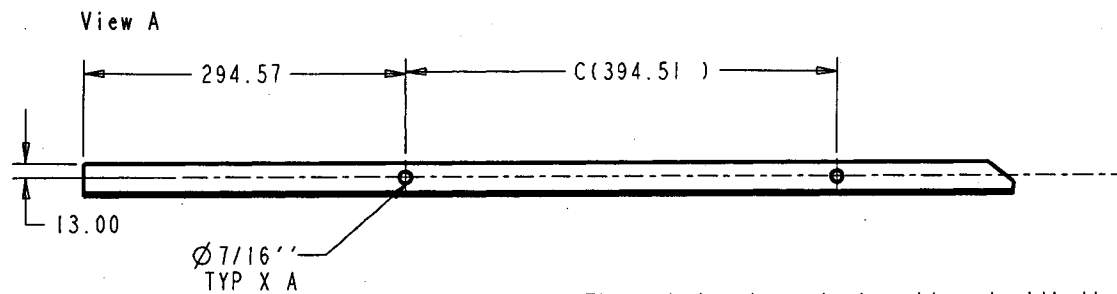
DWG NO.
CD01-403

REV
1

View I



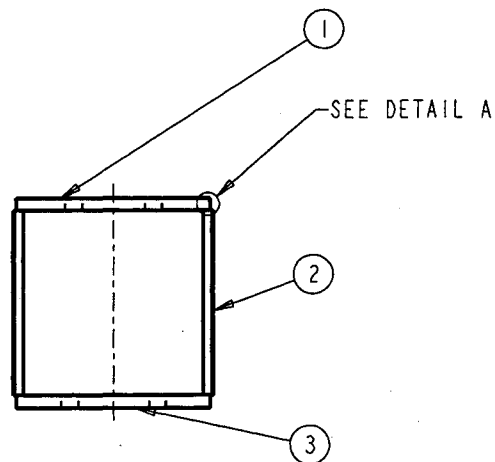
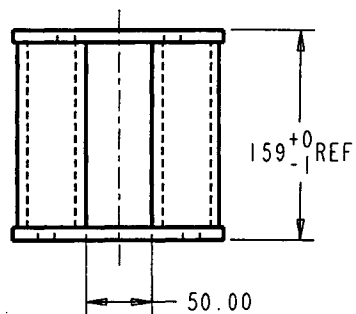
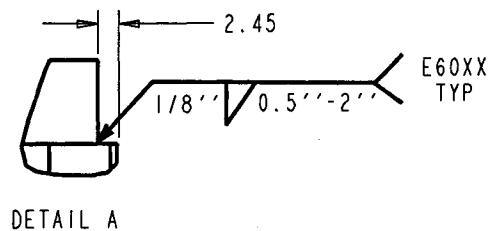
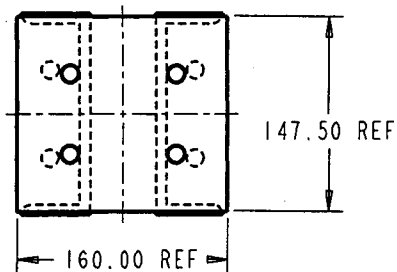
See View A



Note: These holes have to be aligned with the holes on the disc.

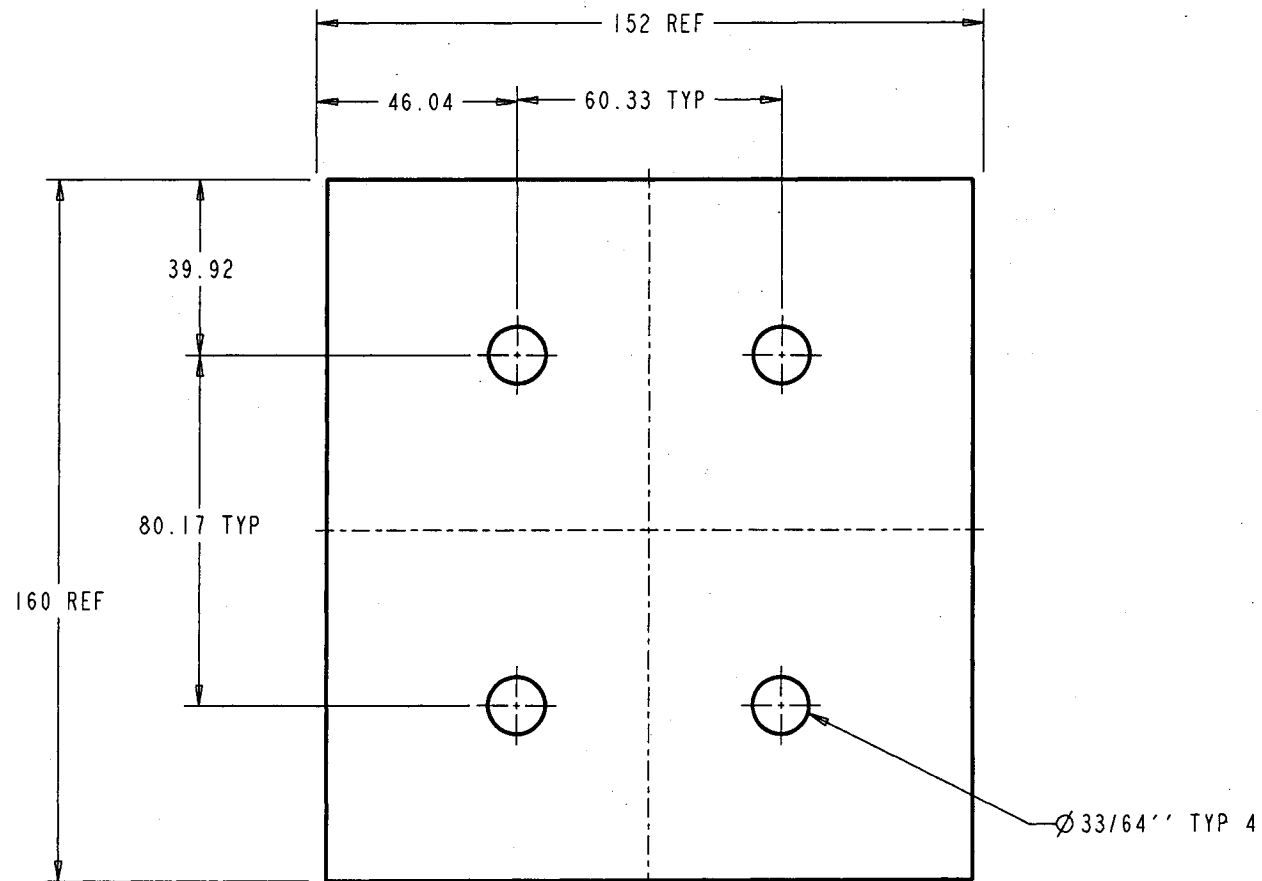
Drum size mm	A	B mm	C mm
1500	12	4734.178	394.51
1250	12	3949.178	329.10
1000	12	3164.178	263.68

PART NAME:		NO REVISION		DATE	BY
Angle unfolded		1	Table	10/12	L.G.
		2			
		3			
		4			
		5			
		6			
		7			
<small>Unless otherwise specified</small> 1. TOLERANCE ON: X: is ± 0.5 X.X is ± 0.2 X.XX is ± 0.05 2. ANGULAR TOLERANCE: ± 0.5 3. LAST REVISION INDICATED BY: <input type="checkbox"/> 4. SURFACE FINISH: 32		MATERIAL A1 2"x2"x3/16" DESIGNED BY: L. GENG CHECKED BY: R. PERLIN APPROVED BY: P. RADZISZEWSKI		MCGILL UNIVERSITY COMMINUTION DYNAMICS LABORATORY	
DWG NO. CD01-404		REV 1			



NO	PART NAME	PART CODE	QTY	MAT.
1	Top plate	CD01-501	1	
2	C-Channel	CD01-502	2	
3	Bottom plate	CD01-503	1	

SUBASSEMBLY NAME:		NO.	REVISION	DATE	BY
Support for rollers		1			
		2			
<small>Unless otherwise specified</small> 1. TOLERANCE ON: X. is ± 0.5 X.X 15 ± 0.2 X.XX 15 ± 0.05 2. ANGULAR TOLERANCE: ± 0.5 3. LAST REVISION INDICATED BY: <input type="checkbox"/> 4. SURFACE FINISH: 32		MATERIAL: STEEL DESIGNED BY: L. GENG CHECKED BY: R. PERLIN APPROVED BY: P. RADZISZEWSKI		MCGILL UNIVERSITY COMMUNION DYNAMICS LABORATORY	
PROJECTION: DIMENSION: mm		SIZE:	SCALE: 1:10	SHEET: 1 of 1	DWG NO. CD01-500 REV 0



NO	REVISION	DATE	BY
1			
2			
3			
4			
5			
6			
7			

PART NAME:

Top Plate

Unless otherwise specified
 1. TOLERANCE ON: X, is ± 0.5
 X.X is ± 0.2
 X.XX is ± 0.05
 2. ANGULAR TOLERANCE: ± 0.5
 3. LAST REVISION INDICATED BY: ☐
 4. SURFACE FINISH: 32

MATERIAL
 MS
 DESIGNED BY:
 L. GENG
 CHECKED BY:
 R. PERLIN
 APPROVED BY:
 P. RADZISZEWSKI

McGILL UNIVERSITY
 COMMUNITION DYNAMICS
 LABORATORY

DWG NO.
 CD01-501

REV
 0

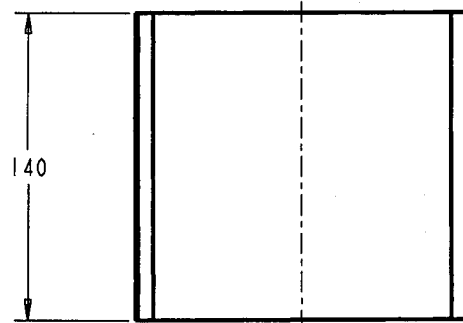
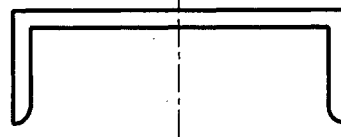


DIMENSION
 MM

SIZE

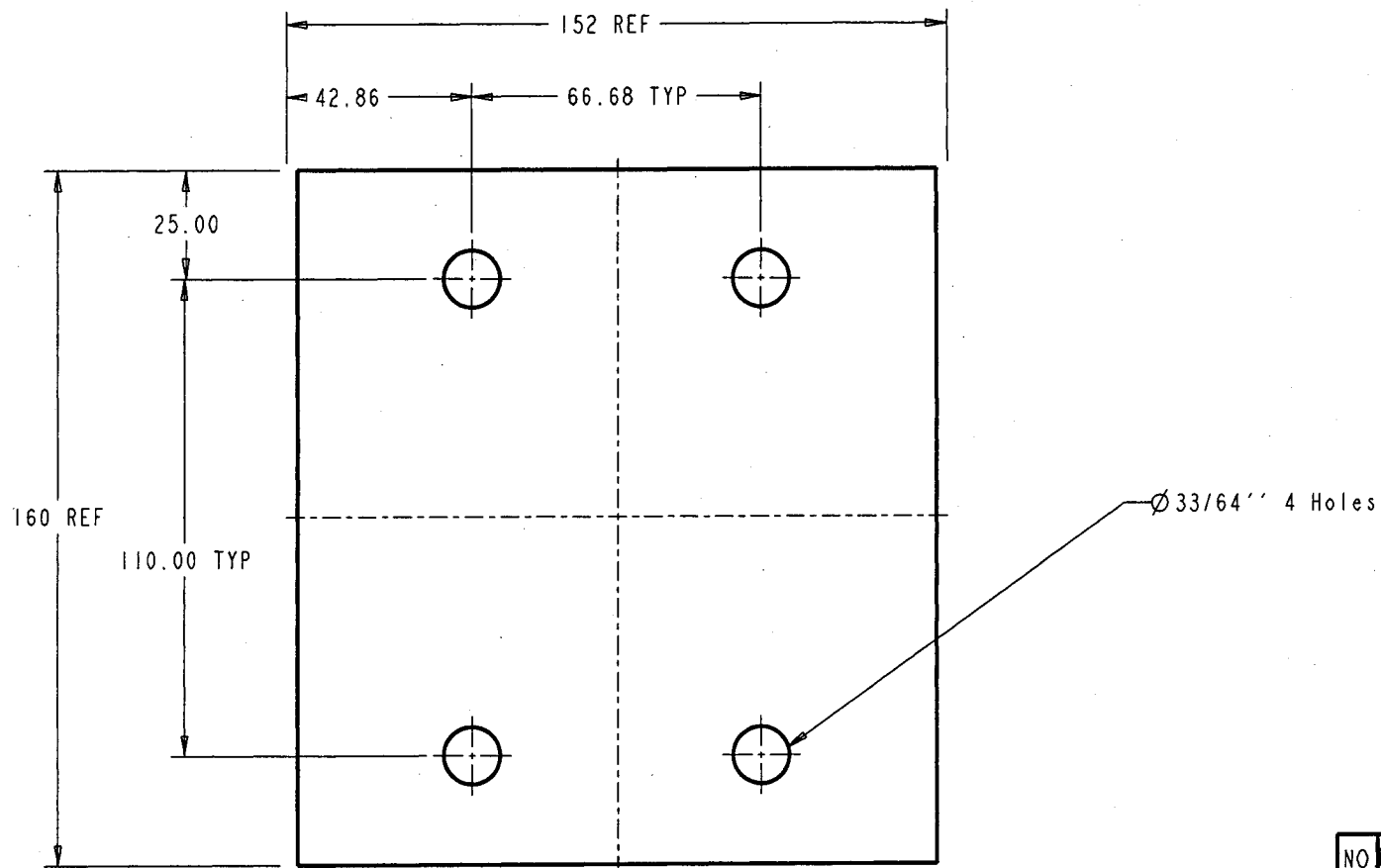
SCALE:
 1:1

SHEET:
 1 of 1



NO	REVISION	DATE	BY
1			
2			
3			
4			
5			
6			
7			

PART NAME: C-Channel				MATERIAL: C8X8.2		MCGILL UNIVERSITY COMMINUTION DYNAMICS LABORATORY			
<small>Unless otherwise specified</small> 1. TOLERANCE ON: X. is ± 0.5 X.X is ± 0.2 X.XX is ± 0.05 2. ANGULAR TOLERANCE: ± 0.5 3. LAST REVISION INDICATED BY: <input type="checkbox"/> 4. SURFACE FINISH: 32				DRAWN BY: L. GENG CHECKED BY: R. PERLIN				DESIGNED BY: L. GENG APPROVED BY: P. RADZISZEWSKI	
PROJECTION 		DIMENSION 		SIZE: 	SCALE: 1:50			SHEET: 1 of 1	
				DWG NO CD01-502				REV 0	



NO	REVISION	DATE	BY
1			
2			
3			
4			
5			
6			
7			

PART NAME:

Bottom plate

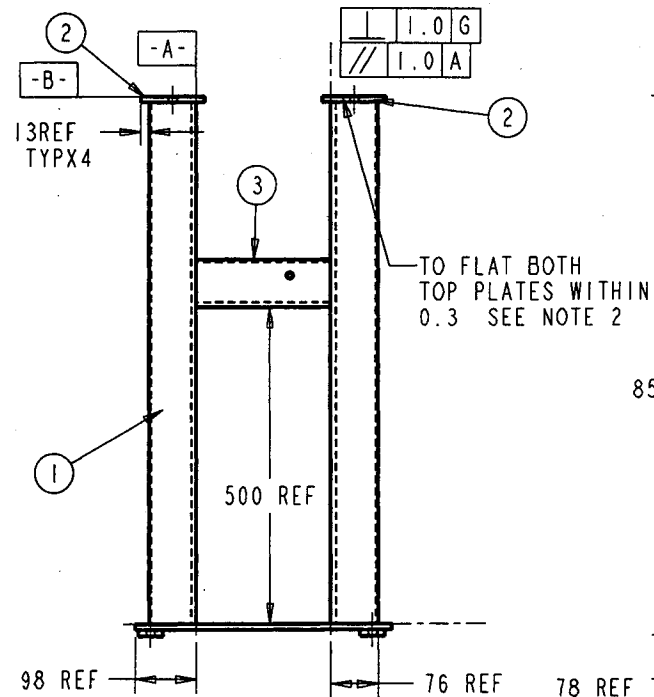
Unless otherwise specified
 1. TOLERANCE ON: X is ± 0.5
 X.X is ± 0.2
 X.XX is ± 0.05
 2. ANGULAR TOLERANCE: ± 0.5
 3. LAST REVISION INDICATED BY: ☐
 4. SURFACE FINISH: 32

DRAWN BY:
L. GENG
 CHECKED BY:
R. PERLIN
 MATERIAL
MS
 DESIGNED BY:
L. GENG
 APPROVED BY:
P. RADZISZEWSKI

PROJECTION: DIMENSION: SIZE: 1:25 SHEET: 1 of 1


McGILL UNIVERSITY
 COMMUNITION DYNAMICS
 LABORATORY

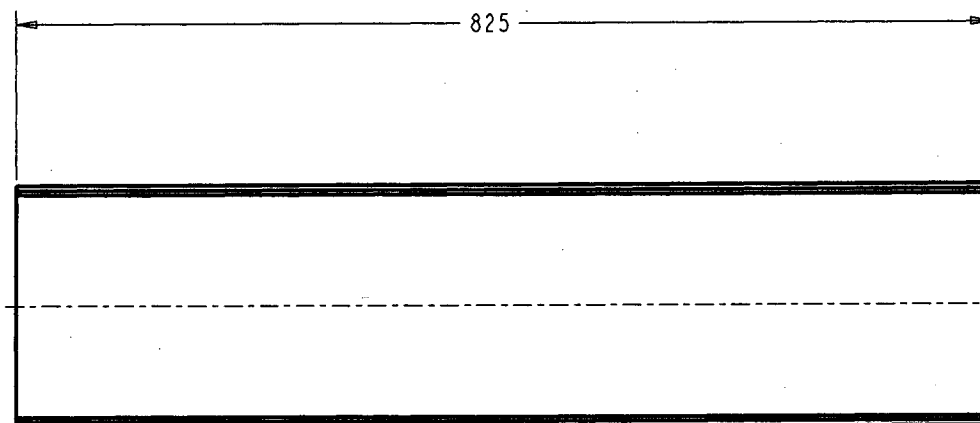
DWG NO. CD01-503 REV 0



-
- | | |
|--|--|
| | |
| | |
| | |
| | |
- IN
2
- 853⁺⁰
-1
- 25 REF TYP
- 4
- 3/16" 0.5"-2" E60XX
TYP
- G-
- F TYP
- 5
- SUBASSEMBLY NAME:
Brake support

[illegible]

SUBASSEMBLY NAME:		NO.		REVISION		DATE		BY	
Brake support		1		New holes		31/7/03		ECP	
		2		New height		5/4/03		ECP	
Unless otherwise specified 1. TOLERANCE ON: X: ± 0.5 X: X IS ± 0.2 X: X IS ± 0.5 2. ANGULAR TOLERANCE: ± 0.5 3. LAST REVISION INDICATED BY: <input type="checkbox"/> 4. SURFACE FINISH: 32		MATERIAL		McGill UNIVERSITY COMMUNITION DYNAMICS LABORATORY					
DRAWN BY: L. GENG		DESIGNED BY: L. GENG							
CHECKED BY: R. PERLIN		APPROVED BY: P. RADZISZEWSKI							
PROJECTION 		DIMENSION		SIZE		SCALE:		SHEET:	
PRT				1:7.5		1 of 1		DWG NO. CD01-600 REV	



PART NAME:
C-Channel Vertical

Unless otherwise specified
1. TOLERANCE ON: X. is ± 0.5
X.Y is ± 0.2
X.XX is ± 0.05
2. ANGULAR TOLERANCE: ± 0.5
3. LAST REVISION INDICATED BY: ☐
4. SURFACE FINISH: 32



DIMENSION
mm

DESIGNED BY:
L. GENG
CHECKED BY:
R. PERLIN

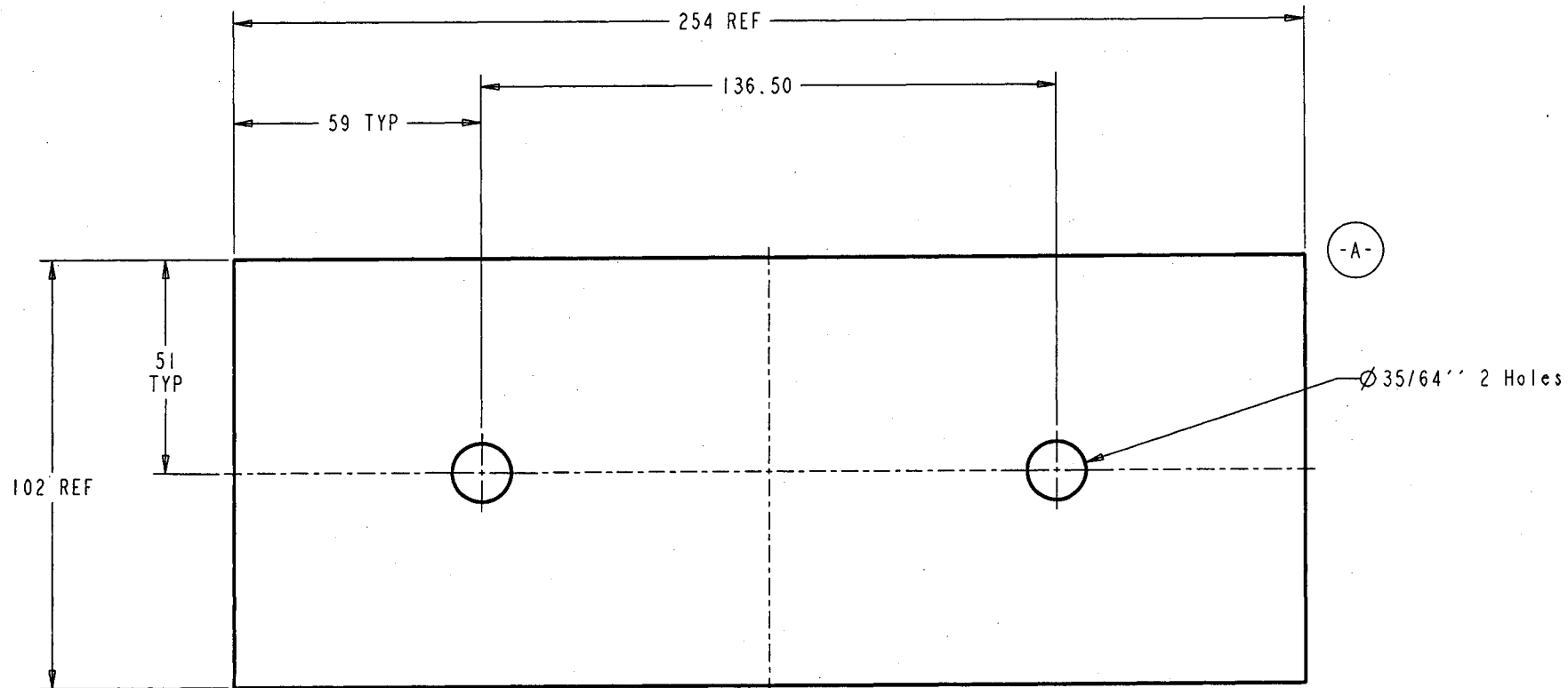
MATERIAL
C8X11.50
DESIGNED BY:
L. GENG
APPROVED BY:
P. RADZISZEWSKI

NO	REVISION	DATE	BY
1	Insert groove	17/7/03	ECP
2	New C.Chnl	23/7/03	ECP
3			
4			
5			
6			
7			

McGILL UNIVERSITY
COMMINUTION DYNAMICS
LABORATORY

DWG NO
CD01-601

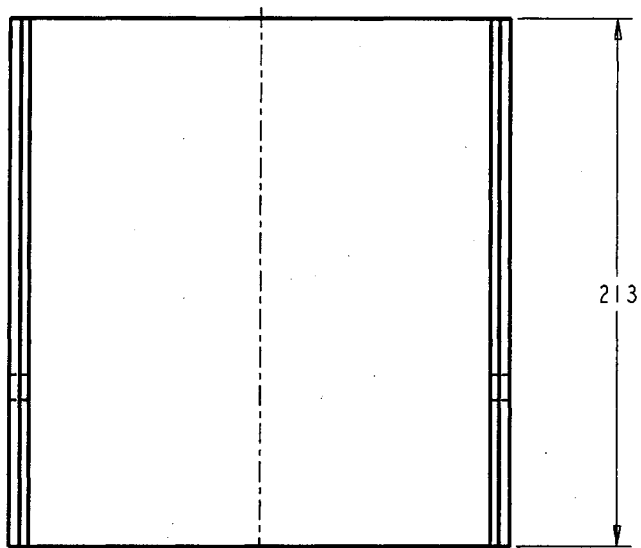
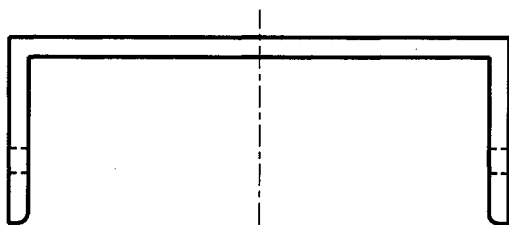
REV
2



-A- Round the corners.

NO	REVISION	DATE	BY
1			
2			
3			
4			
5			
6			
7			

PART NAME: Top plate				THICKNESS 3/8" MATERIAL 304 STAINLESS STEEL GRADE 304	
1. TOLERANCE ON: X, IS ± 0.5 X.X IS ± 0.2 X.XX IS ± 0.05 2. ANGULAR TOLERANCE: ± 0.5 3. LAST REVISION INDICATED BY: <input type="checkbox"/> 4. SURFACE FINISH: 32				DRAWN BY: L. GENG CHECKED BY: R. PERLIN DESIGNED BY: L. GENG APPROVED BY: P. RADZISZEWSKI	
McGill University COMMINUTION DYNAMICS LABORATORY				DWG NO. CD01-602 REV 0	



213

PART NAME:
C-Channel Horizontal

Unless otherwise specified
1. TOLERANCE ON: X, Y ± 0.5
X, X ± 0.2
X, XX ± 0.05
2. ANGULAR TOLERANCE: ± 0.5
3. LAST REVISION INDICATED BY: ☐
4. SURFACE FINISH: 32

MATERIAL:
C8x11.50
DRAWN BY:
L. GENG
DESIGNED BY:
L. GENG
CHECKED BY:
R. PERLIN
APPROVED BY:
P. RADZISZEWSKI

McGILL UNIVERSITY
COMMINUTION DYNAMICS
LABORATORY

DWG NO. CD01-603 REV
0



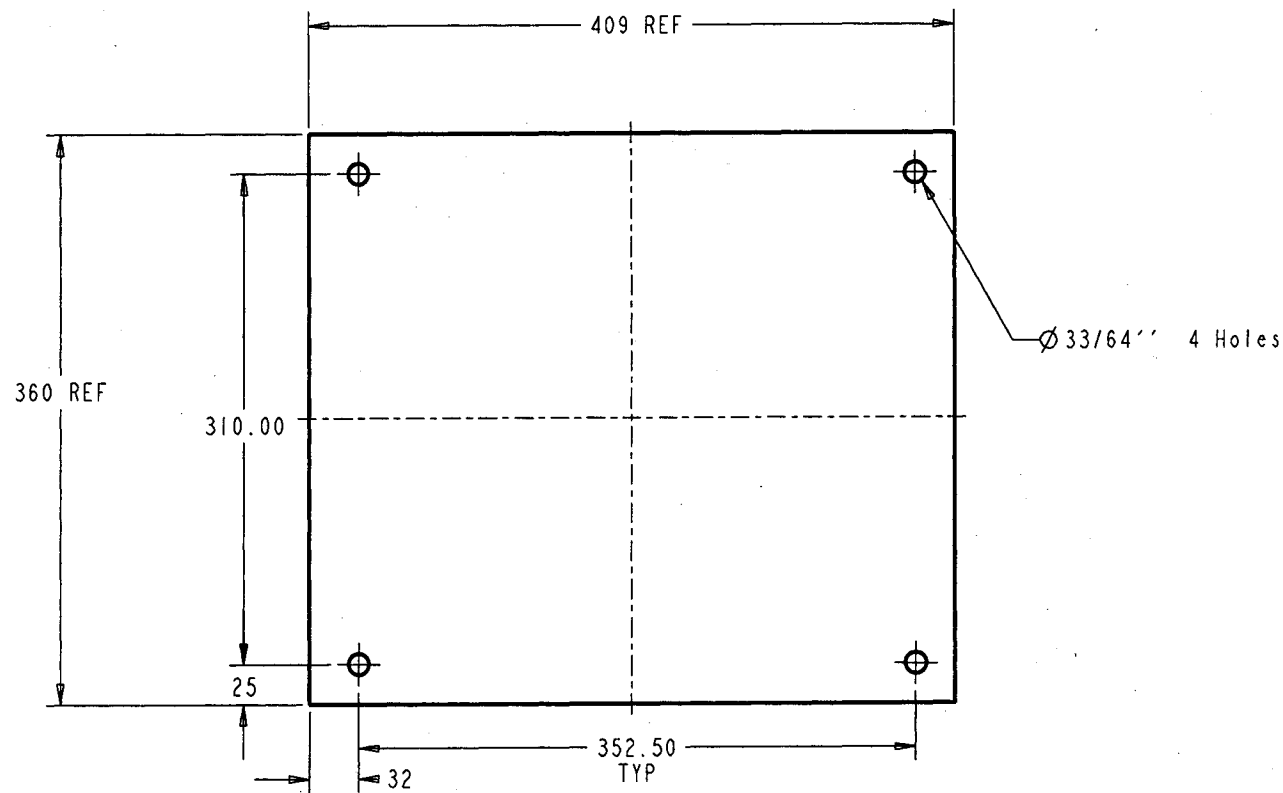
DIMENSION
mm

SIZE:

SCALE:
1:2

SHEET:
1 of 1

NO	REVISION	DATE	BY
1			
2			
3			
4			
5			
6			
7			



PART NAME:
Bottom Plate

Unless otherwise specified
 1. TOLERANCE ON: X is ± 0.5
 X.X is ± 0.2
 X.XX is ± 0.05
 2. ANGULAR TOLERANCE: ± 0.5
 3. LAST REVISION INDICATED BY: ☐
 4. SURFACE FINISH: 32

Thickness **3/8** = MATERIAL
 Wild Steel
 DRAWN BY: L. GENG
 DESIGNED BY: L. GENG
 CHECKED BY: R. PERLIN
 APPROVED BY: P. RADZISZEWSKI

NO	REVISION	DATE	BY
1	Small holes	31/7/03	ECP
2			
3			
4			
5			
6			
7			

McGILL UNIVERSITY
 COMMINUTION DYNAMICS
 LABORATORY

DWG NO.
 CD01-604

REV
 1

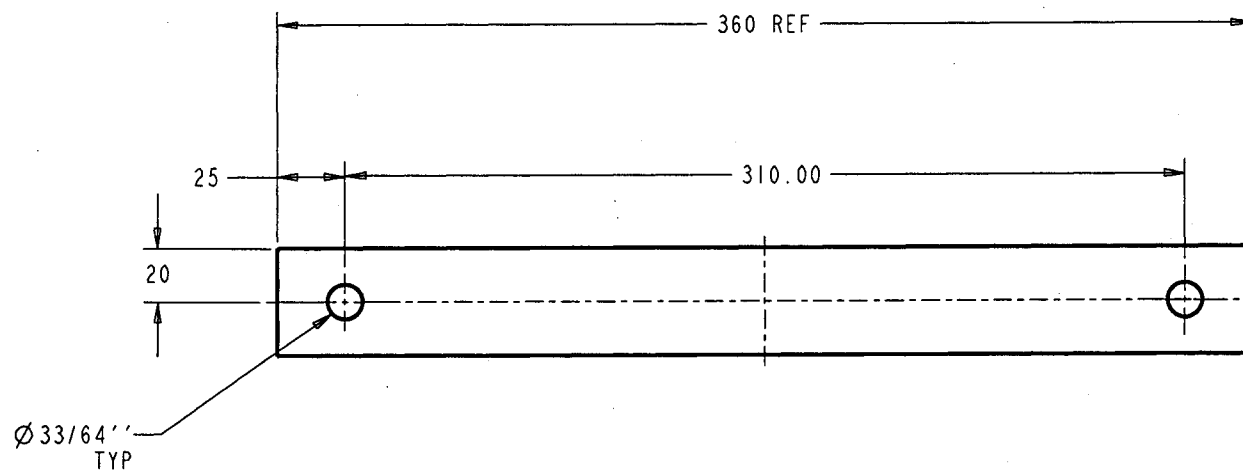


DIMENSION
 mm

SIZE

SCALE:
 1:3

SHEET:
 1 of 1



NO	REVISION	DATE	BY
1	New shape	23/7/03	ECP
2			
3			
4			
5			
6			
7			

PART NAME:
Contact Plate

Unless otherwise specified
1. TOLERANCE ON: X. is ± 0.5
X.X 15 ± 0.2
X.XX 15 ± 0.05
2. ANGULAR TOLERANCE: ± 0.5
3. LAST REVISION INDICATED BY: ☐
4. SURFACE FINISH: 32

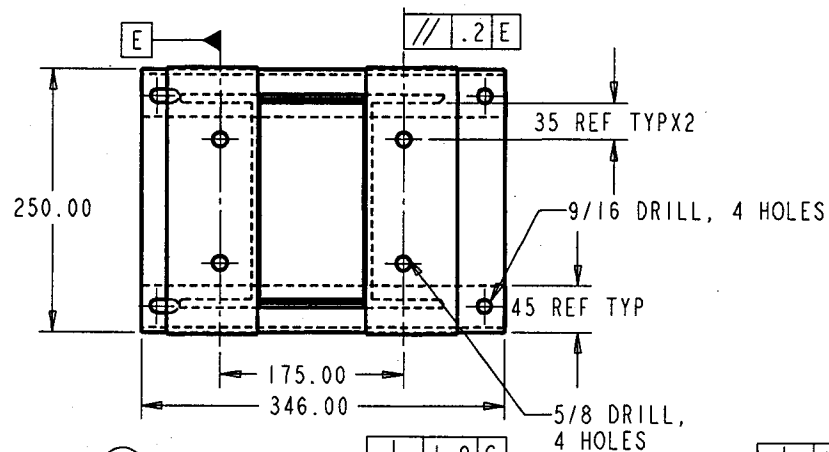
Thickness: 1/4"
MATERIAL: Mild steel
DRAWN BY: L. GENG
DESIGNED BY: L. GENG
CHECKED BY: R. PERLIN
APPROVED BY: P. RADZISZEWSKI

MCGILL UNIVERSITY
COMMINUTION DYNAMICS
LABORATORY

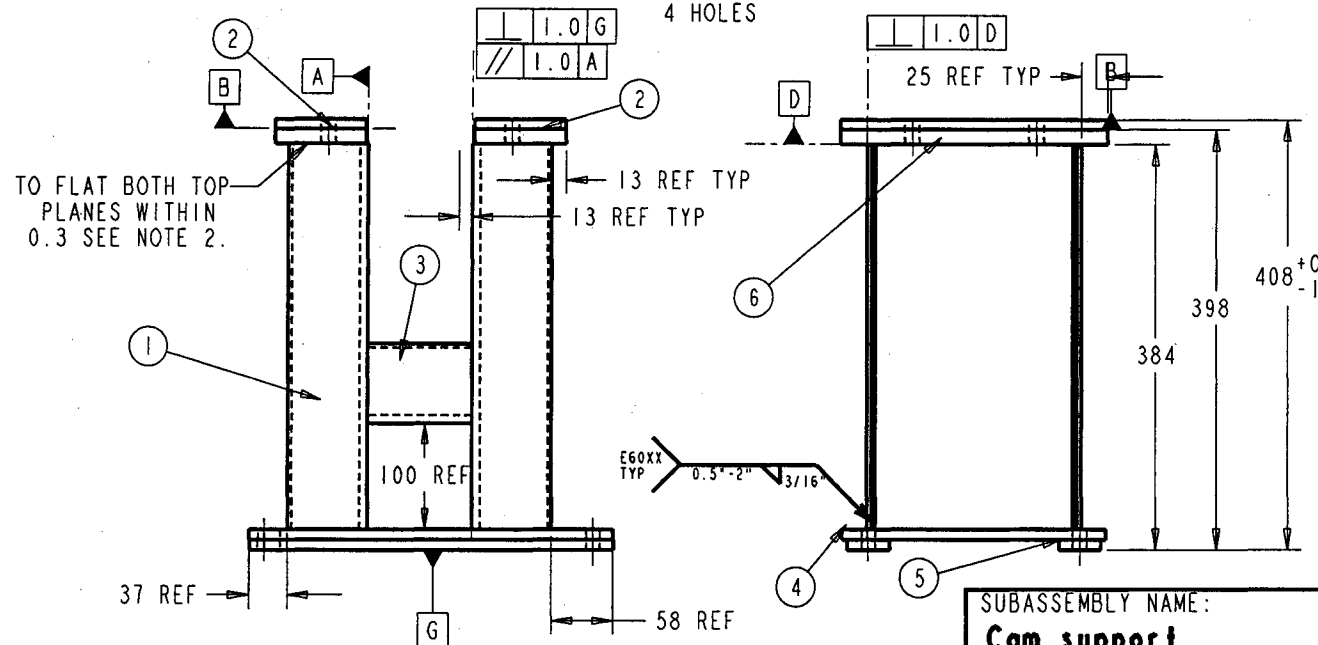
PROJECTION: DIMENSION: mm

SIZE: SCALE: 1:1.75 SHEET: 1 of 1

DWG NO. CD01-605 REV 1

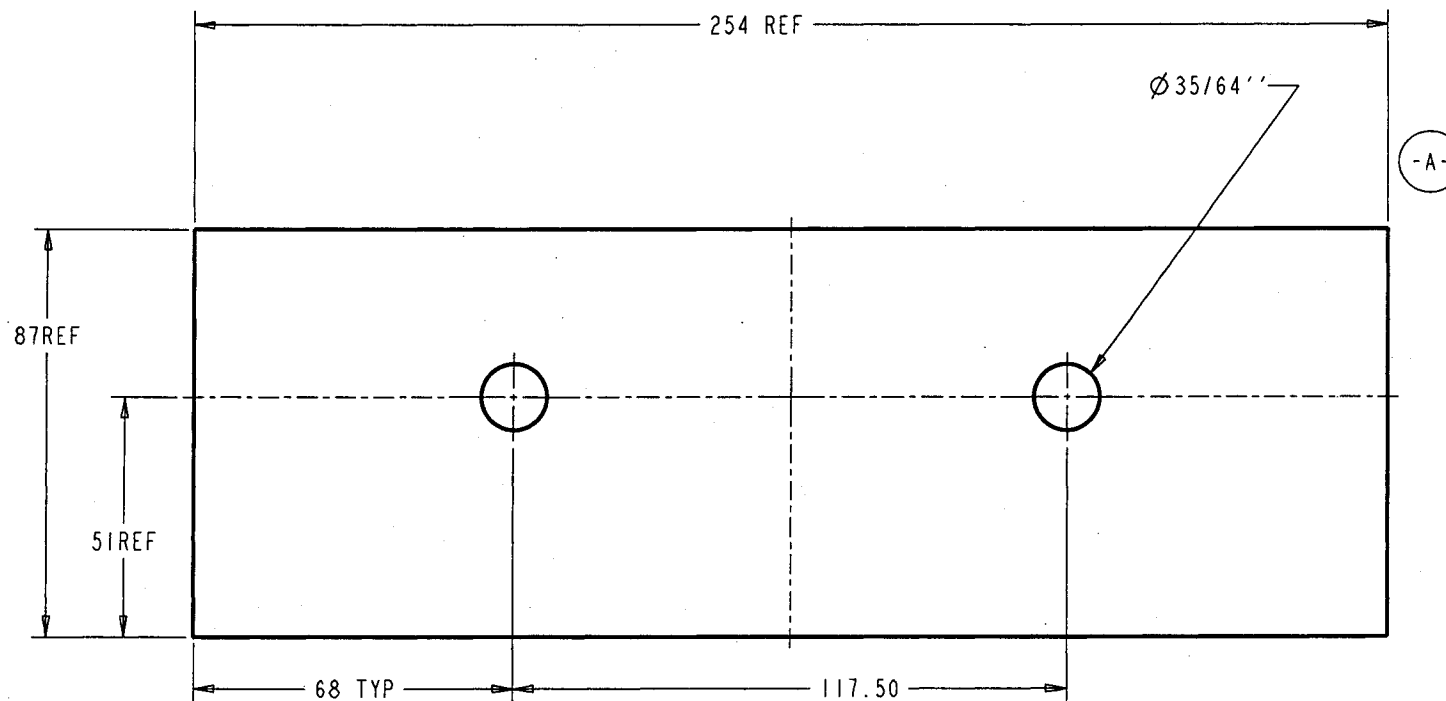


NO	PART NAME	PART CODE	QTY	MAT.
1	C-Channel Vertical	CD01-701	2	
2	Top plate	CD01-702	2	
3	C-Channel Horizontal	CD01-703	1	
4	Bottom plate	CD01-704	1	
5	Contact Plates	CD01-705	2	
6	Spacer	CD01-706	2	



- NOTES: 1. All T-joints and corner joints are typical.
 2. Clamp both parts No.2 to align planes in order to comply with tolerances.
 3. Before welding align holes on bottom plate and contact plates.

SUBASSEMBLY NAME: Cam support		NO.	REVISION	DATE	BY
		1	New holes	31/7/03	ECP
		2	New height	5/4/03	ECP
Unless otherwise specified 1. TOLERANCE ON: X: is ± 0.5 X:1 is ± 0.2 X:XX is ± 0.05 2. ANGULAR TOLERANCE: ± 0.5 3. LAST REVISION INDICATED BY: <input type="checkbox"/> 4. SURFACE FINISH: 32		MATERIAL: DESIGN BY: L. GENG DESIGNED BY: L. GENG CHECKED BY: R. PERLIN APPROVED BY: P. RADZISZEWSKI			
PROJECTION DIMENSION IN		SCALE: 1:4.5		SHEET: 1 of 1	
		DWG NO. CD01-700		REV 3	



-A- Round corners, burres

PART NAME:
Top Plate

Unless otherwise specified
1. TOLERANCE ON: X. is ± 0.5
X.X is ± 0.2
X.XX is ± 0.05
2. ANGULAR TOLERANCE: ± 0.5
3. LAST REVISION INDICATED BY: ☐
4. SURFACE FINISH: 32

Thickness: **3/8"**
DESIGN BY: L. GENG
CHECKED BY: R. PERLIN
MATERIAL: Mild Steel
DESIGNED BY: L. GENG
APPROVED BY: P. RADZISZEWSKI



DIMENSION
IN

SIZE:

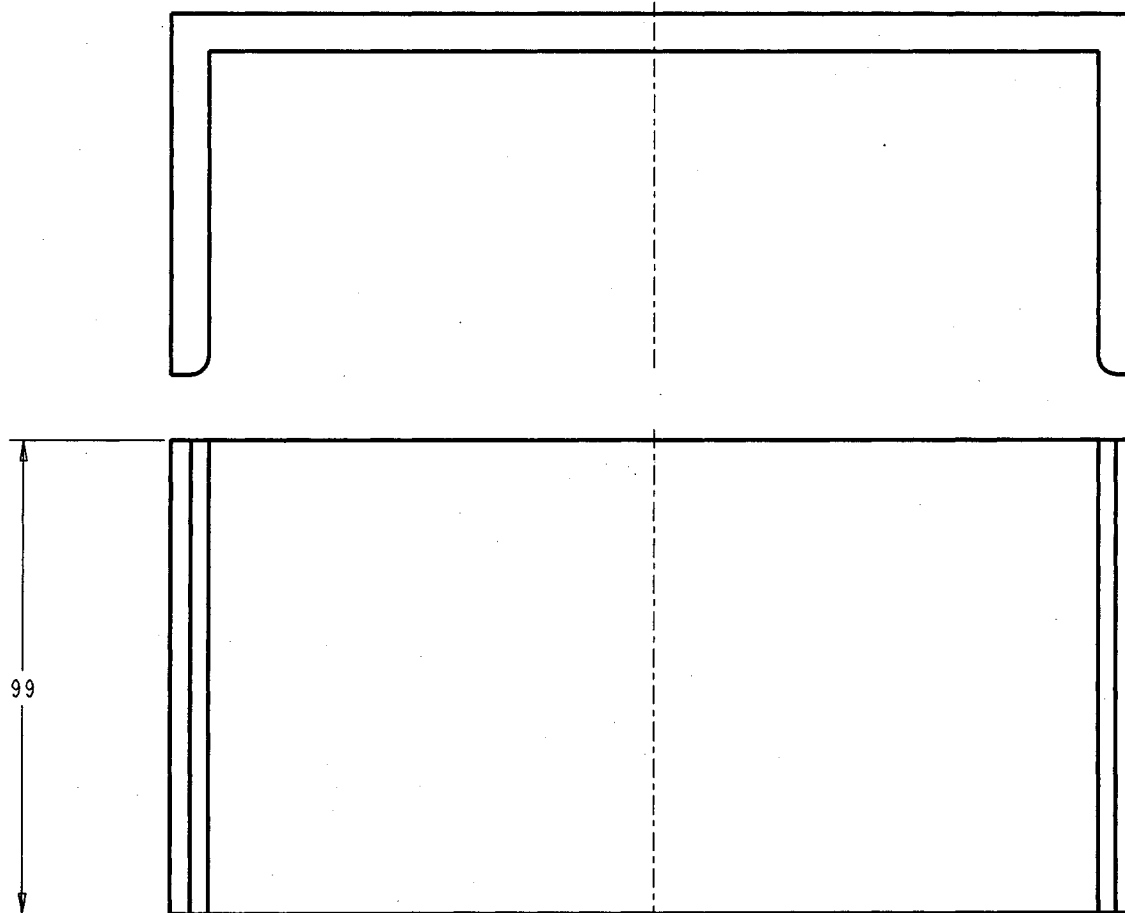
SCALE:
1:25

SHEET:
1 of 1

NO	REVISION	DATE	BY
1	Chng Dim	23/7/03	ECP
2			
3			
4			
5			
6			
7			

McGILL UNIVERSITY
COMMUNITION DYNAMICS
LABORATORY

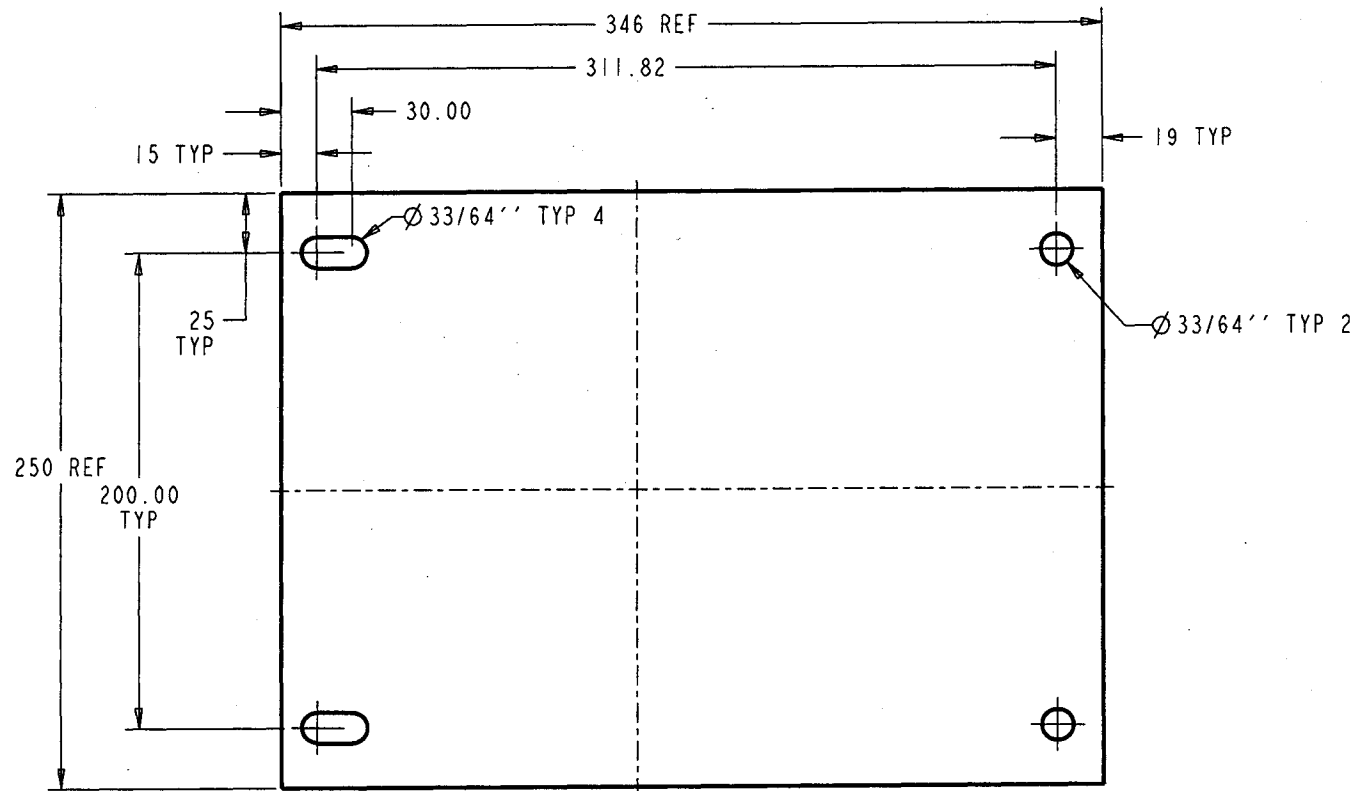
DWG NO. CD01-702 REV 1



NO	REVISION	DATE	BY
1	New length	26/7/03	ECP
2			
3			
4			
5			
6			
7			

PART NAME: C Channel Horizontal			
<small>Unless otherwise specified</small> 1. TOLERANCE ON: X: ± 0.5 X.X: ± 0.2 X.XX: ± 0.05 2. ANGULAR TOLERANCE: ± 0.5 3. LAST REVISION INDICATED BY: <input type="checkbox"/> 4. SURFACE FINISH: 32		MATERIAL: C8x8.2 DESIGNED BY: L. GENG CHECKED BY: R. PERLIN	APPROVED BY: P. RADZISZEWSKI
PROJECTION: 	DIMENSION mm	SIZE: 1:1	SHEET: 1 of 1

MCGILL UNIVERSITY COMMINUTION DYNAMICS LABORATORY	
DWG NO: CD01-703	REV 1



NO	REVISION	DATE	BY
1	Small holes	31/7/03	ECP
2			
3			
4			
5			
6			
7			

PART NAME:

Bottom Plate

Unless otherwise specified
 1. TOLERANCE ON: X. is ± 0.5
 X.X is ± 0.2
 X.XX is ± 0.05
 2. ANGULAR TOLERANCE: ± 0.5
 3. LAST REVISION INDICATED BY: ☐
 4. SURFACE FINISH: 32

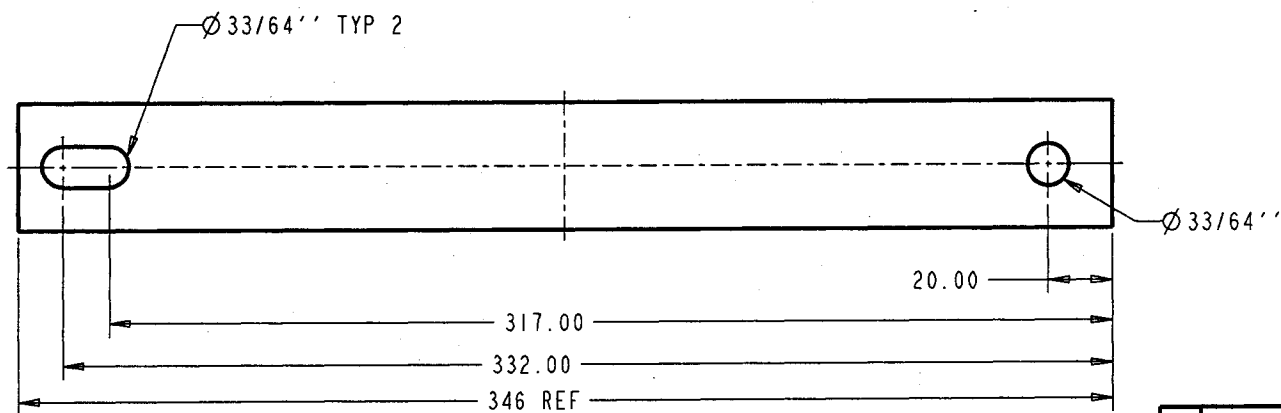
Thickness **3/8"** MATERIAL **Mild Steel**
 DRAWN BY: **L. GENG** DESIGNED BY: **L. GENG**
 CHECKED BY: **R. PERLIN** APPROVED BY: **P. RADZISZEWSKI**

McGILL UNIVERSITY
COMMINUTION DYNAMICS
LABORATORY

PROJECTION DIMENSION SIZE: SCALE: 1:2 SHEET: 1 of 1

DWG NO.
 CD01-704

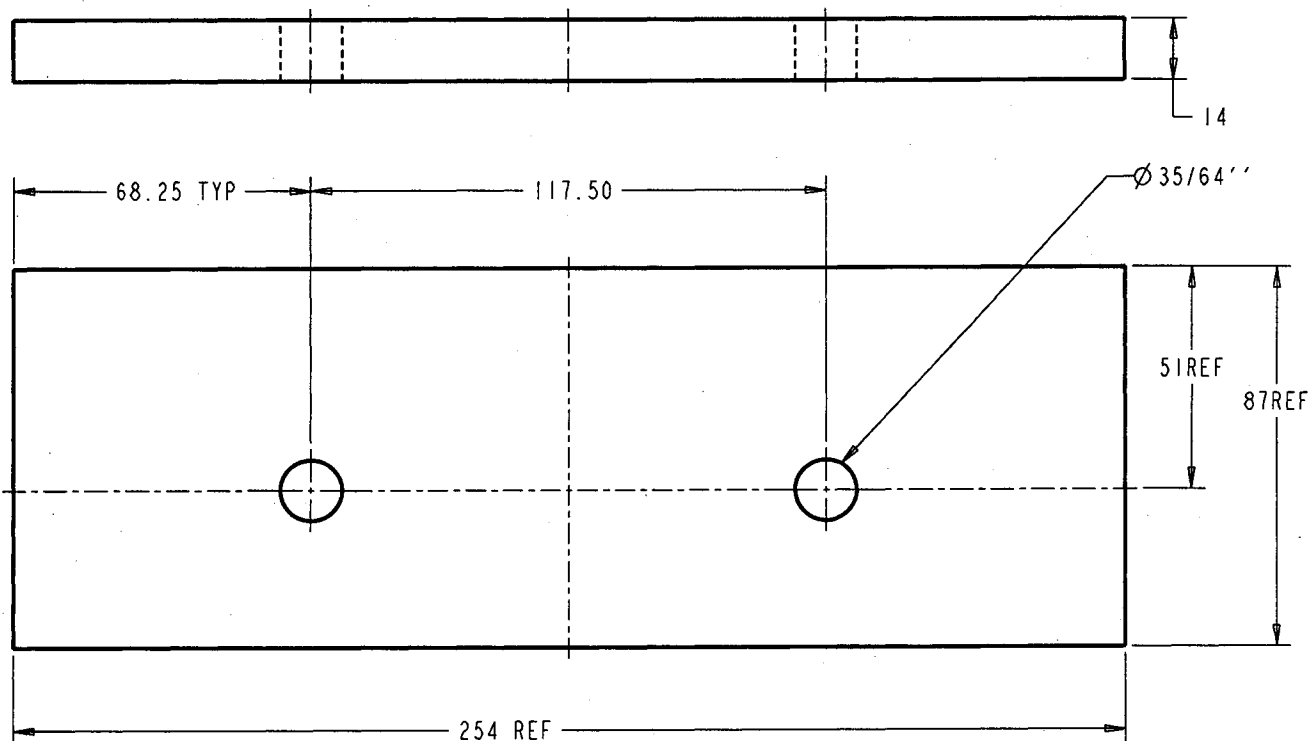
REV
 1



Note: Use flat bar 1/4x1 1/2

NO	REVISION	DATE	BY
1	New size	26/1/03	ECP
2	Small holes	31/7/03	ECP
3			
4			
5			
6			
7			

PART NAME: Support Plate				McGILL UNIVERSITY COMMINUTION DYNAMICS LABORATORY	
<small>Unless otherwise specified</small> 1. TOLERANCE ON: X. is ± 0.5 X.X is ± 0.2 X.XX is ± 0.05 2. ANGULAR TOLERANCE: ± 0.5 3. LAST REVISION INDICATED BY: <input type="checkbox"/> 4. SURFACE FINISH: 32		Thickness 1/4"	MATERIAL Mild steel	DWG NO. CD01-705	
DRAWN BY: L. GENG	DESIGNED BY: L. GENG	CHECKED BY: R. PERLIN	APPROVED BY: P. RADZISZEWSKI	REV 2	SCALE: 1:1.5
DIMENSION <small>mm</small>		SIZE:	SHEET: 1 of 1		



Note: Round corners, burres.

PART NAME:
Spacer for cam

Unless otherwise specified
1. TOLERANCE ON: X. is ± 0.5
 X.X is ± 0.2
 X.XX is ± 0.05
2. ANGULAR TOLERANCE: ± 0.5
3. LAST REVISION INDICATED BY: ☐
4. SURFACE FINISH: 32



DIMENSION
mm

SIZE

SCALE:
1:25

SHEET:
1 of 1

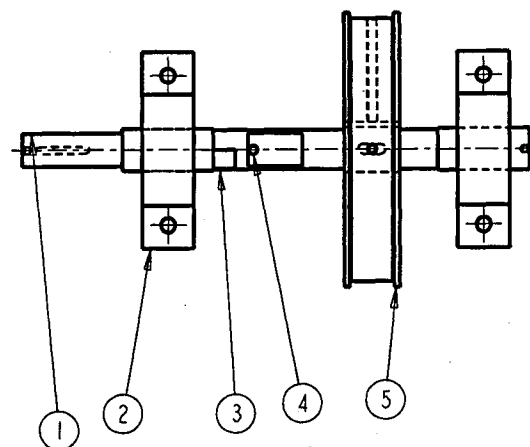
MATERIAL: MS
DRAWN BY: L. GENG
CHECKED BY: R. PERLIN
DESIGNED BY: L. GENG
APPROVED BY: P. RADZISZEWSKI

McGILL UNIVERSITY
COMMINUTION DYNAMICS
LABORATORY

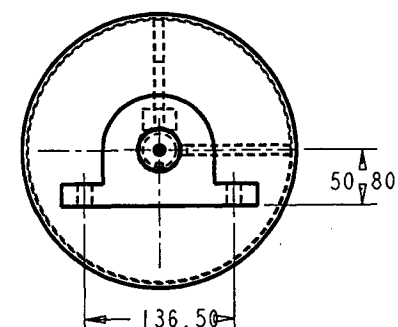
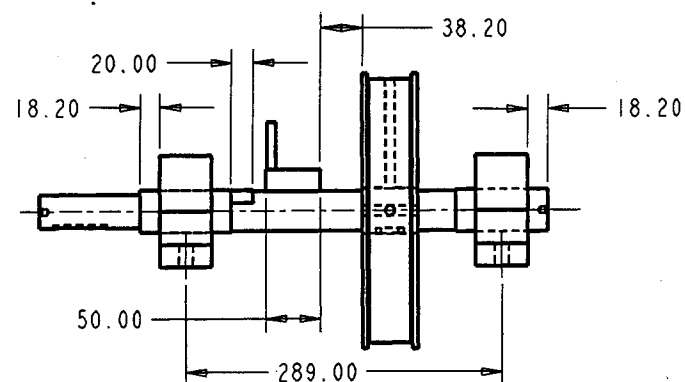
DWG NO.
CD01-706

REV
1

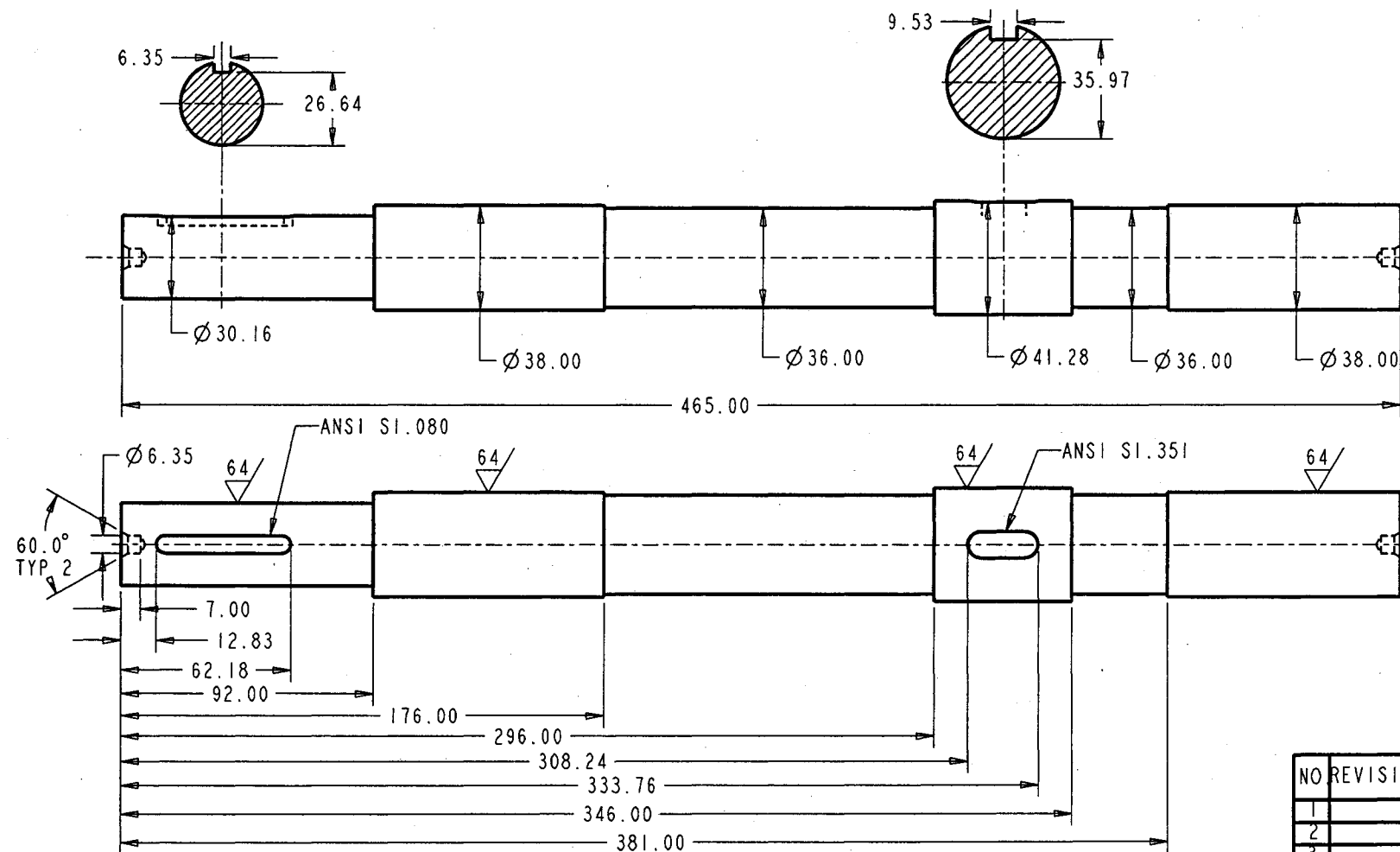
NO	REVISION	DATE	BY
1			
2			
3			
4			
5			
6			
7			



NO	PART NAME	PART CODE	QTY	MAT.
1	Brake shaft	CD01-801	1	Steel
2	Pillow block	P3-U224N	2	
3	Telemetry		1	
4	Sensor		1	
5	Prony brake	CD01-802	1	Steel



SUBASSEMBLY NAME:		NO.	REVISION	DATE	BY
Brake shaft subassembly		1			
		2			
Unless otherwise specified 1. TOLERANCE ON: X: is ± 0.5 X.X is ± 0.2 X.XX is ± 0.05 2. ANGULAR TOLERANCE: ± 0.5 3. LAST REVISION INDICATED BY: <input type="checkbox"/> 4. SURFACE FINISH: 32		MATERIAL DESIGNED BY: L. GENG CHECKED BY: R. PERLIN APPROVED BY: P. RADZISZEWSKI		MCGILL UNIVERSITY COMMUNION DYNAMICS LABORATORY	
PROJECTION DIMENSION mm		SIZE:	SCALE: 1:3	DWG NO. CD01-800 REV 0	



All keyseats are in ANSI B17.1-1967 R1989 standard and the keys are parallel and rectangular.

PART NAME:
Brake Shaft

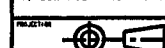
Unless otherwise specified
1. TOLERANCE ON: X is ± 0.5
Y is ± 0.2
Z is ± 0.05
2. ANGULAR TOLERANCE: ± 0.5
3. LAST REVISION INDICATED BY: ☐
4. SURFACE FINISH: 32

DESIGNED BY:
L. GENG
CHECKED BY:
R. PERLIN
APPROVED BY:
P. RADZISZEWSKI

MATERIAL:
CR steel

McGILL UNIVERSITY
COMMUNION DYNAMICS
LABORATORY

DWG NO. CD01-801 REV 0

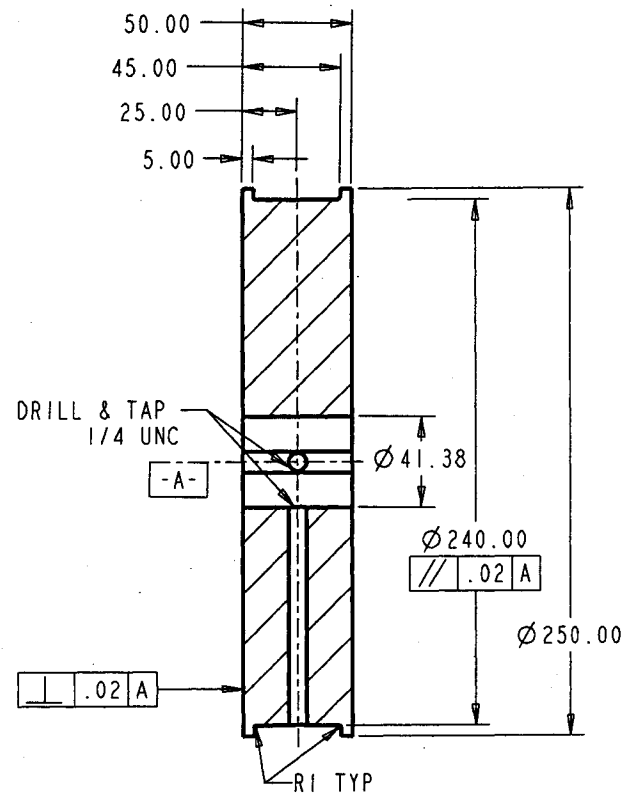
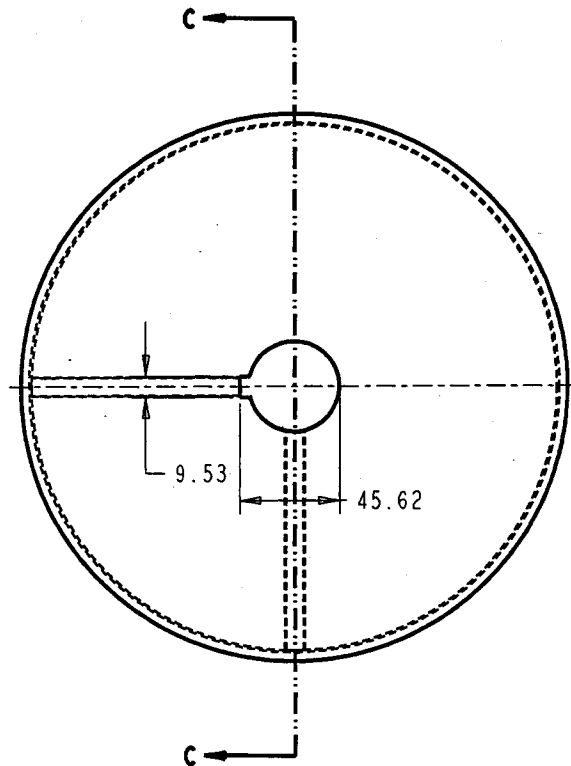


DIMENSION
mm

SIZE:

SCALE:
1:1.5

SHEET:
1 of 1



SECTION C-C

NO	REVISION	DATE	BY
1			
2			
3			
4			
5			
6			
7			

PART NAME:

Brake drum, detail

Unless otherwise specified
 1. TOLERANCE ON: X. is ± 0.5
 X.X 15 ± 0.2
 X.XX 15 ± 0.05
 2. ANGULAR TOLERANCE: ± 0.5
 3. LAST REVISION INDICATED BY: ☐
 4. SURFACE FINISH: 32

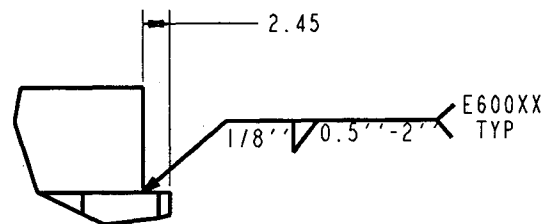
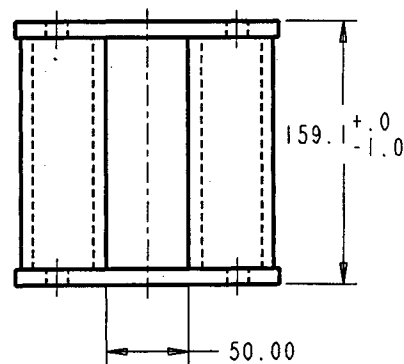
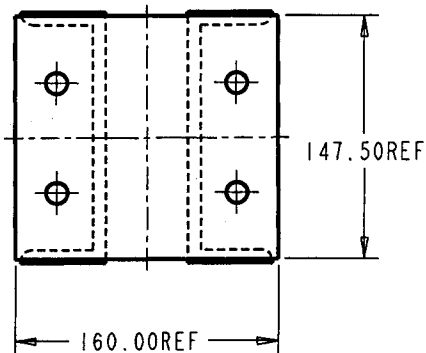
MATERIAL: MS
 DESIGNED BY: L. GENG
 CHECKED BY: R. PERLIN
 APPROVED BY: P. RADZISZEWSKI

McGILL UNIVERSITY
 COMMINUTION DYNAMICS
 LABORATORY

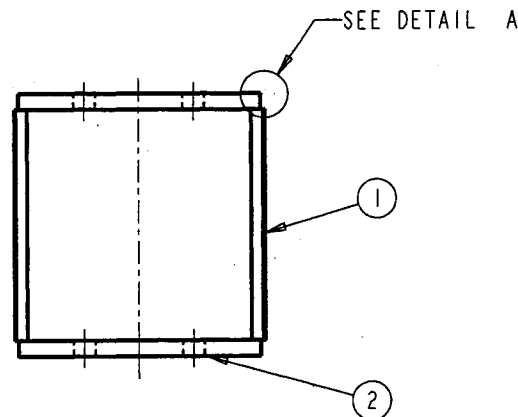
DWG NO. CD01-802 REV

PROJECTION: DIMENSION: mm

SIZE: SCALE: SHEET:

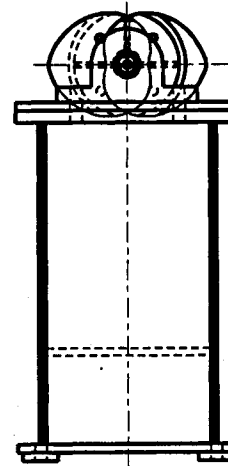
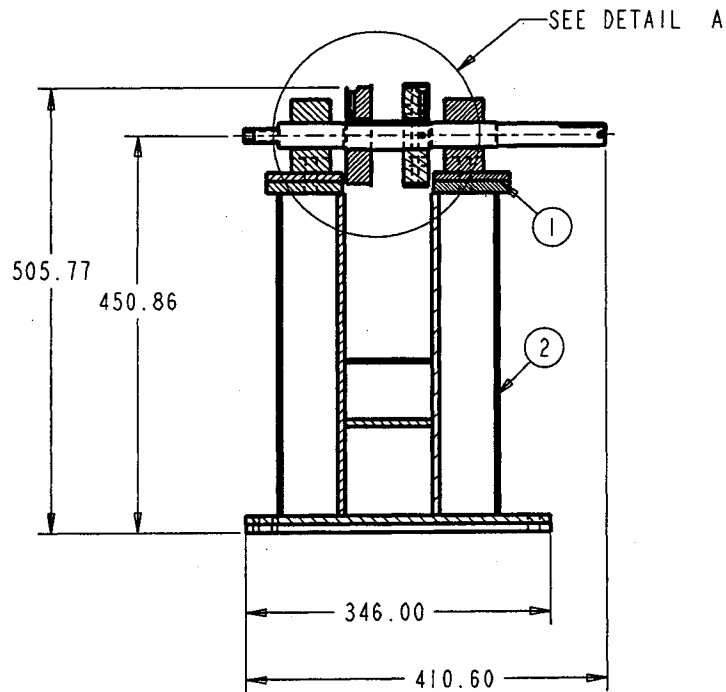
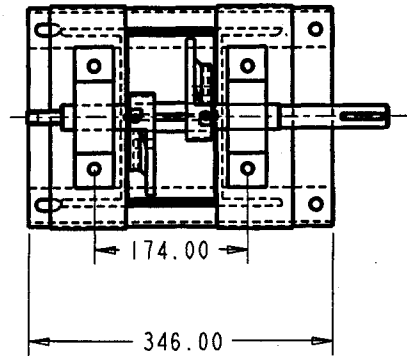


DETAIL A



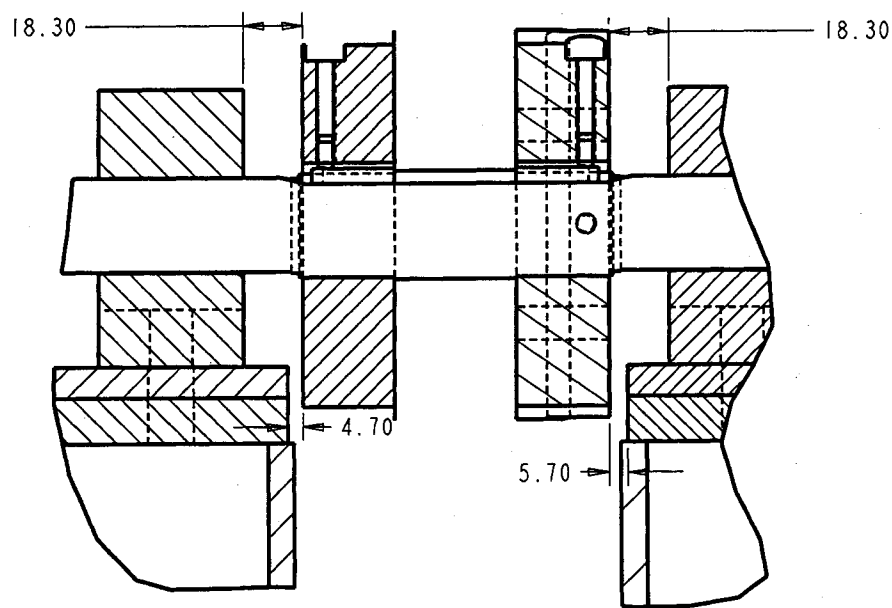
NO	PART NAME	PART CODE	QTY	MAT.
1	C-Chammel	CD01-502	2	Steel
2	Bottom plate	CD01-503	2	Steel

SUBASSEMBLY NAME:		NO.	REVISION	DATE	BY
Support spacer		1			
		2			
<small>Unless otherwise specified</small> 1. TOLERANCE ON: X is ± 0.5 X X is ± 0.2 X XX is ± 0.05 2. ANGULAR TOLERANCE: ± 0.5 3. LAST REVISION INDICATED BY: <input type="checkbox"/> 4. SURFACE FINISH: 32		MATERIAL: DESIGNED BY: L. GENG		DESIGNED BY: L. GENG	
CHECKED BY: R. PERLIN		APPROVED BY: P. RADZISZEWSKI		MCGILL UNIVERSITY COMMINUTION DYNAMICS LABORATORY	
PROJECTION DIMENSION IN MM		SIZE:	SCALE:	DWG NO.	REV
		1:10	1 of 1	CD01-900	0



NO	PART NAME	PART CODE	QTY	MAT.
1	Cam subassembly	CD01-200	1	
2	Cam support	CD01-700	1	

SUBASSEMBLY NAME:		NO.	REVISION	DATE	BY
Cam & support subassembly		1			
		2			
<small>Unless otherwise specified</small> 1. TOLERANCE ON: X.X is ± 0.5 X.XX is ± 0.2 X.XX is ± 0.05 2. ANGULAR TOLERANCE: ± 0.5 3. LAST REVISION INDICATED BY: <input type="checkbox"/> 4. SURFACE FINISH: 32		<small>MATERIAL</small> DRAWN BY: L. GENG CHECKED BY: R. Perlin		DESIGNED BY: L. GENG APPROVED BY: P. RADZISZEWSKI	
<small>PROJECTION</small> 		<small>DIMENSION</small> 		<small>SIZE</small> 1:200	<small>SHEET</small> 1 of 2
		MCGILL UNIVERSITY COMMINUTION DYNAMICS LABORATORY			DWG NO. CD01-1100
					REV 0



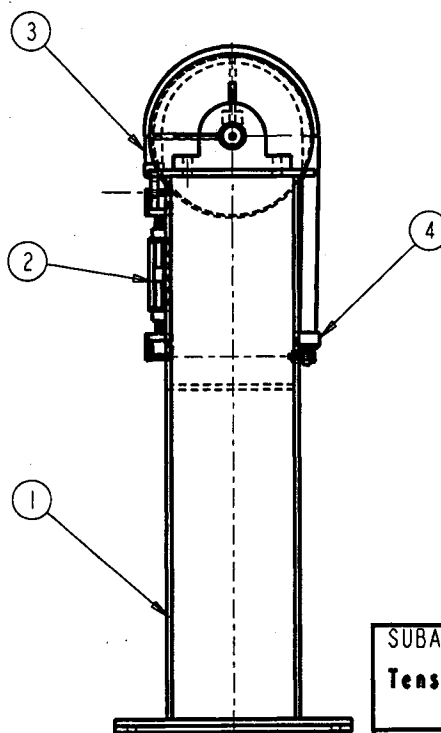
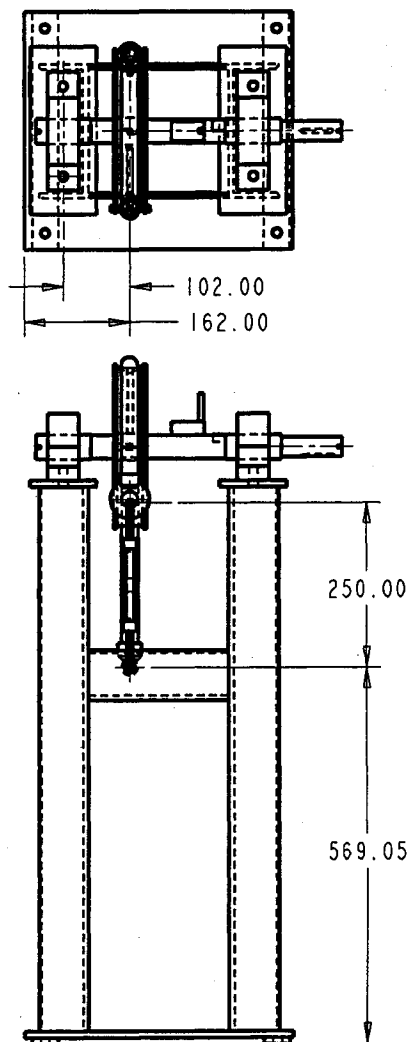
Detail A

NO	PART NAME	PART CODE	QTY	MAT.


SUBASSEMBLY NAME:		NO.	REVISION	DATE	BY
Cam & support subassembly		1			
		2			
<small>Unless otherwise specified</small> 1. TOLERANCE ON: X. is ± 0.5 X.X is ± 0.2 X.XX is ± 0.05 2. ANGULAR TOLERANCE: ± 0.5 3. LAST REVISION INDICATED BY: <input type="checkbox"/> 4. SURFACE FINISH: 32		MATERIAL L. GENG R. Perlin		DESIGNED BY: L. GENG P. RADZISZEWSKI	
PROJECTION 		DIMENSION mm		DWG NO. CD01-1100 SCALE: 1:200 SHEET: 2 of 2	

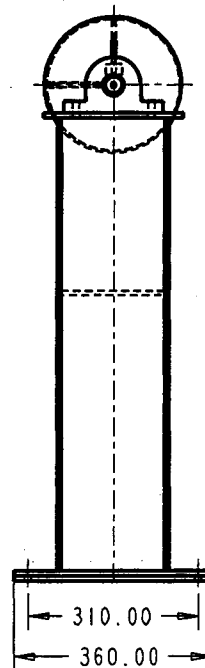
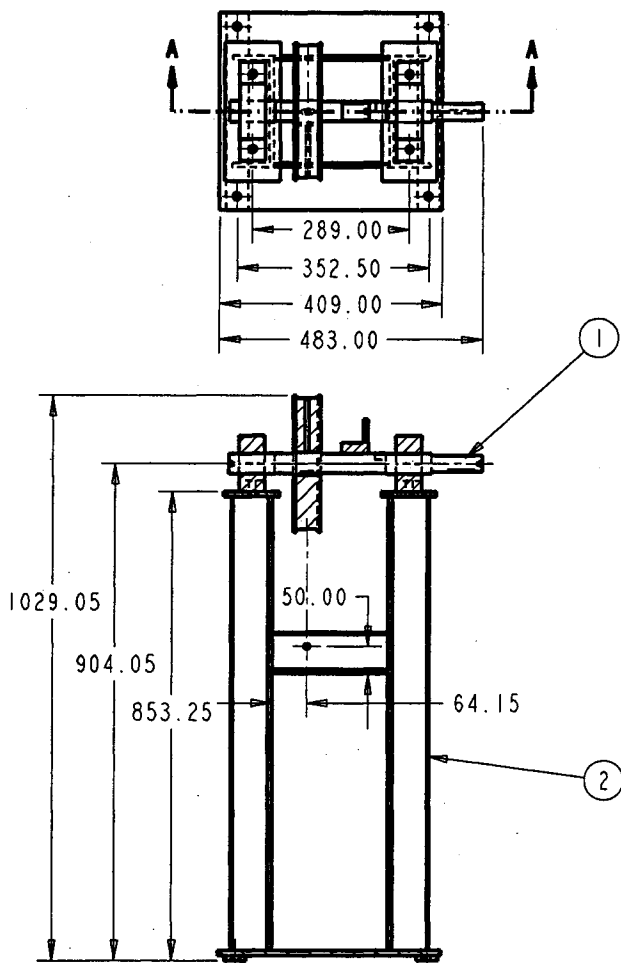
McGILL UNIVERSITY
COMMINUTION DYNAMICS
LABORATORY

REV 0



NO	PART NAME	PART CODE	QTY	MAT.
1	Brake & support subassembly	CD01-1300	1	
2	Turnbuckle Catalog Reid	Jaw and jaw SUN-330	1	
3	Rope	1"	1	
4	Stop sleeve	Eye	2	

SUBASSEMBLY NAME:		NO.	REVISION	DATE	BY
Tension brake & support subassembly		1			
		2			
Unless otherwise specified 1. TOLERANCE ON: X. is ± 0.5 X.X is ± 0.2 X.XX is ± 0.05 2. ANGULAR TOLERANCE: ± 0.5 3. LAST REVISION INDICATED BY: <input type="checkbox"/> 4. SURFACE FINISH: 32		MATERIAL DESIGN BY: L. GENG CHECKED BY: R. Perlin APPROVED BY: P. RADZISZEWSKI			
PROJECTION  DIMENSION IN		SIZE:	SCALE: 1:200	SHEET: 1 of 1	DWG NO CD01-1200 REV



NO	PART NAME	PART CODE	QTY	MAT.
1	Brake shaft subassembly	CD01-800	1	
2	Brake support	CD01-600	1	

SUBASSEMBLY NAME: Brake & support subassembly		NO.	REVISION	DATE	BY
		1			
		2			
<small>Unless otherwise specified</small> 1. TOLERANCE ON: X: is ± 0.5 XX: is ± 0.2 XXX: is ± 0.05 2. ANGULAR TOLERANCE: ± 0.5 3. LAST REVISION INDICATED BY: <input type="checkbox"/> 4. SURFACE FINISH: 32		MATERIAL: DESIGNED BY: L. GENG CHECKED BY: R. Perlin APPROVED BY: P. RADZISZEWSKI		MCGILL UNIVERSITY COMMINUTION DYNAMICS LABORATORY	
PROJECTION	DIMENSION	SIZE	SCALE	SHEET	DWG NO.
	mm		1:200	1 of 1	CD01-1300
					REV

Document Log:

Manuscript Version 1— June, 2004

Typeset by *Microsoft Word*— 30 July 2004

LEI GENG

DEPARTMENT OF MECHANICAL ENGINEERING, MCGILL UNIVERSITY, 817 SHERBROOKE
STREET WEST, MONTREAL (QUEBEC) H3A 2A7, CANADA, *Tel.* : (514) 398-5479
E-mail address: lei.geng@mail.mcgill.ca

Typeset by *Microsoft Word*